Politecnico di Torino

Politecnico di Torino

Master's Degree Course in

ENVIRONMENTAL AND LAND ENGINEERING

A.a. 2021/2022

Graduation Session: March 2024

Spatial and Temporal Variability of Tropospheric Delays estimated from a low-cost GNSS network: A Comparative Analysis

Supervisor
Paolo Dabove

Candidate
Mujtaba Usman

ABSTRACT

The GNSS satellite signals experience a delay in the troposphere layer of the atmosphere, which can be split and modelled into two main parts: the Hydrostatic and Wet Delays, where the latter is due to water vapor. The Precise Point Positioning (PPP) technique which uses dual frequency measurements, demonstrates highly accurate position determination along with Zenith Tropospheric Delay (ZTD) estimation. ZTD estimation is valuable for various applications including climate modelling and determining atmospheric water vapor. Currently, the mean inter-section distance of GNSS Networks does not provide the capability to observe the troposphere at the fine spatial resolution of a few kilometres, necessary to adequately capture the regional variations in water vapor distribution. The expansion of GNSS stations to achieve a denser network, is constrained by financial considerations. The low-cost Centipede-RTK network offers a cost-effective solution to enhance the spatial resolution of tropospheric monitoring. This study analyses spatial and temporal variability of Zenith tropospheric delays derived from the high-cost European Permanent Network (EUREF) and the low-cost Centipede-RTK Network through post-processing of GNSS data in two different open source softwares RTKLIB and the online service CSRS-PPP, have been considered to check the different results that can be obtained, in order to make the analyses independent by the use of the software. The data collection was made by downloading stream data from 5 strategically selected locations across France, ensuring proximate ground stations from both GNSS networks. The ZTD estimates from RTKLIB and CSRS are compared with tropospheric delay product provided by EUREF Permanent GNSSS Network in terms of Root mean squared error. The findings indicate that the Centipede Network, when processed with suitable PPP tools like CSRS-PPP, provides ZTD estimates with accuracy comparable (Root Mean Square Error <_5cm) to the EUREF Network across most locations, except for one in southeastern France. This study emphasizes the feasibility of integrating low-cost GNSS solutions for precise atmospheric monitoring, paving the way for broader application and research in GNSS meteorology.

Acknowledgement

All praises are for ALLAH Almighty, the Most Gracious and the Most Merciful, for bestowing me with the strength, patience, and guidance necessary to complete this journey. It is with His blessings that I have been able to conduct this research and emerge with profound learning and growth. I would like to express my extreme gratitude and respect to the Prophet Muhammad (SAW), whose teachings and exemplary life have always been a beacon of guidance towards leading a better, more purposeful life.

I would like to express my sincere gratitude to my supervisor, Professor Paolo Dabove, for guiding me through this research study. As a very Kind Human being, his expertise, understanding, and patience have been pivotal throughout this journey.

I am indebted to *Politecnico di Torino* for providing me with the necessary resources and state-of-the-art facilities that facilitated the execution of this research.

Lastly, my deepest appreciation goes to my family. Their love, understanding and encouragement served as the bedrock of strength during the challenges encountered during this academic voyage.

Table of Contents

List of Figures

List of Tables

Chapter 1- Introduction

This chapter sets the stage for this research study by providing a comprehensive background on the Global Navigation Satellite System (GNSS), including an overview of GNSS segments and satellite constellations. The concepts of triangulation and the positioning techniques are discussed, which are fundamental to GNSS operations. Among these techniques, Precise Point Positioning (PPP) holds high importance due to the provision of centimetre level accuracy. The chapter further explores the various delays and errors encountered by satellite signals as they travel through the Earth's atmosphere. Following the technical background, the chapter transitions to discuss GNSS networks, with a particular focus on the European Reference Frame (EUREF) and the Centipede network. These networks are essential for providing the data necessary for this research study. The research objectives are then clearly outlined, detailing the aims of investigating the spatial and temporal variability of Zenith Total Delay (ZTD) estimates obtained from GNSS data. Lastly, the significance of this study is articulated, emphasizing its contribution to enhancing the understanding of atmospheric delays on GNSS signals and the potential of low-cost GNSS networks in various applications. This introduction lays the groundwork for the detailed analysis that follows in subsequent chapters.

Background

At its core, GNSS encompasses a constellation of satellites orbiting the Earth, transmitting signals that enable GNSS receivers to determine their location (latitude, longitude, and altitude), velocity, and the precise time, anywhere on or near the Earth’s surface. The development of the Global Navigation Satellite System (GNSS) has seen rapid progress due to its extensive applications in Earth observation and research. GNSS constellations include the European Union’s Galileo, Russia’s Global Navigation Satellite System (GLONASS), and the United States’ Global Positioning System (GPS) [1].

The architecture of GNSS systems consists of three main segments: the space segment, the control segment, and the user segment. The space segment includes the satellites themselves; the control segment comprises ground stations that monitor and control the satellites, ensuring their proper functioning, and the user segment consists of GNSS receivers that interpret the signals from the satellites to provide positioning, navigation, and time.

The basic Principle of GNSS is triangulation to determine user location. The GNSS receiver calculates the time difference between the satellite signal’s transmission and reception times. Using speed of light, the distance between the receiver to the satellite is determined. This distance includes some errors because both the satellite and receiver clocks are not perfectly synchronized. Therefore, it is called Pseudo-range measurement.

Each satellite obtains a message from ground-based antennas that includes details on its orbital parameters, clock condition, and other temporal data. This data is then conveyed to the user via the navigation message. Broadcast data are included in the satellite navigation message, which contains the information about the satellite’s position (orbit) and time (clock).

The accuracy of broadcast orbits is generally within a few meters, and clock accuracies are within a few nanoseconds [2]. Precise orbit and clock data are corrected and validated through ground monitoring stations. The accuracy of precise orbits can be within a few centimetres, and clock accuracies are significantly improved to within fractions of a nanosecond.

Positioning techniques

Single Point Positioning uses the signal from at least four satellites to determine a position in three dimensions. GNSS receivers perform autonomous positioning using broadcast orbits and clocks. The measurements must be corrected for errors [3].

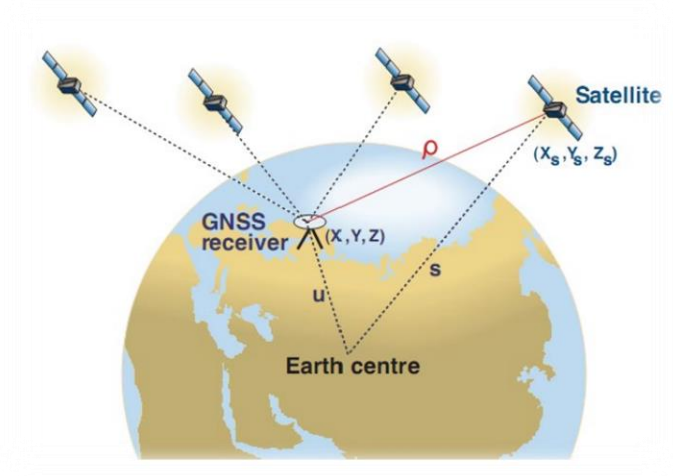

Figure 1 Single Point Positioning Concept

Differential GNSS improves the measurement accuracy using a fixed ground-based reference stations to broadcast the difference between the positions indicated by the satellite systems and the known fixed positions.

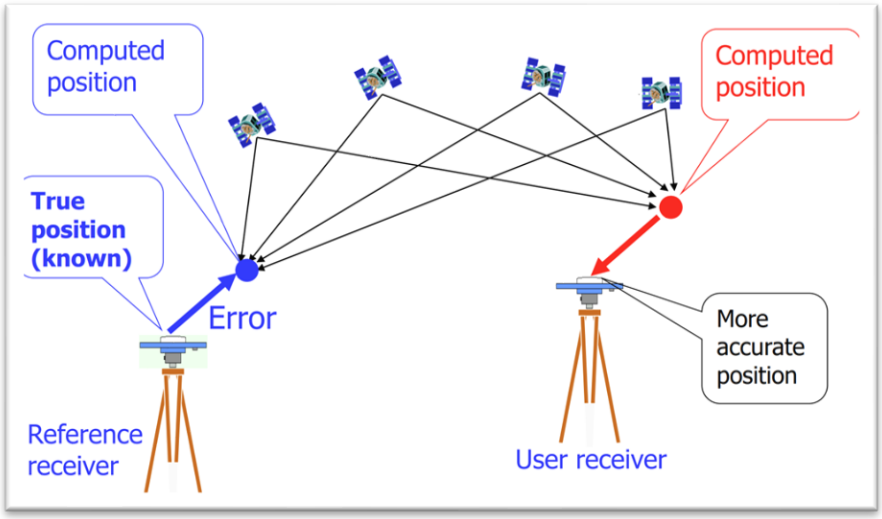

Figure 2 Differential GNSS Positioning (3).

For Differential Positioning, a minimum of two functioning receivers is required. This approach leverages the spatial correlation of errors across stations to reduce or eliminate their impact when operating in differential mode, thereby enhancing accuracy.

Precise Point Positioning

Precise Point Positioning (PPP) is a GNSS data processing technique that allows users to determine their exact location on Earth up to centimetre accuracy. Unlike differential GNSS positioning method that require data from multiple receivers to achieve high levels of accuracy, PPP can achieve this high precision using a single GNSS dual frequency receiver [4]. This capability makes PPP a powerful tool for various applications. PPP utilizes dual-frequency GNSS data along with precise satellite orbit and clock information to correct for the errors in GNSS signal processing.

The presence of cosmic and solar radiation in ionosphere affects the speed of GNSS signals. PPP uses signals at two different frequencies to provide correction for this ionospheric delay. Two-frequency receivers can remove this error source (up to 99.9%) using ionosphere-free combination of pseudo-ranges (PC) or carriers (LC) Ionosphere-free combination [3].

PPP relies on highly accurate satellite orbit and clock products, often provided by international GNSS service providers. These corrections are crucial for eliminating errors due to inaccuracies in the predicted positions of the satellites or in the onboard clocks. The rotation of the satellite antenna as seen from the receiver can introduce errors, which PPP corrects for.

Tropospheric Path Delay

Tropospheric Path delay is a fundamental concept in satellite communications and navigation, which refers to the delay experienced by satellite signals as they pass through the Earth's troposphere (which is the lowest layer of the atmosphere extending from the Earth's surface up to about 8 to 15 kilometres) in altitude. Tropospheric delays arise from the interaction of GNSS signals with atmospheric constituents, with the primary contributing factors being:

- **Atmospheric Moisture**: Water vapor significantly affects signal propagation speed and introduces variability in delay magnitudes due to its uneven distribution across the atmosphere.
- **Temperature**: Variations in atmospheric temperature alter the density of the air, influencing the refractive index and, consequently, the speed of GNSS signals.
- **Atmospheric Pressure**: Changes in air pressure impact the total atmospheric mass that GNSS signals traverse, causing the delay.

Figure 3 Tropospheric Path Delay Concept

GNSS Networks

Traditionally, high-cost GNSS networks like the International GNSS Service, EUREF GNSS Network have been established to provide high quality GNSS data. These networks, equipped with advanced infrastructure and technology, offer highly accurate measurements for atmospheric parameters, and the precise estimation of tropospheric delays.

EUREF Permanent GNSS Network

The EUREF Permanent Network aims to cover the European continent by providing high-quality GNSS data. The EUREF network is characterized by its high-cost, high-accuracy GNSS receivers and antennas, strategically placed to optimize coverage and precision across Europe. The station density varies across different regions as shown in the below map.

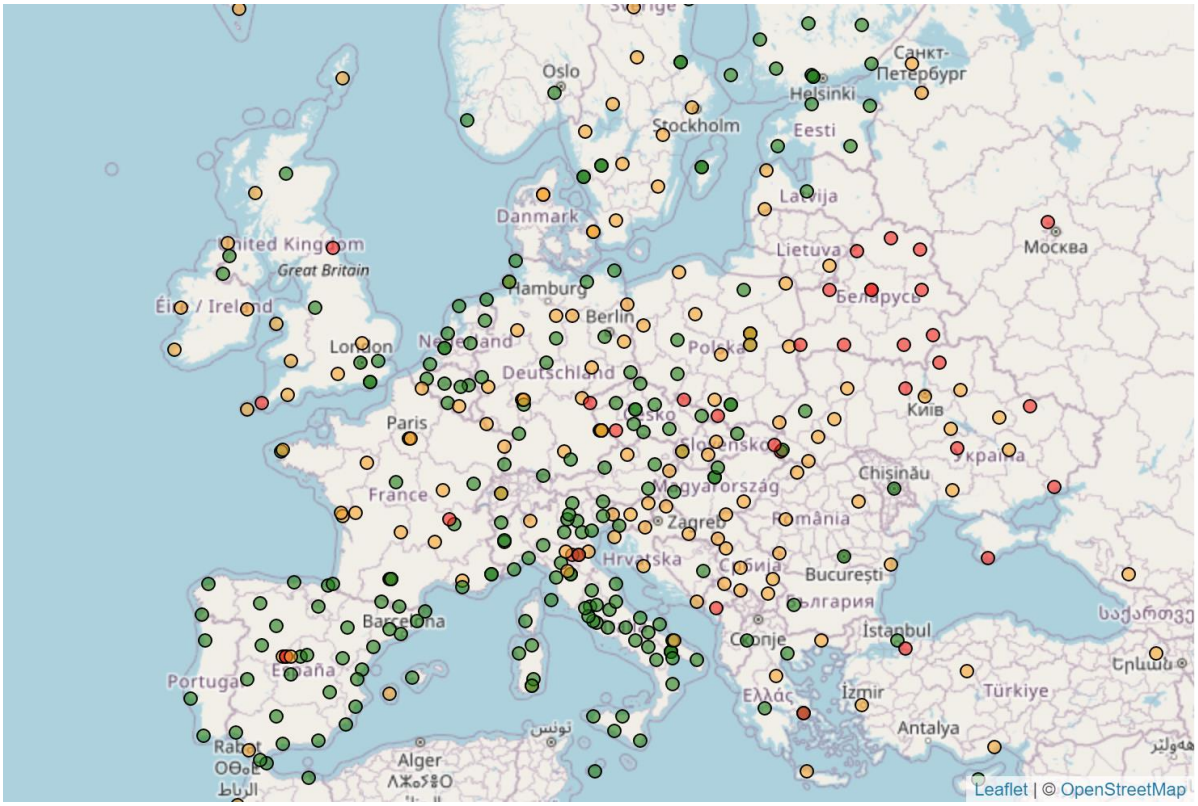

Figure 4 EUREF GNSS Network Map

The EUREF Permanent Network (EPN) is a collaborative effort of over 100 self-funding entities, including agencies, universities, and research institutions across more than 30 European countries. Their collective aim is to uphold the European Terrestrial Reference System (ETRS89. ETRS89 is established through EUREF by providing access to precise coordinates and GNSS observation data from over 200 permanent GNSS stations across Europe. This network supports both static and kinematic spatial referencing and has become essential for various applications, including ground deformation monitoring, sea level tracking, space weather observation, and numerical weather prediction. The EUREF Permanent Network offers a suite of products based on GNSS data to support various applications, including the maintenance and accessibility of the European Terrestrial Reference Frame (ETRS89) and monitoring the Earth's troposphere.

Product	Description
Daily Position Estimates	Calculated from one day of GNSS data and refreshed daily, instrumental for ongoing station monitoring activities.
Weekly Position Estimates	Derived from a week's worth of data and updated weekly, occasionally reprocessed to align with current best practices. Serves as a snapshot realization of the ETRS89.
Long-term Positions and Velocities	Compiled from the entirety of available EPN data and revised every 15 weeks, representing EUREF's official implementation of the ETRS89.
Zenith Tropospheric Path Delay Estimates	Crucial for understanding atmospheric conditions.
ETRS89 Satellite Orbit and Clock Correction Streams	Vital for precision in GNSS applications.

Figure 5 EUREF Network Products [5]

Centipede-RTK Network

The Centipede Network represents a newer generation of GNSS networks that leverage low-cost GNSS receivers to achieve broader coverage. Centipede-RTK represents a cooperative network of GNSS base stations, accessible to all. This network has been expanded through contributions from public institutions, private entities like agriculturalists, individuals, and other public collaborators. The project's goal is to ensure comprehensive coverage across metropolitan areas. Financial backing is provided by INRAE [6]. While initially, the Centipede Network may not match the precision level of networks like EUREF, its strength lies in the potential for high density of stations, especially in urban areas or regions previously underserved by GNSS stations. Following is a map of Centipede-RTK network stations.

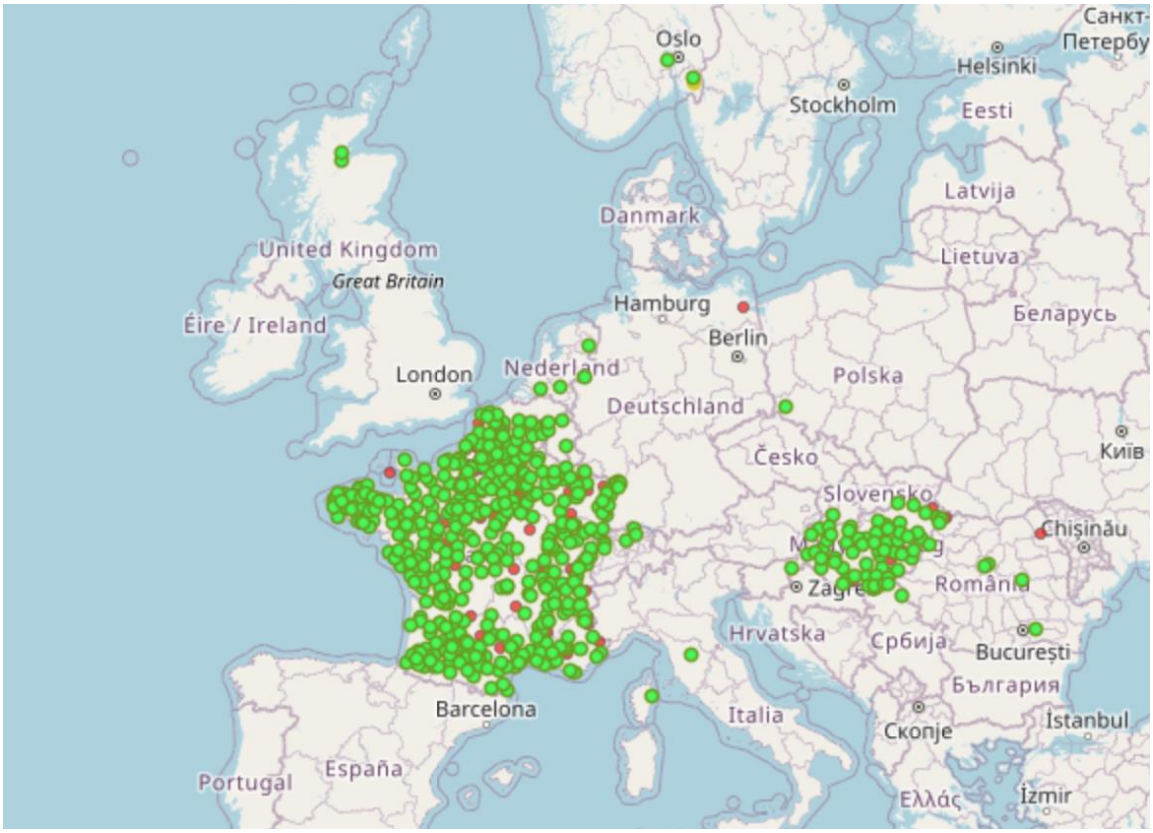

Figure 6 Centipede-RTK Network Station Map [6]

A significant development is the collaboration between the Centipede-RTK network and the Permanent National GNSS Network (RENAG), which has integrated about thirty RENAG stations, especially in the south-east of France, into the Centipede-RTK network. This partnership not only expands the Centipede-RTK network with valuable data but also ensures the longevity of network data through archival in RENAG's databases. This mutual exchange marks a significant step towards improving geolocation precision and data sustainability in environmental research.

Research Objectives

The Main objectives of this research study are presented below.

- The selection of GNSS stations from the EUREF and Centipede Networks in such a geographical location where there are proximate stations from both the networks.
- To acquire Real time GNSS data, simultaneously for the EUREF and the Centipede network stations.
- To Process the acquired GNSS data using different software packages to obtain the ZTD estimates over time. This is done to make the analyses independent of software usage.
- To assess the Temporal variability of ZTD estimates obtained from the low-cost Centipede network.
- To assess the spatial variability of ZTD estimates provided by the Centipede network.

- Through statistical indicators, the comparison of spatial and temporal variability of tropospheric delays estimated from the Centipede-RTK low-cost GNSS network and the EUREF Permanent GNSS network.
- To check the accuracy of ZTD estimates of Centipede network against the EUREF tropospheric product.
- This study seeks to determine the feasibility and potential limitations of employing low-cost GNSS solutions for atmospheric analyses and research. The final goal is to assess whether these cost-effective networks can serve as viable alternatives to traditional, more expensive systems in the context of atmospheric studies, thereby broadening the accessibility and applicability of GNSS technology in meteorological and climatological applications.

Significance of this Research

Accurately estimating the tropospheric path delay poses significant challenge due to the dynamic nature of the troposphere, which varies spatially and temporally. Variations in temperature, pressure, and water vapor content can significantly influence the amount of delay, requiring sophisticated models and continuous monitoring to achieve high resolution. Precise estimation of ZTD plays a critical role in improving weather prediction models, studying climate change, and advancing our understanding of atmospheric dynamics.

Enhancing Spatial Resolution

GNSS meteorology significantly benefits from the extensive network of over thousands of permanent GNSS stations globally. Europe alone possesses more than 2000 stations, offering tropospheric data with a spatial resolution of approximately 30 to 100 kilometres. Japan's GEONET, recognized as one of the densest national GNSS networks with over 1300 stations, enhances this resolution to about 20 kilometres. However, despite these advances, current networks do not provide the capability to observe the troposphere at the fine spatial resolution of a few kilometres, a scale that regional climate and weather models are beginning to incorporate [7] [8]. Moreover, neither these extensive networks nor any other existing observational method can adequately capture the regional variations in water vapor distribution.

The expansion of GNSS stations to achieve a denser network, is constrained by financial considerations. The high costs associated with the deployment and maintenance of such networks limit their expansion and the density of GNSS stations, which is crucial for capturing the spatial and temporal variability of the troposphere. The geodetic GNSS receiver's high cost ($30.000 to $70.000 each) is a major challenge for the high-resolution monitoring of the atmosphere [9].

The low cost GNSS networks present a promising opportunity for network densification. They offer a cost-effective solution to enhance the spatial resolution of tropospheric monitoring. The resulting improvement in our knowledge of water vapor distribution would enable more

accurate forecasts of rainfall and extreme weather events and would contribute to climate change studies.

Performance of Low-Cost Receivers

Recent studies point out that the performance of low-cost GNSS receivers approaches to that of geodetic grade equipment. To meet the ever-increasing demand for affordable GNSS equipment across a wide range of applications, the recent low cost GNSS antennas allow kinematic and static positioning with high precision [10].

Studies have shown that dual-frequency low-cost GNSS receivers can achieve precise positioning and are effective for hazard monitoring in optimal conditions. However, their performance in determining positions falls short when compared to geodetic-grade receivers [10]. Nonetheless, when it comes to post-processed Zenith Tropospheric Delay (ZTD) estimates, low-cost GNSS receivers deliver accuracy comparable to that of geodetic-grade receivers. This highlights the significant potential of affordable devices for use in meteorological applications, despite some limitations in position accuracy [9].

Specific case studies have explored the performance of low-cost GNSS receivers in detecting atmospheric water vapor variations and estimating ZTD with various antenna qualities. These studies highlight the potential of low-cost receivers in numerical weather prediction and other high-accuracy applications, with the quality of the receiving antenna identified as a limiting factor. [11]. For static GNSS experiments, low-cost receivers show that an accuracy of a few millimetres can be achieved in comparisons to geodetic-grade equipment.

Chapter 2- Literature Review

This chapter includes the foundational concepts and prevailing research studies relevant to this study. The concept of tropospheric delay is discussed in detail, due to its critical significance to this research. The discussion extends to atmospheric refractivity, Zenith Tropospheric Delay (ZTD) and Slant Tropospheric Delay (STD). Furthermore, the chapter provides literature review of Neil mapping function and Global mapping function used by the software packages utilized in this study. Precise point positioning technique along with the discussion on the PPP software packages is provided in the last section of this chapter.

Tropospheric Delay

The troposphere's influence on GNSS signals is quantified through the concept of refractivity, denoted as N. Refractivity is a measure of how much the atmosphere bends or refracts the path of a GNSS signal, altering its speed and ultimately its arrival time at the receiver. This bending is caused by variations in air density within the troposphere, which are influenced by factors such as temperature, pressure, and humidity. The formula for calculating the total refractivity N of the troposphere is given by:

$$N = 10^6(n-1) \qquad (1)$$

where *n* represents the refractive index of the troposphere. The refractive index, in turn, indicates the ratio of the speed of light in a vacuum to its speed through the troposphere; a higher refractive index implies greater slowing and bending of GNSS signals. The multiplier 10^6 is used to scale the refractivity to a practical range for measurement and analysis.

This refractivity, denoted as *N*, can be deconstructed into two primary components: the hydrostatic (or dry) component, N_{dry} , and the wet component, N_{wet}.

Hydrostatic component is attributable to the dry gases in the atmosphere, primarily nitrogen and oxygen. It is relatively stable and can be predicted with high accuracy based on surface air pressure. The hydrostatic component is significant because it constitutes the majority of the tropospheric delay, yet its stability allows for effective modelling and correction in GNSS applications.

Unlike the hydrostatic component, the wet component results from the variable content of water vapor in the atmosphere. Water vapor distribution is highly variable in time and space, making the wet component more challenging to model and correct. It accounts for a smaller portion of the tropospheric delay compared to the hydrostatic component but introduces significant variability due to its dependence on local atmospheric conditions.

The total refractivity *N* is separated into its dry and wet components [12]. Total refractivity can also be mathematically expressed as a function of meteorological parameters—air pressure (*p*), temperature (*T*), and water vapor partial pressure (*e*)—and is given by the equation [13].

$$N = N_{dry} + N_{wet} = k_1.\frac{(p-e)}{T} + k_2.\frac{e}{T} + k_3.\frac{e}{T^2} \quad (2)$$

In this equation, k_1, k_2 , and k_3 represent empirically determined coefficients that are critical for calculating the refractivity based on observed atmospheric conditions. The values of these coefficients are as follows [14].

- $k_1 = 77.689\ K.hPa^{-1}$
- $k_2 = 71.295\ K.hPa^{-1}$
- $k_3 = 375{,}463\ K^2.hPa^{-1}$

These coefficients facilitate the translation of meteorological data into a refractivity value that quantifies the atmospheric impact on GNSS signal speed and trajectory.

The equation (2) can be rewritten in terms of dry air and water vapor compressibility factors [15].

$$N = k_1.\frac{(P_d)}{T}{Z_d}^{-1} + k_2.\frac{e}{T}{Z_w}^{-1} + k_3.\frac{e}{T^2}{Z_w}^{-1} \quad (3)$$

Where P_d is the pressure of dry air and e is the partial pressure of water vapor respectively in (hPa), T is the temperature in Kelvin, Z_d and $Z_w$are the dry air and water vapor compressibility factors, that consider the deviation of air from an ideal gas. The calculation of Z_d and Z_w can be performed from the following equations [16].

$${Z_d}^{-1} = 1 + P_d\left[57.97 * 10^{-8}(1 + \frac{0.52}{T}) - 9.4611 * 10^{-4}(\frac{T-273.15}{T^2})\right] \quad (4)$$

$${Z_w}^{-1} = 1 + 1650\frac{P_w}{T^3}[1 - 0.01317(T - 273.15) + 1.75 * 10^{-4}(T - 273.15)^3 + 1.44 * 10^{-6}(T - 273.15)^3] \quad (5)$$

The tropospheric delay (Δ^{PD}) is calculated as an integral of the total refractivity (*N*) along the signal's path (*s*) from the receiver (*r*) to the satellite (*w*). This is mathematically represented as:

$$\Delta^{PD} = 10^{-6}\int_r^w N.ds \quad (6)$$

This equation shows that the delay is proportional to the integral of refractivity over the distance that the signal travels through the troposphere. The factor 10^{-6} is used to scale the refractivity to the appropriate units for the delay calculation.

The equation for tropospheric delay considering both the dry and wet components of the refractivity N, separately is:

$$\Delta^{PD} = 10^{-6}\int_r^w N_{dry}.ds + 10^{-6}\int_r^w N_{wet}.ds \quad (7)$$

Zenith Tropospheric Delay

Zenith Tropospheric delay is the total delay experienced by a signal from a Global Navigation Satellite System (GNSS) as it passes through the Earth's troposphere in a direction perpendicular to the Earth's surface as shown in the figure below. Zenith Tropospheric Delay (ZTD) encompasses both the zenith hydrostatic delay (ZHD), which correlates with atmospheric gases present in the troposphere, and the zenith wet delay (ZWD), characterized by its dynamic variations due to atmospheric water vapor content. The ZHD is the stable, predictable part while the ZWD is the variable which is challenging-to-model.

The ZTD is defined as the addition of the Zenith Hydrostatic Delay (ZHD) and the Zenith Wet Delay (ZHD):

$$ZTD = ZHD + ZWD \qquad (8)$$

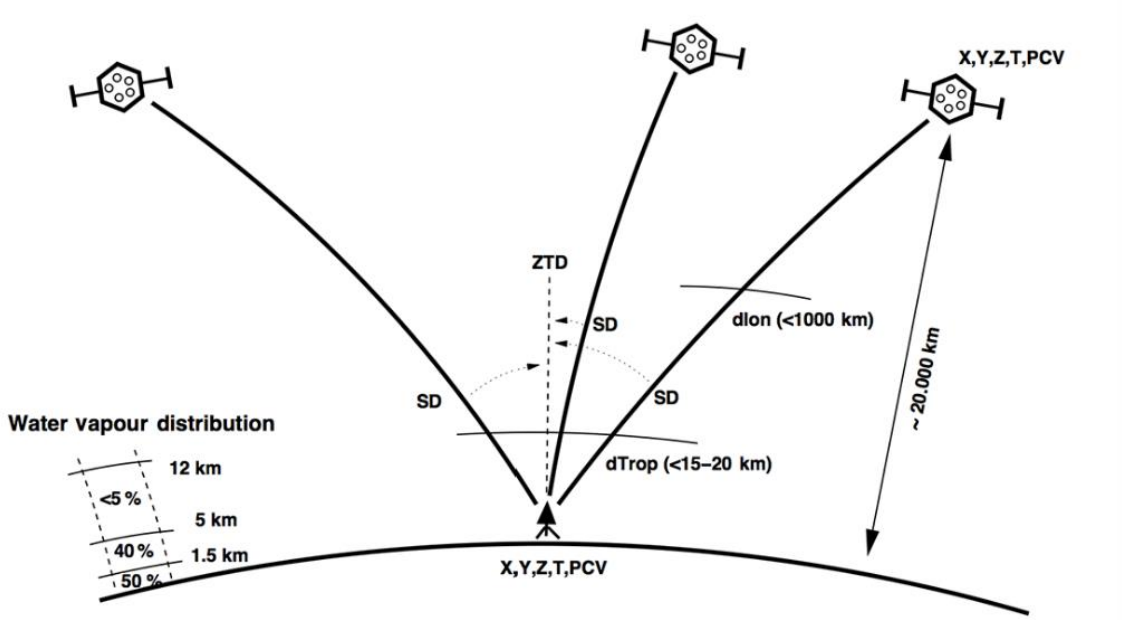

Figure 7 ZTD and STD [17]

Slant Tropospheric Delay refers to the delay experienced by a GNSS signal as it travels through the troposphere at an angle to the Earth's surface, from the satellite to the GNSS receiver as shown in the figure above. This path is not straight down but slanted, hence the name "slant" delay. The conversion from Zenith Tropospheric Delay to STD is achieved using mapping functions. The mapping functions, which are empirical or theoretical models, provide a factor that scales the ZTD to an equivalent STD [18].

$$\mathrm{STD} = ZHD * m_h(E) + ZWD * m_w(E) \qquad (9)$$

Where m_h is the hydrostatic mapping function, m_w is the wet mapping function while E is the elevation angle of the Satellite. These functions are crucial because they allow for a standardized way to account for the impact of the troposphere on signal delays.

Zenith Hydrostatic Delay (ZHD)

It is assumed that the mean molar mass is equal to the mean molar mass of only the “dry” components excluding the water vapor. If it is assumed that the atmosphere is in hydrostatic equilibrium, the zenith dry delay is very well modelled - with an RMS of approximately 0.5 mm [19]. The hydrostatic part is described by:

$$ZHD = 10^{-6} k_1 \int \frac{(P_d)}{T} {Z_d}^{-1} \, ds \tag{10}$$

Zenith Wet Delay (ZWD)

ZWD is due to the water vapor and includes a correction for the "dry mean molar mass”. Since the water vapor is present in the form of water drops which causes the “unmixed” condition of the troposphere, the wet delay estimation is very inaccurate and can have RMS errors of several centimetres [19]. The wet part is described by:

$$ZWD = 10^{-6} k_2 \int \frac{(e)}{T} {Z_w}^{-1} \, ds + 10^{-6} k_3 \int \frac{e}{T^2} {Z_w}^{-1} \, ds \tag{11}$$

Mapping Functions

The two software packages used in this research study estimate the Zenith Tropospheric Delay by using a model to estimate the hydrostatic slant delay, then use a mapping function to estimate the delay in the zenith direction and estimate the wet delay as an unknown in the parameter estimation process typically done with an Extended Kalman Filter [20].

The mapping functions play a crucial role in translating slant tropospheric delays (STD) to zenith tropospheric delays (ZTD) across different elevation angles. The mapping functions commonly use the Herring-style continued fraction, as presented in Equation (11). Each mapping function adopts a distinct approach to calculating its coefficients, a method initially proposed by Herring in 1992. [21]

$$m_i(E) = \frac{1 + \dfrac{a_i}{1 + \dfrac{b_i}{1 + c_i}}}{\sin(E) + \dfrac{a_i}{\sin(E) + \dfrac{b_i}{\sin(E) + c_i}}} \tag{12}$$

where a_i, b_i, and c_i are empirically derived coefficients that vary based on the type of mapping function used and potentially the location and time of year. The mapping function $m_i(E)$ for

a given elevation angle (E) can be expressed as a *function of* (E, a_i, b_i, c_i). In this context, 'i' denotes either 'h' for the hydrostatic mapping function or 'w' for the wet mapping function [18]

Calculations are performed for determining the refractivity at different altitudes; calculating both hydrostatic and wet delays in the zenith direction; and assessing hydrostatic and wet delays along with the bending effect in the slant path direction. The formation of a mapping function involves the integration of zenith and slant delays obtained through raytracing into Equation (11), with the coefficients being optimized through a least-squares adjustment method [22].

Neill Mapping Function

The software package RTKLIB uses the Niell Mapping Function (NMF), developed by Arthur Niell, for converting slant tropospheric delays to zenith tropospheric delays. For the implementation of raytracing, NMF relies on data from radiosondes. NMF uses raytracing through Numerical Weather Models (NWM) to calculate mapping function coefficients, it can also incorporate empirical data, climatology, and other atmospheric models. For the Niell Mapping Function (NMF), coefficients are established through the application of raytracing across nine elevation angles ranging from 3° to 90°. These coefficients are specifically available for four latitudinal positions: 15°, 30°, 45°, and 60° North [23] .

The NMF is defined separately for hydrostatic (m_h) and wet (m_w) components of the tropospheric delay as functions of the elevation angle (E) of the satellite.

The coefficients of the wet mapping function are defined as a constant by latitude, and those of the hydrostatic mapping function are defined as a function of latitude and observation time for the Neil mapping function [23].

$$a_h(\varphi, t) = a_{avg}(\varphi) - a_{amp}(\varphi)cos(2\pi\frac{DOY - 28}{365.25}) \qquad (13)$$

In the Equation (13), φ is the site latitude and Day-of-Year (DOY) is the date based on UT (Universal Time). a_{avg} and a_{amp} stand for the mean value and an amplitude, respectively; and they are given as constants. The hydrostatic mapping function of NMF needs correction terms to make up for the height difference of observation site. Therefore, the hydrostatic mapping function of NMF should be re-defined:

$$m_h(E) = f(E, a_h, b_h, c_h) - (\frac{1}{sin(E)} - f(E, a_{ht}, b_{ht}, c_{ht}) * H \qquad (14)$$

H is the height of the site in km, and the constants a_{ht}, b_{ht}, c_{ht} are constants. [23]

The simple temporal and latitudinal functions of the NMF can't capture the high-resolution variations over space and time that are found in mapping functions using Numerical Weather Model data. [22]

Global Mapping Function (GMF)

The online service CSRS-PPP uses the Global Mapping Function to estimate the Zenith tropospheric delay from STD. The GMF introduces $a_h \, and \, a_w$ as hydrostatic and wet coefficients respectively, leveraging raytracing across ERA40 monthly averages from 1999 to 2002. This function calculates coefficients by analysing ray-traced values at 312 global points for 36 months, demonstrating a comprehensive coverage that enhances its utility. GMF includes latitude, day of the year, and height as factors in its calculations [24]. The GMF provides better precision than the NMF and smaller height biases with respect to the Vienna Mapping Function. It can be implemented very easily because it uses the same input parameters as NMF. [25]

Precipitable Water

Precipitable Water (PW) in the atmosphere refers to the total amount of water vapor contained in a vertical column of the atmosphere, if all the water vapours were condensed into liquid water. It is typically represented in millimetres or inches and represents the depth of water that would accumulate on a flat surface if all the water vapor in that column were to precipitate out. The zenith wet delay (ZWD) and Precipitable water (PW) are related as:

$$PW = \mathbb{\Pi} * ZWD \qquad (15)$$

ZWD is in the units of length and the dimensionless proportionality constant is a function of refractivity of the moist air and the weighted mean temperature of the atmosphere.

Precise Point Positioning

Precise Point Positioning (PPP) technique in GNSS data processing is utilized to determine the exact location of a GNSS receiver by analysing carrier phase and pseudo-range observations used with high-accuracy products from different sources such as the International GNSS Service (IGS), enabling measurements with centimetre-level precision [4]. Typically, this level of precision requires the use of GNSS receivers and antennas, which can be quite costly. In the PPP approach, observations from a single receiver are used to estimate the receiver position, the ambiguities, the receiver clock offset and the wet tropospheric delay [4].PPP serves a wide range of applications such as: precise positioning , atmospheric water vapor sensing [26], earthquake and tsunami monitoring [27], orbit determination of low Earth orbiting satellites [28] and precision agriculture [29]. PPP have demonstrated a high ability to become the next-generation positioning technology. The the use of a single receiver reduces the equipment costs and makes the processing less labour and resources intensive.

PPP Software Packages

In Recent years, there has been an emergence of several open-source PPP software packages, enriching the field with diverse tools such as RTKLIB, GAMP, CSRS-PPP, Magic. Each of these software solutions presents unique benefits and features, catering to various research and practical needs. However, the ease of use and the quality of documentation significantly differ

among these packages and softwares, often posing challenges during the initial setup and usage phases. The study by [20] has evaluated software packages and online processing services like APPS, CSRS-PPP, MagicGNSS, POINT, RTKLIB, and gLAB, with their estimated ZTDs checked against International GNSS Tropospheric Product values using the Root Mean Square Error (RMSE) to gauge the accuracy. CSRS-PPP and gLAB demonstrated low RMSE values [20], indicating more accurate estimation of ZTD values than the other services compared under study.

RTKLIB

RTKLIB is an open-source software, developed by Tomoji Takasu from the Tokyo University of Marine Science and Technology, designed for processing GNSS raw data. It enables users to achieve precise positioning through real-time or post-processing analysis, using data from dual receivers for relative positioning (RTK/PPK) or data from a single receiver for absolute positioning (PPP) [30]. The Following Table 1 presents features supported by the RTKLIB v2.4.3 [31].

RTKLIB Features	Details
Supported GNSS Constellations	GPS, GLONASS, Galileo, QZSS, BeiDou, SBAS
Positioning Modes	Single, DGPS/DGNSS, Kinematic, Static, Moving-Baseline, Fixed, PPP-Kinematic, PPP-Static, PPP-Fixed
Standard Formats and Protocols	RINEX 2.10, 2.11, 2.12 OBS/NAV/GNAV/HNAV/LNAV/QNAV, RINEX 3.00, 3.01, 3.02 OBS/NAV, RINEX 3.02 CLK, RTCM ver.2.3, RTCM ver.3.1 (with amendment 1-5), ver.3.2, BINEX, NTRIP 1.0, RTCA/DO-229C, NMEA 0183, SP3-c, ANTEX 1.4, IONEX 1.0, NGS PCV and EMS 2.0
External Communication	Serial, TCP/IP, NTRIP, local log file (record and playback), FTP/HTTP (automatic download)

Table 1 RTKLIB Features

Table 2 shows the different RTKLIB tools for Graphical user interface application program and Command line interface application program [31].

Function	GUI AP	CUI AP
AP Launcher	RTKLAUNCH	-
Real-Time Positioning	RTKNAVI	RTKRCV
Communication Server	STRSVR	STR2STR
Post-Processing Analysis	RTKPOST	RNX2RTKP
RINEX Converter	RTKCONV	CONVBIN
Plot Solutions and Observation Data	RTKPLOT	-
Downloader for GNSS Data	RTKGET	-
NTRIP Browser	SRCTBLBROWS	-

Table 2 RTKLIB Tools

Demo5 version of RTKLIB is based on RTKLIB 2.4.3 but modified to improve the solutions for lower cost receivers and lower quality data. The demo5 version is developed by Tim Everett and is maintained on GitHub. The GitHub contains code versions and changelogs which describe changes or improvements in the code [32].

CSRS-PPP

The Canadian Spatial Reference System Precise Point Positioning (CSRS-PPP) service is an online tool provided by Natural Resources Canada (NRCan). It offers users the ability to obtain precise GNSS positioning information by processing single or dual-frequency GNSS. CSRS-PPP supports both real-time and post-processing applications. The Canadian Geodetic Survey (CGS) provides a set of tools including CSRS-PPP, to achieve precise point positioning. By utilizing precise orbit and clock data, CSRS-PPP enables the determination of positions globally. [33]. Users can upload observation data in the Receiver Independent Exchange (RINEX) format, supporting either static or kinematic modes. As an online service, CSRS-PPP provides a user-friendly interface that allows users to upload GNSS data files and receive processed results via email, facilitating ease of use for professionals and researchers. The output is downloadable through email which contains the position estimates, quality indicators, Zenith tropospheric delay, corrections for satellite and receiver clock errors, and a pdf report containing graphics of the outputs over time.

Chapter 3- Methodology

This chapter presents the methodology employed in this research to obtain the tropospheric delays from the low-cost Centipede Network, the delay estimates from the EUREF Network and their comparison. The ZTD values are also compared with the EUREF Tropospheric Product, as indicated by the Flowchart below. The GNSS stations are introduced, followed by the GNSS data acquisition and processing methodology. To assess the spatial and temporal variability, the methodology adopted for the analysis is also discussed in the last section of this chapter. The Following diagram illustrates the main methodology adopted for this research study.

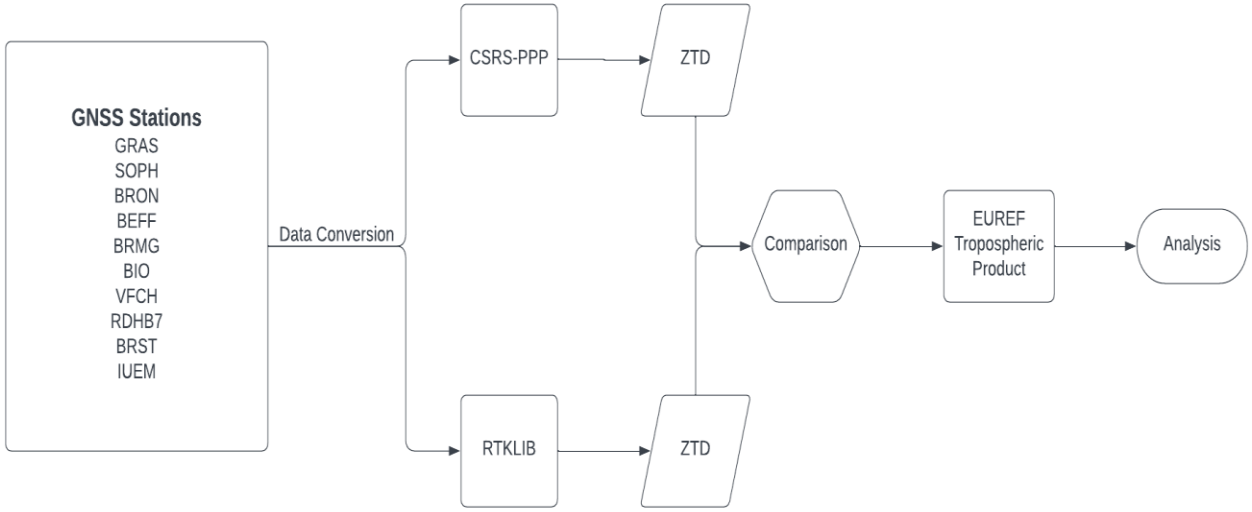

Figure 8 Methodology of the Research

GNSS Stations

For this study, five stations across France are selected, one each from the Centipede-RTK and the EUREF GNSS Network. The coordinates (X, Y, Z) for the EUREF Network stations are available in ETRF2000 (European terrestrial reference frame 2000), are converted to WGS84 reference coordinate system with QGIS Software. The coordinates for the EUREF Network stations are listed below in table 3.

	EUREF Network Station	Latitude	Longitude	Altitude (m)
1	GRAS00FRA (Caussols, FRA)	43.7547	6.9206	1319.35
2	BRMF00FRA (Bron, FRA)	45.7261	4.9384	256.85
3	BRST00FRA (Brest, FRA)	48.3805	-4.4966	67.84
4	BRMG00DEU (Bremgarten, DEU)	47.9077	7.6329	261.60
5	VFCH00FRA (Villefranche-sur-Cher, FRA)	47.2942	1.7197	153.24

Table 3 EUREF Network Station Coordinates

The coordinates for the stations from the Centipede-RTK Network are given below in table 4.

	Centipede-RTK Network Station	Latitude	Longitude	Altitude (m)
1	SOPH	43.6114	7.0541	178.85
2	BEFF	45.7666	4.8796	280.86
3	IUEM	48.3585	-4.5626	123.64
4	BIO	48.0228	7.5629	249.05
5	RDHB7	47.3345	1.4216	151.76

Table 4 Centipede Network Station Coordinates

As indicated by the coordinates, the corresponding stations from the EUREF and Centipede Networks are geographically close to each other.

The stations are carefully selected to compare the ZTD estimation of both the Network stations under variable geographic and atmospheric conditions of GNSS signal propagation. The first three stations belong to Eastern part of France while the last two are located in Central and Western part of France respectively. Located in the Alpes-Maritimes, the GRAS and SOPH stations provide an opportunity for observing tropospheric delays in a climate, influenced by both the Mediterranean Sea and alpine topography. The Bron and BEFF stations are situated near Lyon in the Auvergne-Rhône-Alpes region of France. It is a part of Alpine region of France having urban influence. The BRMG and BIO stations are located on the Eastern border of France shared with Germany, along the Rhine River. This landscape is typical of the Upper Rhine Plain, providing relatively stable conditions of the atmosphere.

The VFCH and RDHB7 stations belong to Villefranche-sur-Cher, in the Central region of France. This location has minimal urban influence and proximity to rivers, particularly useful in understanding the interaction between surface water bodies and the atmosphere. The BRST and IUEM stations are on the western Brittany coast of France, characterized by mild temperatures, high humidity, and significant precipitation throughout the year.

Hence, these stations encompass different geographical and atmospheric conditions. The assessment of Spatial variability of ZTD with low cost GNSS Networks is performed through the comparison of ZTD values for these stations.

Using the coordinates of all these stations, it is possible to mark their geographical location on the basemap as shown in the figure 10 below.

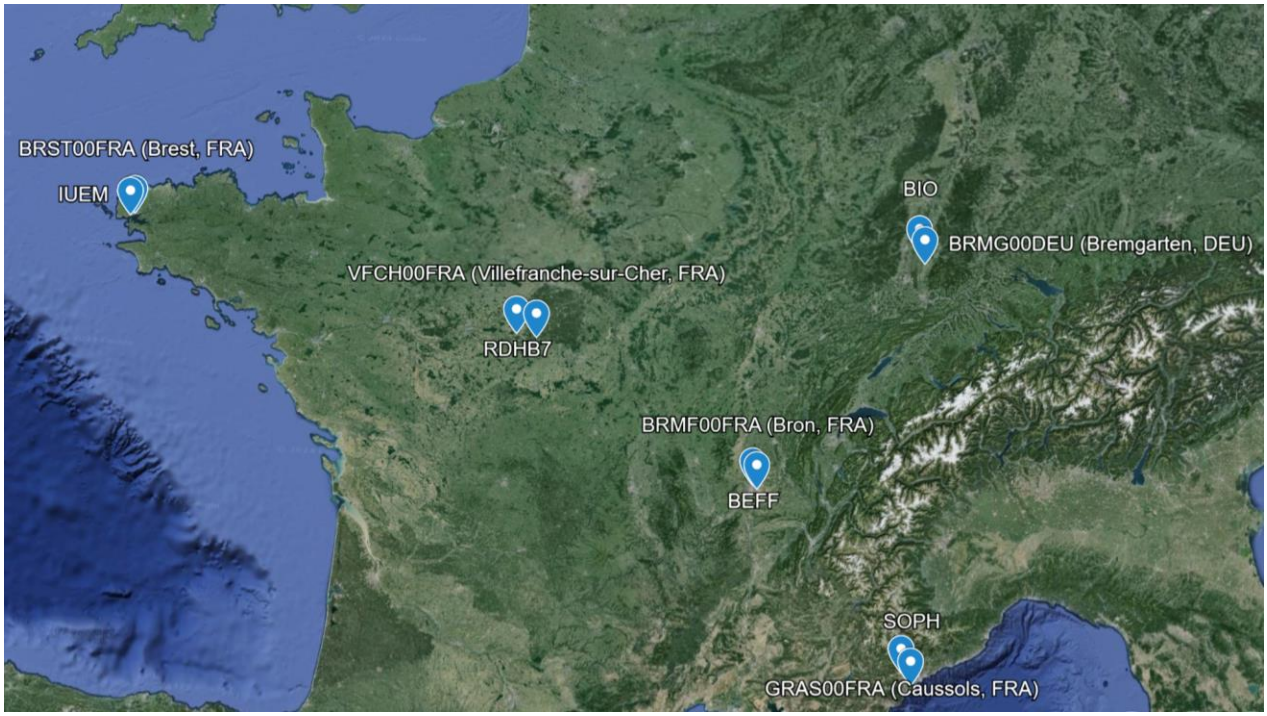

Figure 9 Map of the Observed Stations

For the analysis of temporal variability of zenith tropospheric delay estimates, GNSS data is streamed from both stations (Proximate EUREF and Centipede Stations) simultaneously for 24 hours. This ensures that the data is gathered across all phases of the day, including diurnal temperature variations and changes in atmospheric water vapor content. To accurately capture the trends of ZTD variability, data is sampled at high frequency, every 30 seconds. For each station, the data is acquired and processed for 5 different days in the winter season. This allows for the comparison of ZTD estimation and the temporal trends from the Centipede Network stations.

Data Acquisition

The GNSS data streaming and acquisition methodology is discussed in this section. NTRIP (Networked Transport of RTCM via Internet Protocol) is a protocol for streaming GNSS data over the internet. NTRIP is designed to broadcast all kinds of GNSS streaming data to stationary or mobile users over the Internet, allowing simultaneous PC, Laptop, or receiver connections to a broadcasting host.

NTRIP Casters act as the central hub in the NTRIP system, facilitating the distribution of correction data from NTRIP Servers to NTRIP Clients. For this study, to stream GNSS data from the EUREF Network, NTRIP client credentials were requested from the ASI Broadcaster. ASI (Italian Space Agency) has been operating as EUREF NTRIP Broadcaster since 2009.

For this research study, Data is streamed and stored through STRSVR (Stream Server) tool in RTKLIB software package. STRSVR is configured to receive data streams from GNSS receivers.

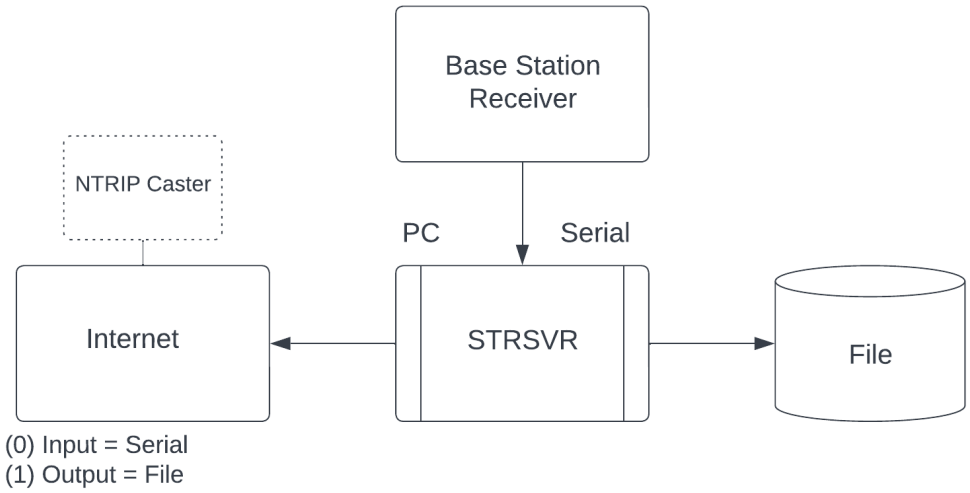

Figure 10 Data Streaming through NTRIP Client

The configuration in STRSVR involves setting up the NTRIP Caster address, Port, Station mountpoint and the user credentials obtained from the broadcaster. The following figure shows the NTRIP client configuration for streaming GNSS data from a EUREF Network station.

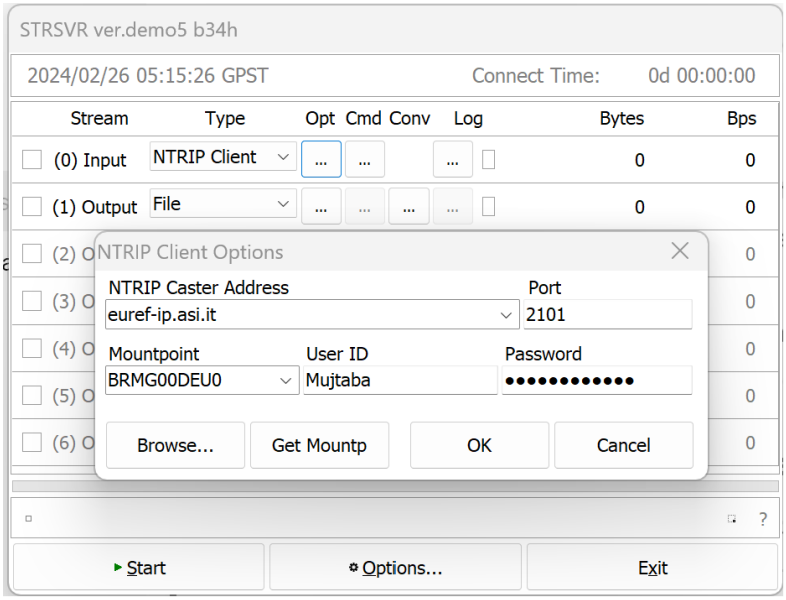

Figure 11 NTRIP Client Configuration for EUREF Network

For the connection to the Centipede-RTK Network, the caster address is configured along with the user credentials which are available on the network's web page. A sample configuration for the connection to a centipede network station is given below.

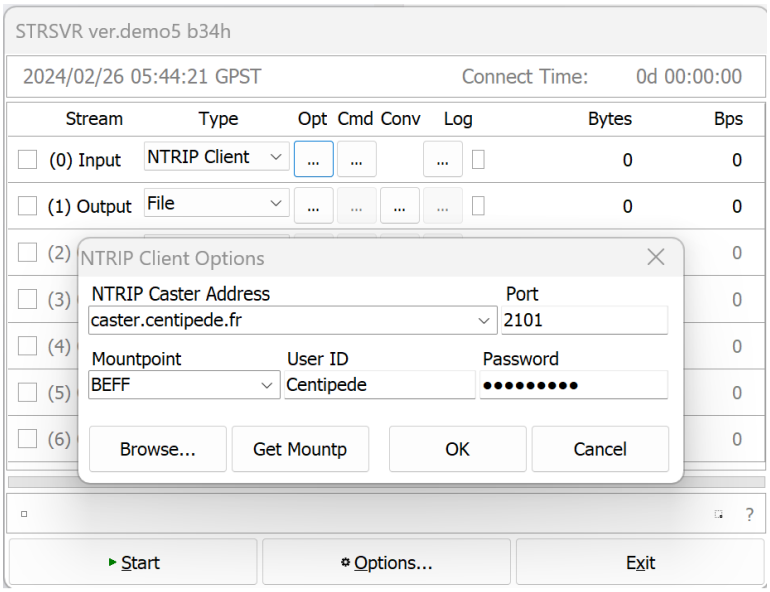

Figure 12 NTRIP Client configuration for Centipede Network

The file containing raw GNSS data is saved in RTCM format. RTCM (Radio Technical Commission for Maritime Services) is a standard format developed for the real-time transmission of GNSS correction data. RTCM3 file is obtained through stream server as output which consists of information necessary to correct GNSS signal errors, including ionospheric and tropospheric delays, satellite orbital errors, and clock corrections. RTCM3 utilizes a binary encoding scheme that reduces the size of correction messages compared to the previous versions of the same format, enabling efficient data transmission over limited bandwidth.

Data Conversion

The RTCM3 files contain different GNSS data and other information. Hence, they are to be converted to Receiver Independent Exchange Format (RINEX). RINEX format allows a standardized way for storing and sharing observation data and navigation messages across different receivers and post-processing softwares. To convert RTCM3 file into the universally compatible RINEX format, RTKLIB offers the conversion tool named “RTKCONV”. The Following figure shows the interface of RTKCONV, with interval time set at 30 seconds to ensure high sampling rate.

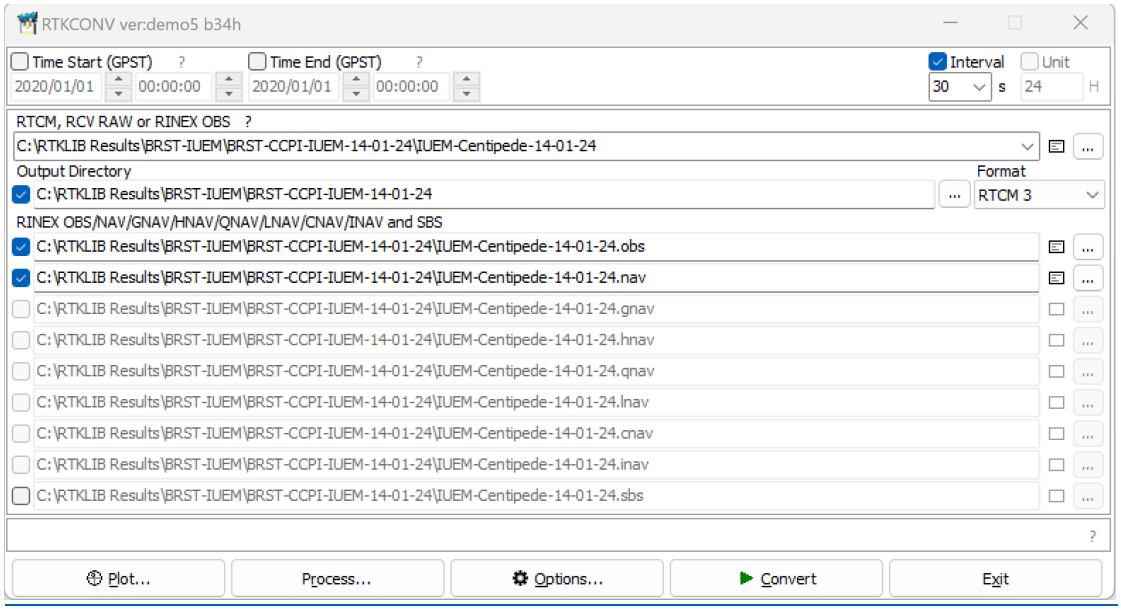

Figure 13 RTKCONV Interface

RTKCONV can convert raw GNSS data, including RTCM and BINEX formats. RTKCONV converts the RTCM file into two primary RINEX files which are explained below.

RINEX OBS (Observation Data) file contains the raw satellite observations recorded by the GNSS receiver, such as satellite positions, signal strength, and phase information. These RINEX OBS files are of interest for the estimation of Zenith Tropospheric Delay (ZTD).

RINEX Navigation data file includes the navigation messages broadcasted by GNSS satellites, containing information about satellite orbits, clock corrections, and other parameters necessary for computing precise positions.

Data Processing

The RINEX files must be post processed to obtain the zenith tropospheric delay estimates for the Centipede and EUREF Network for the comparison. To make the analyses of the low-cost centipede network independent of the processing method, two post processing options are chosen for this study. The first adopted method is post-processing through RTKLIB, and the second method is the online service Canadian Spatial Reference System (CSRS-PPP). Existing studies reveal the ZTD estimates from the online CSRS-PPP service show good agreement (<1 cm) with the International GNSS Service ZTD values [20]. The data processing methodology for RTKLIB and CSRS-PPP service is discussed below.

Post Processing in RTKLIB

The data processing is performed in RTKLIB using the RTKPOST tool. The Input data is provided in the RINEX format, which includes both the observation and navigation files. Following figure shows the interface of RTKPOST.

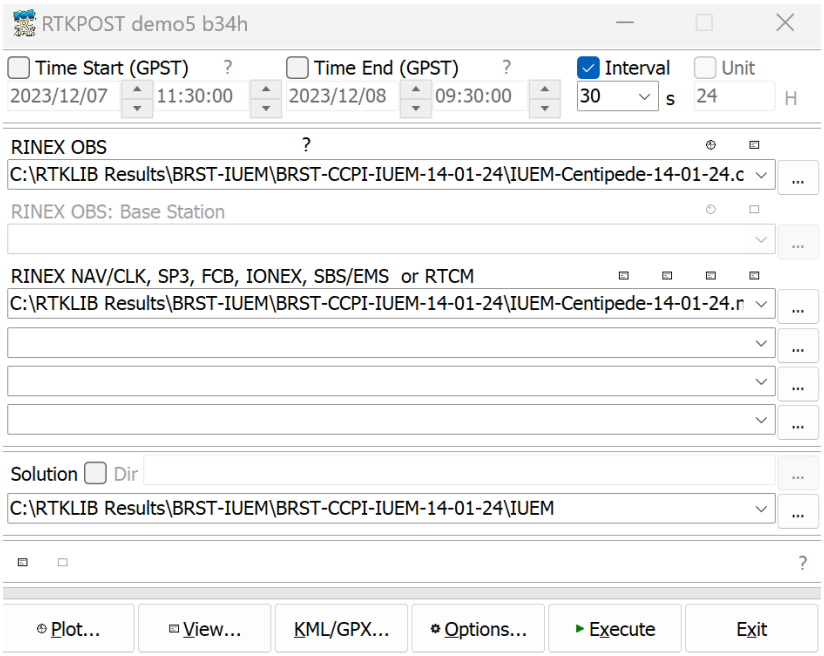

Figure 14 RTKPOST Interface

Aimed at extracting the ZTD for the GNSS Stations data, the configuration options are carefully set. Precise Point Positioning Static Mode is selected. The static nature of the receiver during data collection ensures consistency in atmospheric measurements, enabling analysis of temporal ZTD variability. The filter type is chosen to be Forward Filter which processes the data in a chronological sequence. It allows to understand how atmospheric conditions evolve over the course of the data collection period. Setting an Elevation Mask of 10 degrees helps mitigate the effects of multipath errors and atmospheric noise, which are more pronounced at lower elevation angles. This threshold ensures that only signals from satellites well above the horizon are considered, eliminating low elevation noise. For this study, Ionosphere-free Linear Combination (LC) is used as the tropospheric correction method. It is because the ionospheric delay effects can be significantly reduced, leading to more accurate tropospheric delay estimations. The following figure shows the configuration options for the processing of data in RTKPOST. The rest of the options are left to default settings.

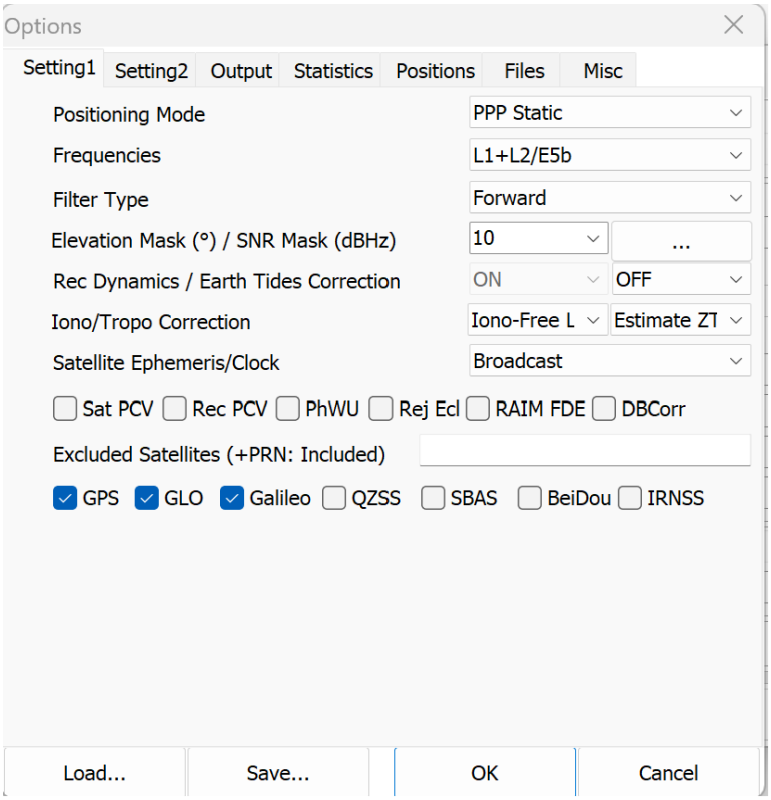

Figure 15 RTKPOST Configuration for ZTD Estimation

The output path is selected for the stat and position files along with other auxiliary files. The following figure shows a typical stat file processed in this research study.

File Edit View

```
$POS,2296,467820.000,6,4245557.3751,568959.1257,4710201.3981,7.2171,5.3496,8.5681
$VELACC,2296,467820.000,6,-0.0114,0.0038,0.0021,0.00000,-0.00000,0.00000,0.0000,0.0000,0.0000,0.00000,0.00000,0.000
00
$CLK,2296,467820.000,6,1,-0.000,73.249,22.078,-0.000,200.138,25.795,27.795,27.795
$TROP,2296,467820.000,6,1,2.2934,0.1200
$SAT,2296,467820.000,R05,1,160.2,29.8,-2.1382,-0.0147,1,53,0,1,1,0,1,0,0.00,0.000000,0.00000
$SAT,2296,467820.000,R06,1,274.9,73.7,-5.8210,0.0000,0,43,0,1,0,1,1,0,0.00,0.000000,0.00000
$SAT,2296,467820.000,R07,1,324.7,27.2,0.0746,0.0005,1,51,0,1,1,0,1,0,0.00,0.000000,0.00000
$SAT,2296,467820.000,R09,1,237.0,24.4,2.9242,0.0202,1,52,0,1,1,0,1,0,0.00,0.000000,0.00000
$SAT,2296,467820.000,R15,1,43.1,38.4,0.1871,0.0013,1,55,0,1,1,0,1,0,17.13,78.467883,0.00000
$SAT,2296,467820.000,R16,1,282.8,78.4,-0.3290,-0.0023,1,55,0,1,1,0,1,0,0.00,0.000000,0.00000
$SAT,2296,467820.000,E03,1,303.6,45.5,-0.7413,-0.0020,1,51,0,1,1,0,1,0,11.88,3600.000000,0.00000
$SAT,2296,467820.000,E05,1,160.3,76.7,-0.0996,-0.0003,1,52,0,1,1,0,1,0,0.00,0.000000,0.00000
$SAT,2296,467820.000,E09,1,134.4,23.0,-0.2446,-0.0007,1,49,0,1,1,0,1,0,-18.37,32.467926,0.00000
$SAT,2296,467820.000,E24,1,97.9,71.8,0.7565,0.0020,1,52,0,1,1,0,1,0,0.00,0.000000,0.00000
$SAT,2296,467820.000,E31,1,48.4,26.7,0.0260,0.0001,1,49,0,1,1,0,1,0,7.60,3600.000000,0.00000
$POS,2296,467850.000,6,4245557.2462,568958.9147,4710201.2881,5.1511,3.8115,6.1259
$VELACC,2296,467850.000,6,-0.0114,0.0038,0.0021,0.00000,-0.00000,0.00000,0.0000,0.0000,0.0000,0.00000,0.00000,0.000
00
$CLK,2296,467850.000,6,1,0.000,73.022,21.898,0.000,200.138,19.029,20.092,20.092
$TROP,2296,467850.000,6,1,2.2934,0.1200
$SAT,2296,467850.000,R05,1,160.3,29.5,-1.4566,-0.0089,1,53,0,0,2,0,1,0,0.00,0.000000,0.00000
$SAT,2296,467850.000,R06,1,273.9,73.8,-49.8274,-49.8274,0,43,0,0,0,2,1,2,0.00,0.000000,0.00000
$SAT,2296,467850.000,R07,1,324.6,27.4,-0.2850,-0.0091,1,51,0,0,2,0,1,0,0.00,0.000000,0.00000
$SAT,2296,467850.000,R09,1,237.2,24.6,1.8207,0.0344,1,52,0,0,2,0,1,0,0.00,0.000000,0.00000
$SAT,2296,467850.000,R15,1,43.2,38.2,0.4116,-0.0171,1,55,0,0,2,0,1,0,17.31,39.875084,0.00000
$SAT,2296,467850.000,R16,1,284.2,78.5,-0.1740,-0.0148,1,54,0,0,2,0,1,0,0.00,0.000000,0.00000
$SAT,2296,467850.000,E03,1,303.5,45.7,-0.6141,-0.0190,1,51,0,0,2,0,1,0,11.88,3600.000000,0.00000
$SAT,2296,467850.000,E05,1,160.2,76.5,0.4099,-0.0199,1,52,0,0,2,0,1,0,0.00,0.000000,0.00000
$SAT,2296,467850.000,E09,1,134.5,22.8,-0.0409,-0.0253,1,49,0,0,2,0,1,0,-18.30,16.368312,0.00000
$SAT,2296,467850.000,E24,1,97.3,71.7,0.2083,-0.0175,1,52,0,0,2,0,1,0,0.00,0.000000,0.00000
$SAT,2296,467850.000,E31,1,48.4,26.6,0.2668,-0.0206,1,49,0,0,2,0,1,0,7.60,3600.000000,0.00000
$POS,2296,467880.000,6,4245557.0217,568959.0044,4710201.1134,4.2214,3.1213,5.0197
$VELACC,2296,467880.000,6,-0.0114,0.0038,0.0021,0.00000,-0.00000,0.00000,0.0000,0.0000,0.0000,0.00000,0.00000,0.000
00
```

Figure 16 Stat file obtained from RTKPOST.

The stat file is of particular interest here for the extraction of ZTD values. The stat file contains variety of data such as positioning solution, velocity, and the satellite clock error information. $TROP line in this file contains tropospheric delay data and its estimated error. The Tropospheric delay estimates are to be filtered from the stat file which is discussed later in this chapter.

Post Processing in CSRS-PPP

The Canadian Spatial Reference System Online Precise Point Positioning service supports the RINEX file to be uploaded online. It is possible to access the CSRS-PPP service through its web interface by obtaining the user credentials. The RINEX OBS files obtained through RTKCONV are uploaded to CSRS for both the GNSS networks. The positioning mode is chosen to be static. The CSRS service does not allow the flexibility of altering the configuration options as in RTKLIB. The default sampling rate for ZTD estimation set by CSRS is 30 seconds which is in agreement with the RTKLIB processing conducted in this study. The cut-off angle used is 7.5 degrees which cannot be changed. The output files from CSRS-PPP are received through email as zip file. The zip file consists of different files: CLK, POS, SUM, TRO, and a PDF report. The TRO file contains the tropospheric delay estimations over the data acquisition period. The pdf report contains a comprehensive overview of the processing results including station coordinates and metadata, Observation start and end times, graphics of ZTD, station clock offsets, Ambiguities, and residuals. The Tropospheric data file (TRO) is of importance to this study. It is imported into QGIS software for obtaining the ZTD data in excel file.

Data Filtering

This section describes the methodology for importing GNSS data files: stat files (from RTKLIB Processing) and TRO files (from CSRS-PPP Processing) into QGIS, applying filters specifically to tropospheric delay information, and exporting the refined dataset for further analyses.

Data filtering in QGIS

QGIS software version 3.30.3 is used in this research study. The stat file is imported as delimited text layer. Filtering is applied through query builder function of QGIS as shown in the figure below.

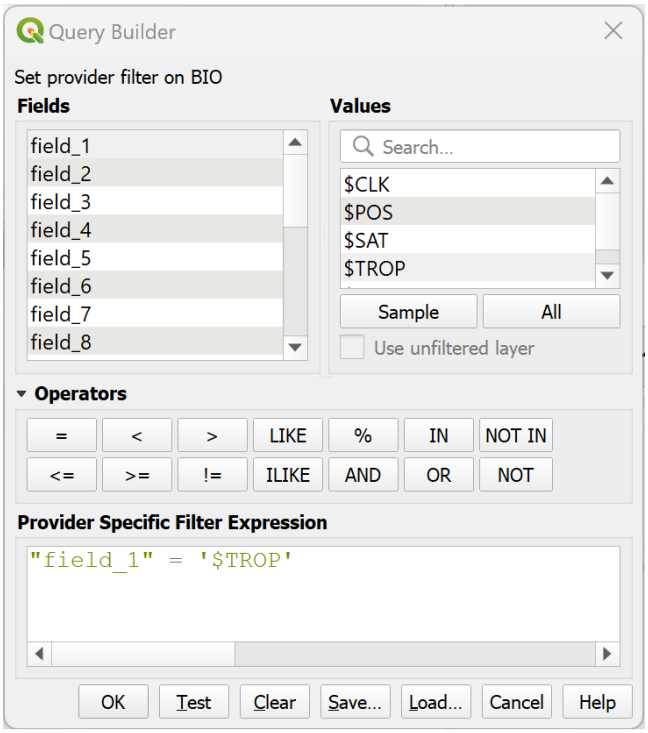

Figure 17 Data filtering in QGIS.

After applying the filer, the resulting layer is exported as excel file, containing the ZTD estimates and standard deviation values for the corresponding time epochs.

The TRO file obtained through CSRS-PPP online service, is imported into QGIS as a delimited text layer and exported as excel file. This allows the consistent representation of ZTD values against time epochs in the form of columns in the excel files.

In this way, Zenith tropospheric delay estimates are obtained for a duration of 24 hours at 30 seconds sampling rate. This methodology is adopted to obtain ZTD estimates from the EUREF Permanent GNSS network stations and the low-cost Centipede-RTK network stations.

Data Analysis

This section outlines the methodology adopted to compare Zenith Total Delay (ZTD) estimates processed from the GNSS networks: EUREF (European Permanent Network) and Centipede, utilizing both the RTKLIB and the Canadian Spatial Reference System Precise Point Positioning (CSRS-PPP) service. The objective is to assess the spatial and temporal variability and accuracy of ZTD estimates. This comprehensive analysis involves a multi-step approach, including data processing, alignment of epochs, and statistical evaluation to understand the spatial and temporal variability of ZTD results.

Tropospheric Delay Timeseries

The ZTD estimates are plotted against time (24 hours) to obtain the ZTD timeseries. Each timeseries plot incorporates ZTD data from the two GNSS network stations, processed through both software solutions, alongside the EUREF tropospheric product (provided for hourly interval). By observing the temporal trends of ZTD variability provided by the two networks, a

comparison can be established. Such a comparative visualization aids in identifying differences, and patterns in ZTD variability for the Centipede network.

Statistical and Quality Indicators

To quantitatively assess the spatial and temporal variability of ZTD estimates for the Centipede Network, statistical indicators such as mean and maximum of differences of ZTD values, and root mean square error are calculated. RMSE values are calculated with the EUREF tropospheric product. These indicators provide insights into the consistency, accuracy, and reliability of ZTD estimates for the Centipede GNSS network.

Due to the higher cut-off angle (10 degrees) and processing algorithm of the RTKLIB, it results in the rejection of some epochs and the corresponding ZTD values. CSRS has a default cut-off angle set at 7.5 degrees and the processed results do not undergo rejection of epochs. Hence, to compare the ZTD values for the Centipede and EUREF stations and the EUREF tropospheric product, the datasets must be aligned for the common epochs.

A Python code within a Jupyter Notebook environment is used to synchronize the datasets. It is then possible to calculate the Mean of Differences and Maximum of Differences between:

- EUREF and Centipede station's ZTD estimates processed with RTKLIB.
- EUREF and Centipede station's ZTD estimates processed with CSRS-PPP.
- The cross software ZTD comparison for the two stations.

The Root mean square error (RMSE) is calculated with respect to the EUREF Tropospheric product. This allows a standardized way to access the accuracy of ZTD estimation from the Centipede low-cost networks. These RMSE values are compared to that obtained for the EUREF Network processed ZTD. Lower RMSE values indicate higher accuracy while higher RMSE values suggest greater discrepancies.

Chapter 4- Results and Discussion

In order to assess the spatial and temporal variability of ZTD estimates for the low-cost Centipede Network, observation data from the 5 Centipede Network stations and their nearest stations from the EUREF Network is processed to obtain the tropospheric delay estimates and compared in this chapter. The data processing is performed using RTKLIB and CSRS-PPP to make the analyses independent of the processing method. The processing yields the ZTD estimates against time epochs which are plotted as ZTD Timeseries. The first section of this chapter presents a discussion on the ZTD timeseries. Through statistical measures, it is possible to assess the temporal and spatial variability of ZTD estimates. In this study, mean and maximum of differences of ZTD for the Centipede Network are presented against the ZTD provided by the EUREF Network data. To assess the spatial variability of the ZTD obtained from the Centipede network, the statistical indicators are compared for the five different geographical locations across France. Finally, to assess the quality of the ZTD estimates provided by the Centipede Network, Root mean square error is used as the quality indicator. The RMSE values for the Centipede and EUREF Network data are presented and discussed in detail. The last section of this chapter includes the discussion about the assessment of temporal and spatial variability, and quality of ZTD estimates from the Centipede Network.

Tropospheric Delay Timeseries

The 24-hour ZTD timeseries are plots of tropospheric delay estimates from the GNSS stations processed by the two software packages. The plots for each station for the observed days are attached in the Annex section of this document.

First, the plots for the three observation locations in Eastern France are compared. Starting with the geographical region having lowest latitudinal coordinate, the stations are in the region of Alpes-Maritimes. The GRAS(EUREF) and SOPH(Centipede) stations are in Caussols, France, and their ZTD plots are attached in the Annex A for the five different observed days. The actual ZTD provided by the EUREF network remains stable throughout the 24 hours and does not exhibit much temporal variability. The ZTD values are in between 2.0m and 2.1m. The processed ZTD estimates from both stations by CSRS-PPP show similar ZTD variability over time. With the trend being similar, the GRAS station seems to provide accurate ZTD values while the SOPH station provides ZTD values in between 2.3m and 2.4m. The ZTD values for the two stations processed through RTKLIB also show similar trend over time. The quality of these datasets is determined through RMSE later in this study.

The second observed location is near Lyon in the Auvergne-Rhône-Alpes region of France. The BRON(EUREF) and BEFF(Centipede) stations are also located in Eastern part of France but at relatively higher latitude than the previously discussed GRAS and SOPH station. CSRS-PPP is found to model the ZTD values accurately for both the BRON and BEFF stations for all the days observed. The delay values obtained from CSRS are about 2.3-2.4m. If processed through RTKLIB, ZTD estimates from the BEFF station show similar trends over time as of BRON station.

The exceptions are the observed Day4 and Day14 in January 2024 with relatively high ZTD values from the BEFF station. The graphs are attached in the Annex B.

The third location observed in the Eastern France is located on the Eastern border of France shared with Germany, along the Rhine River. The BRMG(EUREF) and BIO(Centipede) stations are at higher latitude than the previous two locations analysed. CSRS processed values for both stations show accurate temporal variability between 2.3m and 2.4m. RTKLIB processed estimates from both the stations also show comparable trend with each other. The temporal variability of these estimates is better analysed through statistical measures later in this study rather than the visual comparison. The related graphs are attached in Annex C.

To check the temporal variability of tropospheric delays in the central part of France, the VFCH(EUREF) and RDHB7(Centipede) stations provided delays are analysed. The ZTD values exhibit a higher range of variability (between 2.3m and 2.5m) than the previously seen results. The data processed by CSRS for the stations provide ZTD values close to those provided by the EUREF Network consistently over time. If processed by RTKLIB, the ZTD estimates from the VFCH station show similar trends over time as of RDHB7 station.

The performance of low-cost stations in the Western part of France is checked by observing the stations located on the western Brittany coast of France. The ZTD values at this location also show a higher range of variability (between 2.3m and 2.5m). The stations BRST(EUREF) and IUEM(Centipede) provide accurate ZTD values over time, processed by CSRS. RTKLIB processed values for both stations exhibit comparable trends but higher variability with respect to the EUREF provided ZTD values. The graphs are attached in the Annex E. The variability of ZTD estimates is analysed through the use of statistical indicators in the next section.

Statistical Comparison of Delay Estimates

The following discussion in this section compares the mean & maximum of Differences of ZTD estimates along with Root mean square values (RMSE) of for five different days. Through graphical representation, the consistency of the ZTD estimates is checked through Mean of differences. The comparison of Maximum of differences allows to determine the reliability of ZTD estimates against the rapidly changing atmospheric conditions. Finally, to check the ZTD estimates accuracy, Root mean square error values are presented in the form of graphs. These RMSE values are calculated by benchmarking the hourly ZTD estimates provided by the EUREF permanent GNSS network as a Processed Product. This comprehensive comparison allows to the check the temporal and spatial variability of ZTD estimates obtained by processing low-cost Centipede stations data against the EUREF GNSS Network station data.

Eastern France

The three observed locations in the Eastern part of France are discussed below. The following figures 18 and 19 present the Mean and Maximum of ZTD differences respectively for the GRAS and SOPH stations situated at lower latitudinal region.

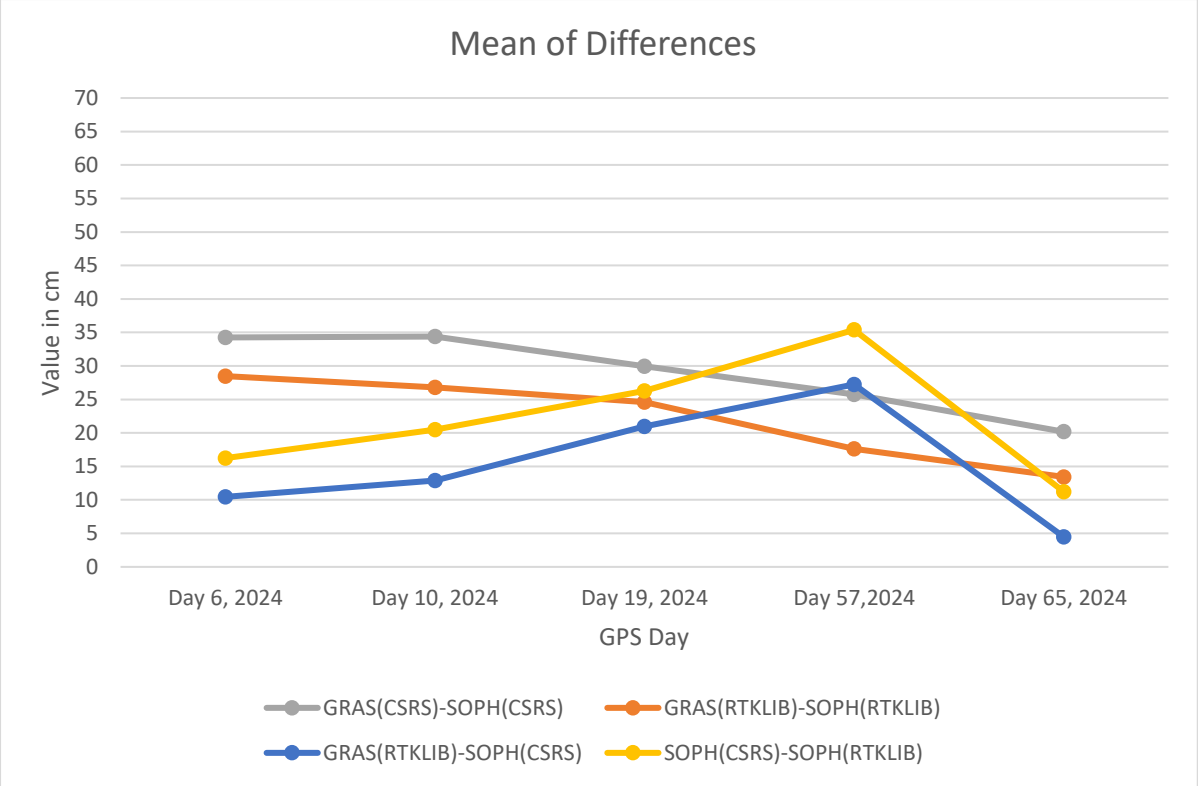

Figure 18 Mean of Differences of ZTD for GRAS-SOPH Stations

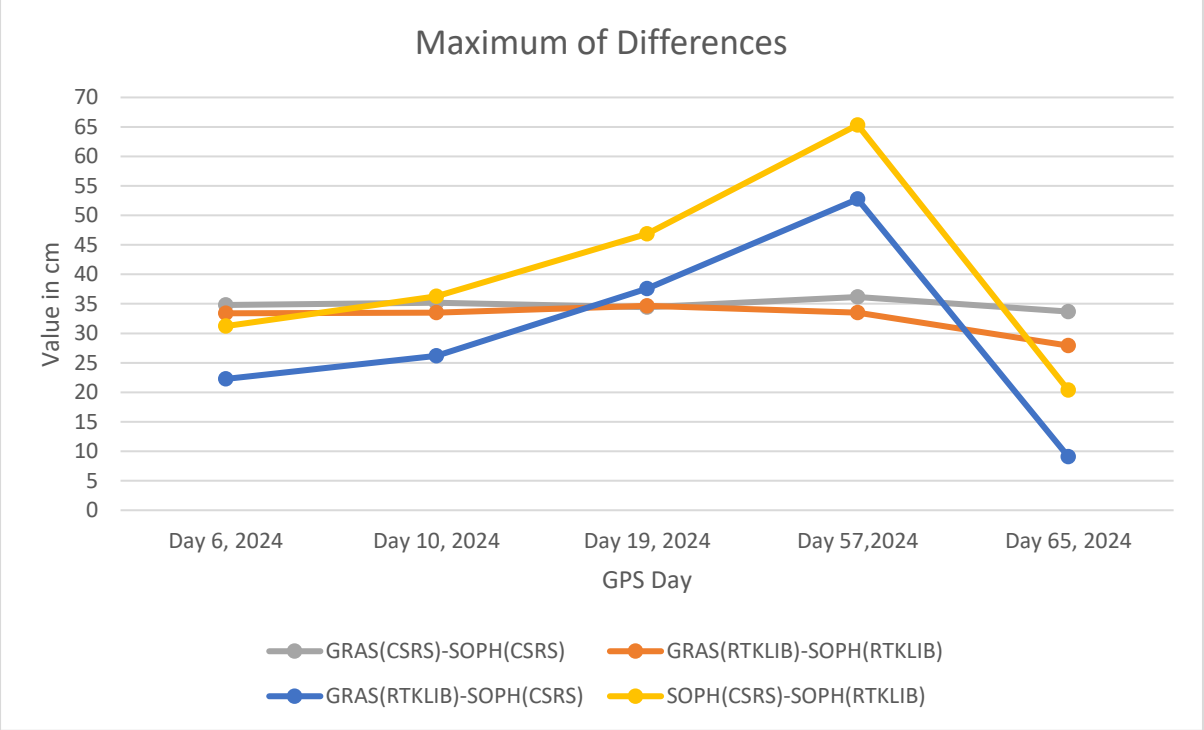

Figure 19 Maximum of Differences of ZTD for GRAS-SOPH Stations

- The ZTD estimates from the two stations (GRAS and SOPH) processed by RTKLIB show closest agreement to each other among the datasets analysed. These values are relatively higher as compared to other locations with mean and maximum of differences of ZTD less

than 40cm. It shows that the ZTD values provided by the VFCH and RDHB7 stations exhibit similar trends in terms of temporal variability.

- The Maximum of ZTD differences for the two stations processed by RTKLIB and CSRS-PPP show similar values for all the days observed. The values are less than 40cm, which indicate rapid fluctuations in ZTD values due to changing atmospheric conditions.
- Variability of ZTD estimates is also checked when GRAS station data is processed by RTKLIB and the SOPH station data is processed by CSRS and vice versa. This comparison yields lower values of mean and maximum of ZTD differences for GRAS(RTKLIB)-SOPH(CSRS), with Day57,2024 as an exception.

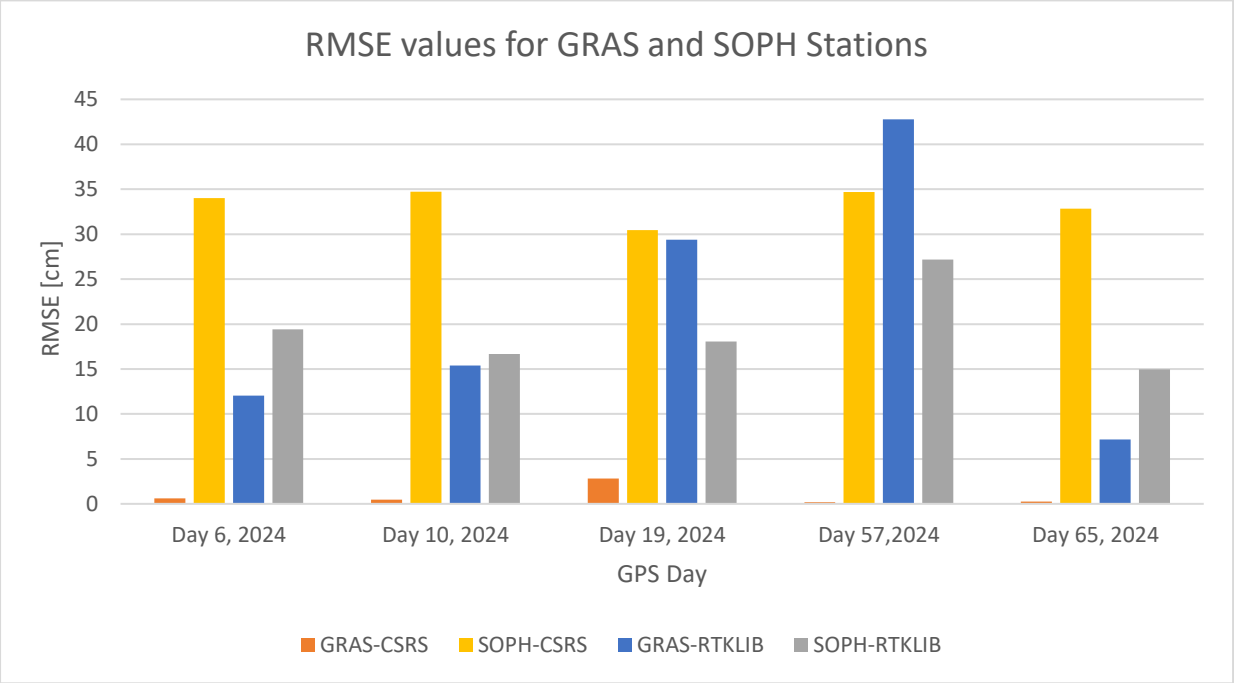

Figure 20 Mean RMSE values for GRAS-SOPH Stations

- The ZTD estimates from the GRAS station processed by CSRS-PPP show very low RMSE values (less than 3cm) for all the days observed. The ZTD estimates of BEFF station processed by CSRS-PPP show high RMSE values, around35cm, for all the days observed.
- If the RMSE values are compared for the estimates processed through RTKLIB, GRAS station has lower RMSE values for Day6, Day10 and Day65, 2024. On Day19 and Day57,2024 the RMSE values for the SOPH station are lower than that of GRAS.

The statistical measures calculated for the BRON and BEFF stations are presented in figures below.

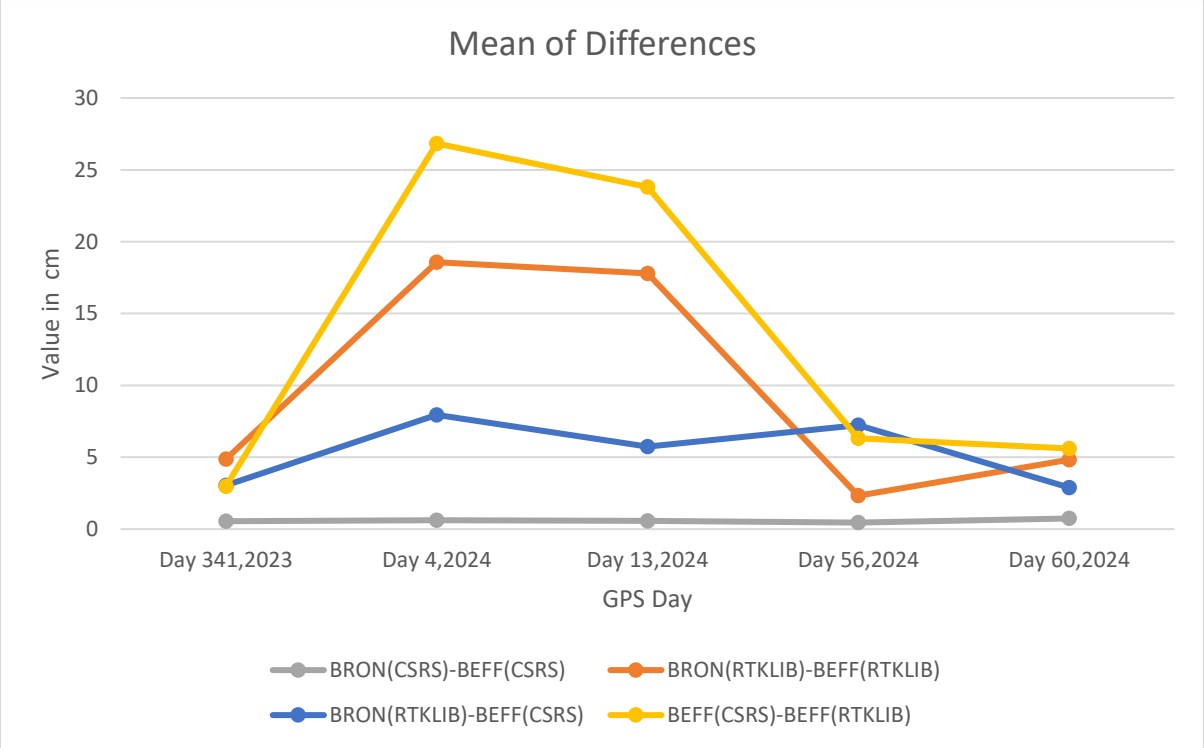

Figure 21 Mean of Differences of ZTD for BRON-BEFF Stations

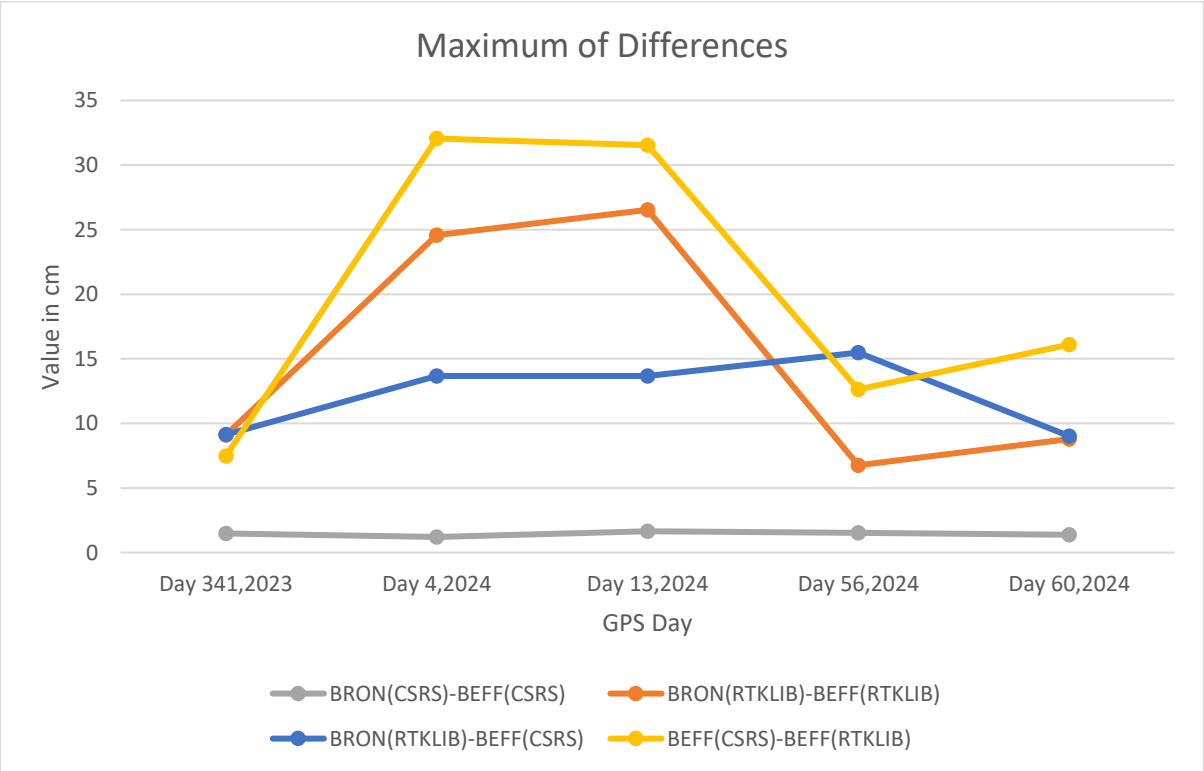

Figure 22 Maximum of Differences of ZTD for BRON-BEFF Stations

- The ZTD estimates from the BRON and BEFF stations processed by CSRS-PPP show closest agreement to each other with mean of ZTD differences less than 1cm and maximum of ZTD differences less than 2cm. It shows that the ZTD values provided by the BRON and BEFF stations exhibit similar trends in terms of temporal variability.
- If we analyse the Mean and Maximum of ZTD differences, processed by RTKLIB, the datasets of ZTD from both he stations exhibit similar trend except for January (Day4 and Day13).
- Variability of ZTD estimates is also checked when BRON station data is processed by RTKLIB and the BEFF station data is processed by CSRS and vice versa. The values observed in this case are less than 10cm for mean of differences and maximum of differences being 15cm or less. Again, the exception here is Day4,2023 and Day13,2024.

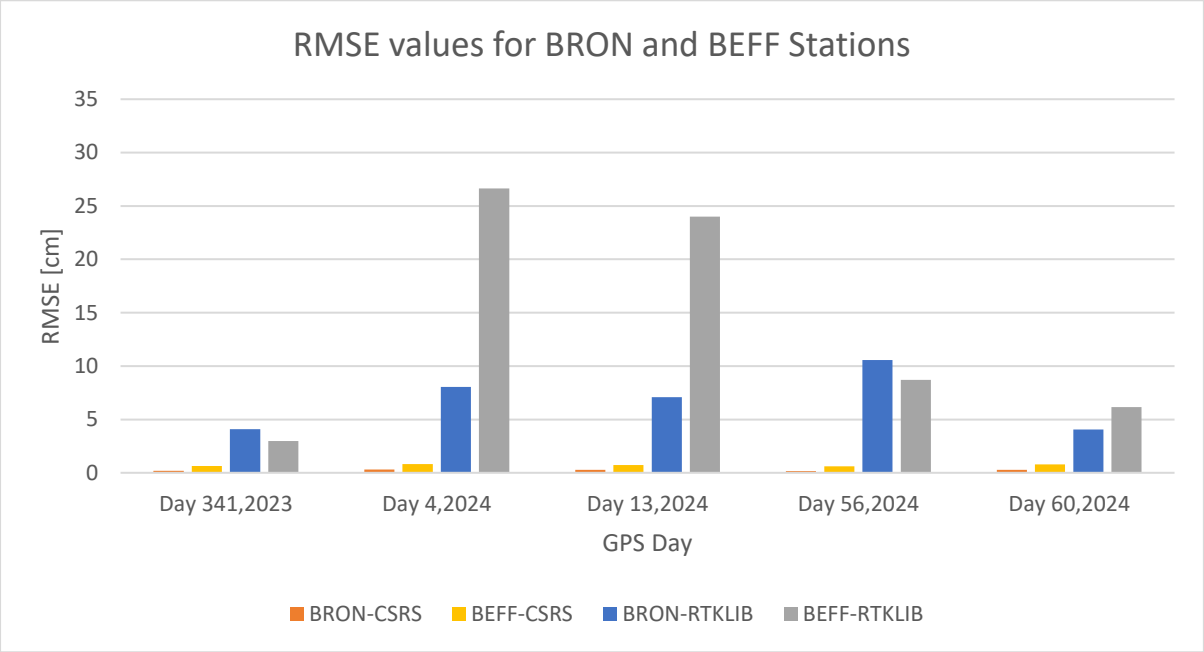

Figure 23 Mean RMSE values for BRON-BEFF Stations ZTD

- The ZTD estimates from BRON and BEFF stations processed by CSRS-PPP show very close agreement to the EUREF provided ZTD. It is evident that the ZTD estimates provided by the two stations are highly accurate (RMSE less than 1cm), if processed by CSRS-PPP.
- If we compare the RMSE values for the ZTD obtained by the BRON and BEFF stations, processed through RTKLIB, BRON station has lower RMSE values for Day4-2024, Day13-2024, and Day60-2024. The mean RMSE value for BEFF station is lower on Day341-2023 and Day56,2024.

The Mean and Maximum of ZTD differences for the BRMG and BIO stations processed by RTKLIB and CSRS are shown in figure 24 and 25 below.

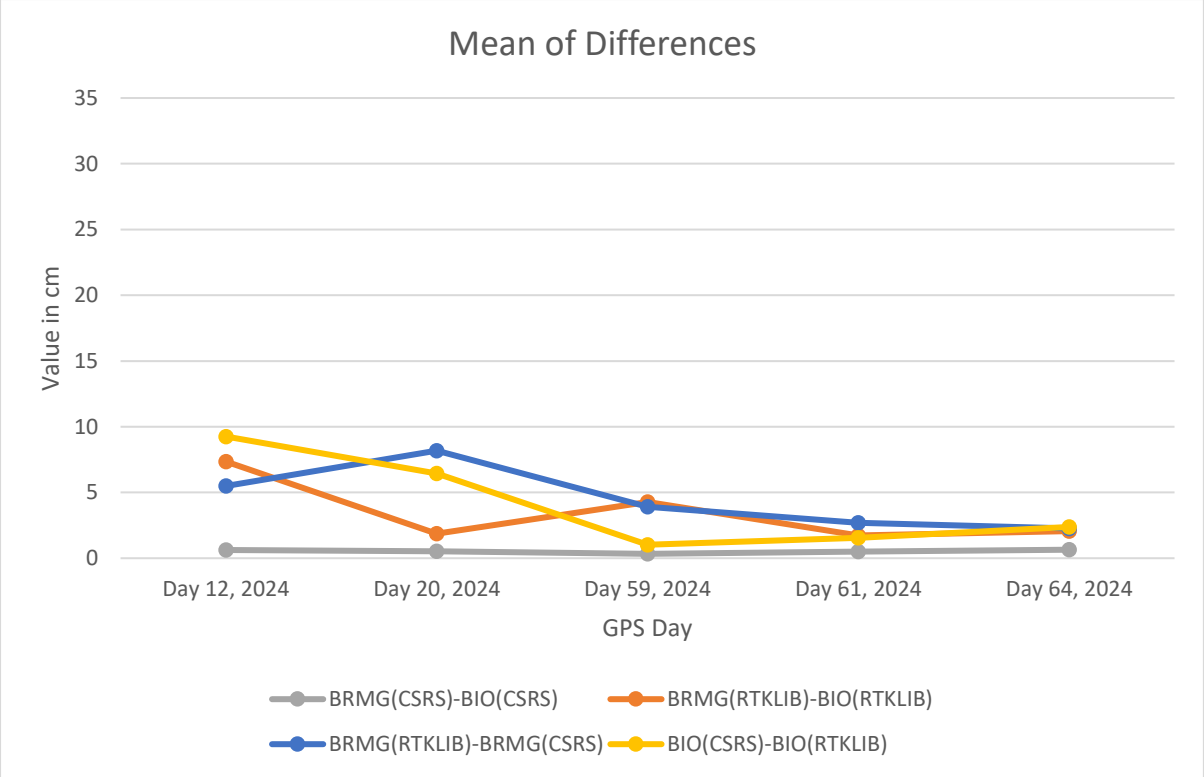

Figure 24 Mean of Differences of ZTD for BRMG-BIO Stations

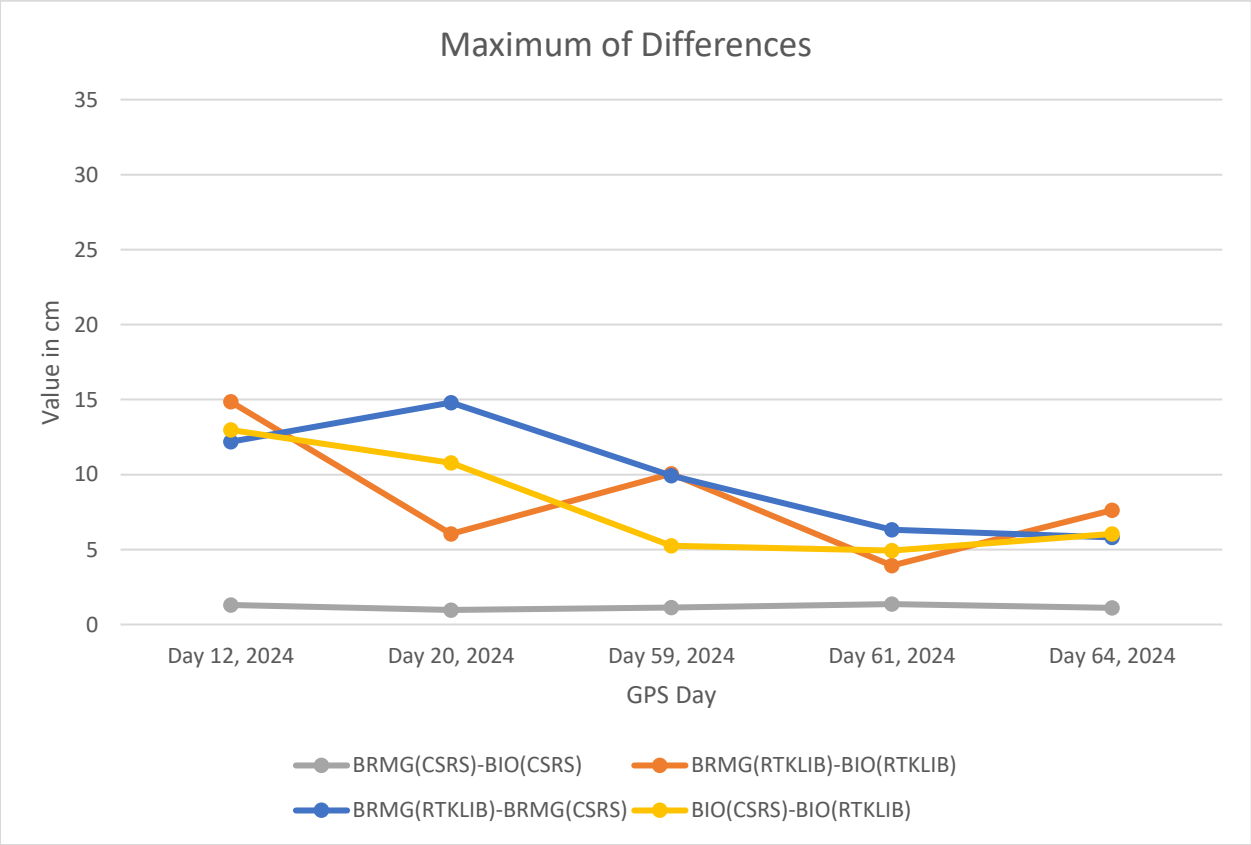

Figure 25 Maximum of Differences of ZTD for BRMG-BIO Stations

- The ZTD estimates from the two stations (BRMG and BIO) processed by CSRS-PPP show consistent estimation of ZTD with mean of differences less than 1cm and maximum of differences of ZTD less than 2cm. It shows that the ZTD values provided by the BRMG and BIO stations exhibit similar trends in terms of temporal variability.
- The ZTD estimates for the two stations processed by RTKLIB, are less consistent with each other as compared to CSRS processed estimates. The Mean of differences observed in this case is less than 10cm and maximum of differences being less than 15cm.
- Variability of ZTD estimates is also checked when BRMG station data is processed by RTKLIB, and the BIO station data is processed by CSRS and vice versa. This comparison yields values less than 15 cm for mean and maximum of ZTD differences.

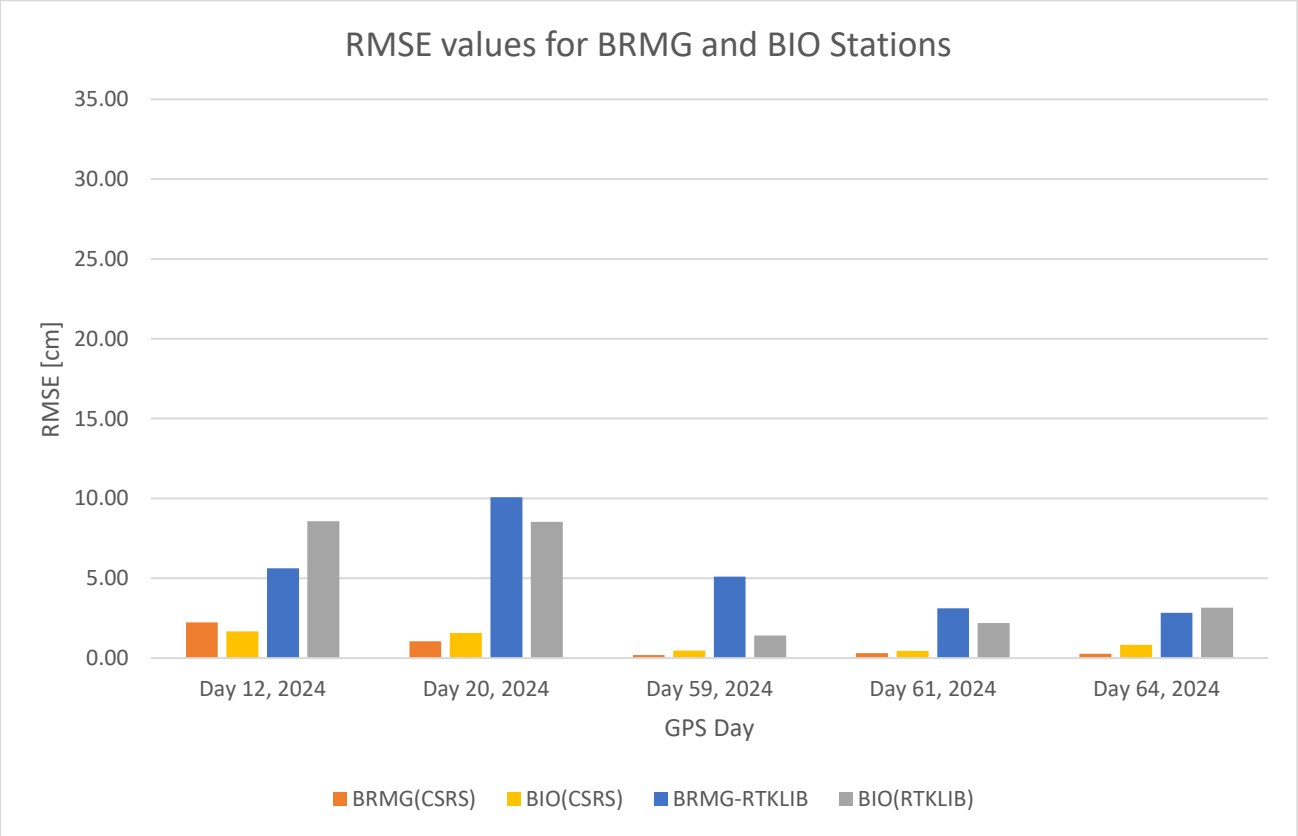

Figure 26Mean RMSE values for BRMG-BIO Stations

- The ZTD estimates from the BRMG and BIO stations processed by CSRS-PPP indicate comparable accuracy for all the days observed. The ZTD estimates provided by the BRMG station has RMSE value less than 3cm while the BIO station has RMSE value less than 2cm.
- Processed through RTKLIB, the BIO station ZTD has lower RMSE values than that of BRMG station with the only exception on Day12 2024.

Central France

To check the temporal variability of tropospheric delays in the central part of France, the analysis on the mean and maximum of differences along with the RMSE values are presented in the figures below.

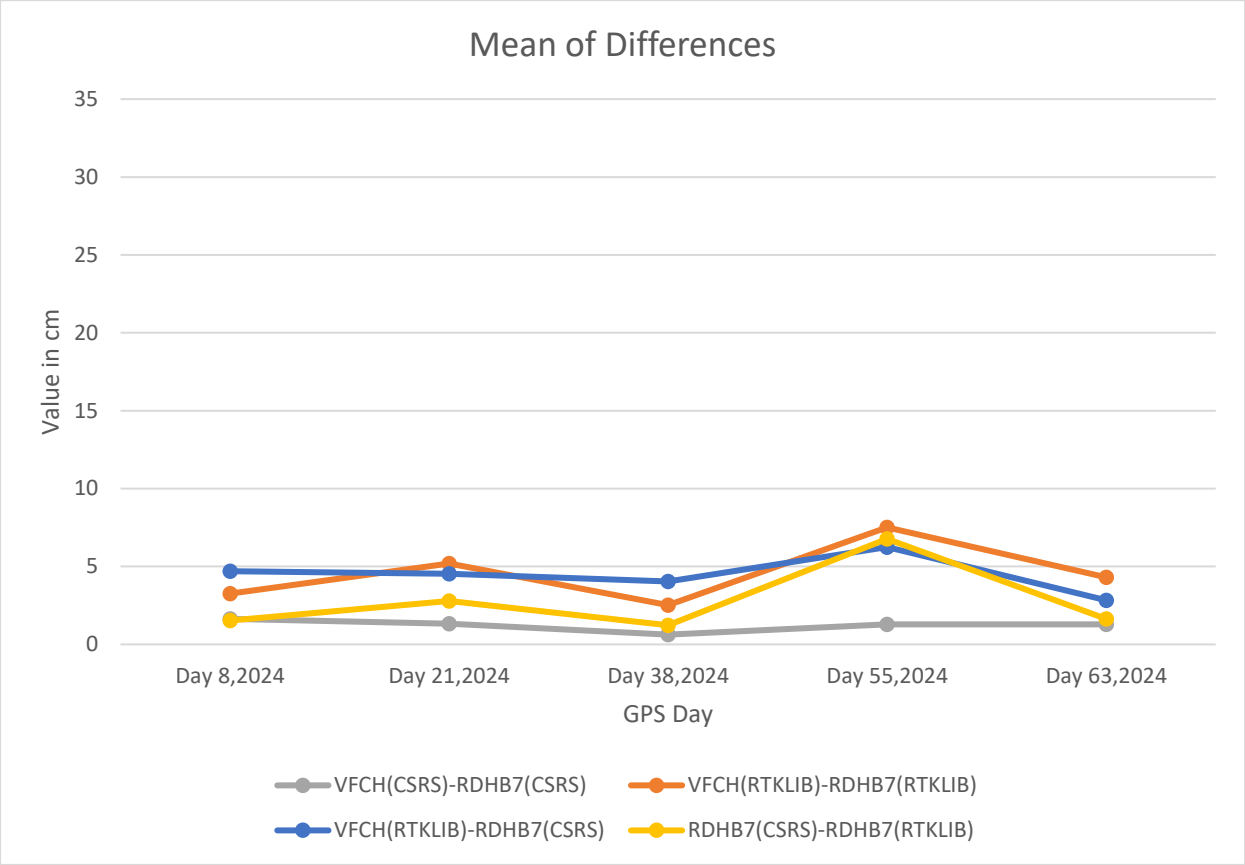

Figure 27 Mean of Differences of ZTD for VFCH-RDHB7 Stations

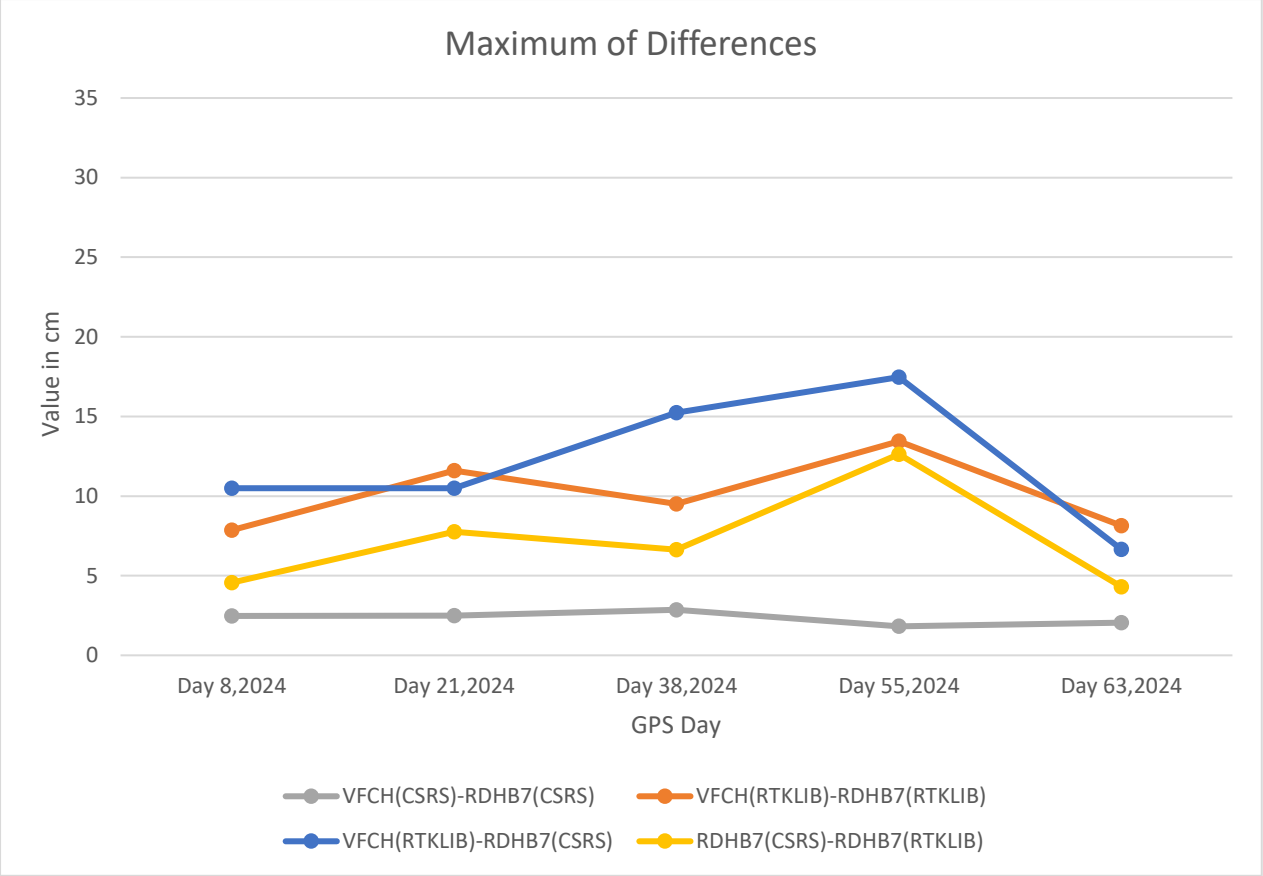

Figure 28 Maximum of Differences of ZTD for VFCH-RDHB7 Stations

- The ZTD estimates from the two stations (VFCH and RDHB7) processed by CSRS-PPP show closest agreement to each other with mean and maximum of differences of ZTD less than 3cm. It shows that the ZTD values provided by the VFCH and RDHB7 stations exhibit similar trends in terms of temporal variability.
- Mean and Maximum of ZTD differences for the two stations processed by RTKLIB show reasonable agreement with each other. The Mean of differences observed in this case is less than 10cm and maximum of differences being less than 15cm.
- Variability of ZTD estimates is also checked when VFCH station data is processed by RTKLIB and the RDHB7 station data is processed by CSRS and vice versa. This comparison yields Low values of mean and maximum of ZTD differences, suggesting similar trend of ZTD values for all the five days. For Day55,2024, there are relatively high values of mean and maximum.

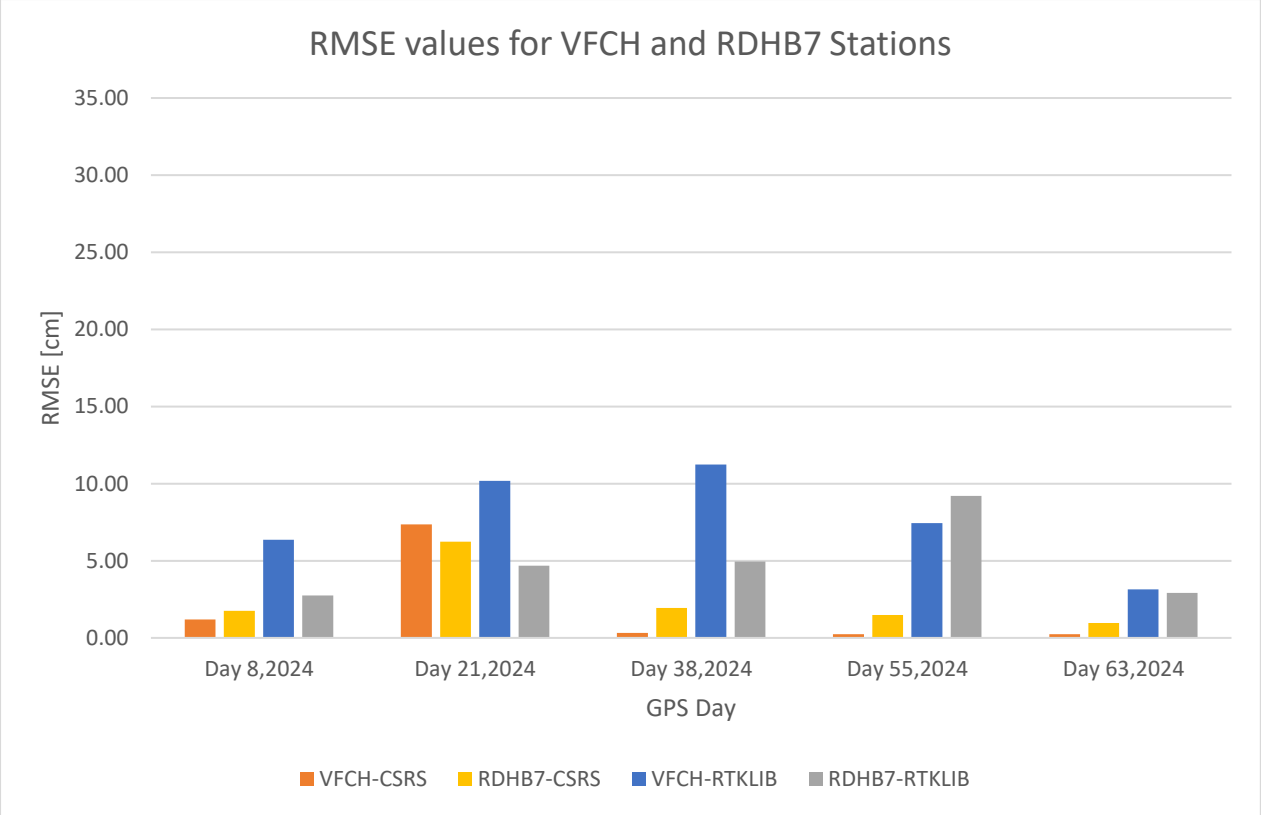

Figure 29 Mean RMSE values for VFCH-RDHB7 Stations

- The ZTD estimates from the VFCH and RDHB7 stations processed by CSRS-PPP show comparable accuracy for all the days observed. The ZTD estimates provided by the two stations have very low RMSE values (less than 2cm). For Day21, 2024, RMSE value for the RDHB7 station ZTD is lower than that of VFCH station data.
- If we compare the RMSE values for the ZTD obtained by VFCH and RDHB7 stations, processed through RTKLIB, RDHB7 provides better accuracy with respect to EUREF provided ZTD values on 4 occasions. On Day55, 2024 the mean RMSE value for the VFCH station is lower but comparable to that of RDHB7.

Western France

To assess the ZTD estimates from low-cost networks in western France, the quality indicators for the BRST and IUEM processed data are presented in the following figures.

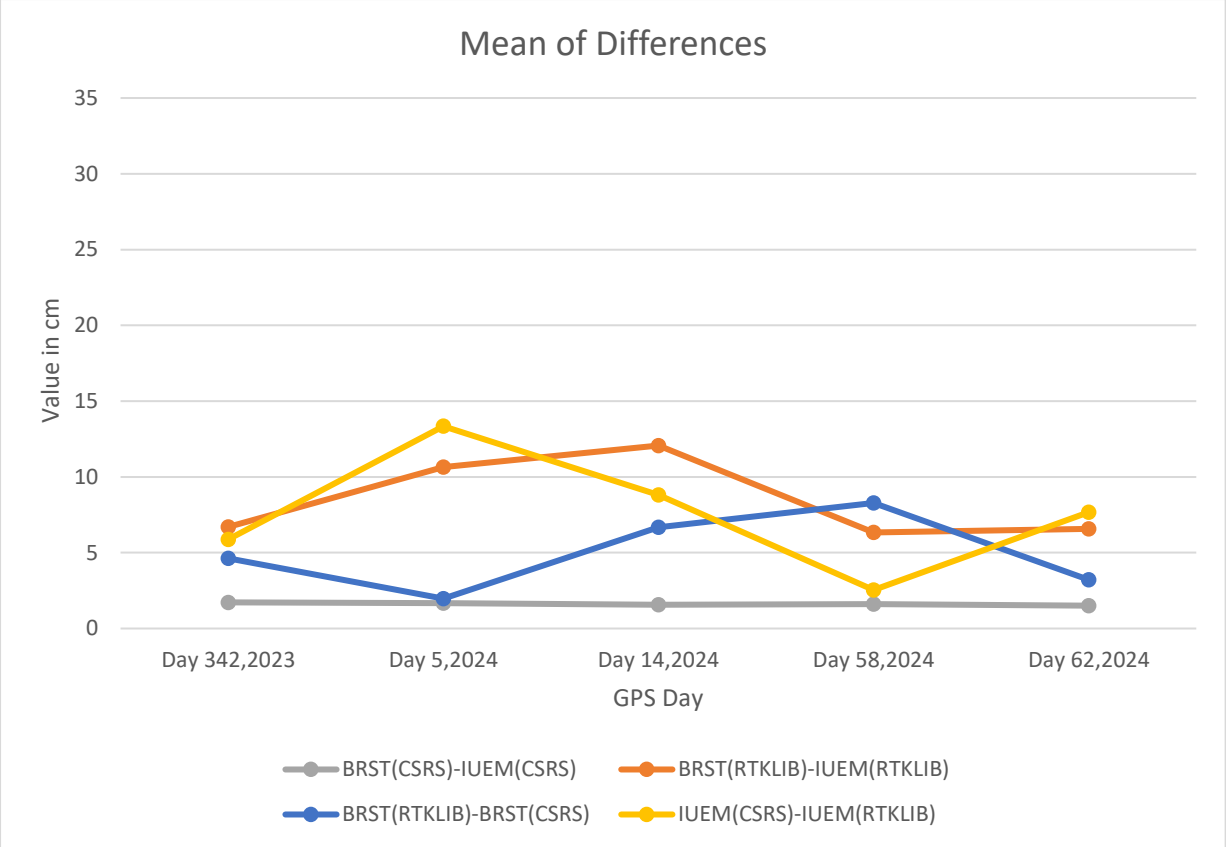

Figure 30 Mean of Differences of ZTD for BRST-IUEM Stations

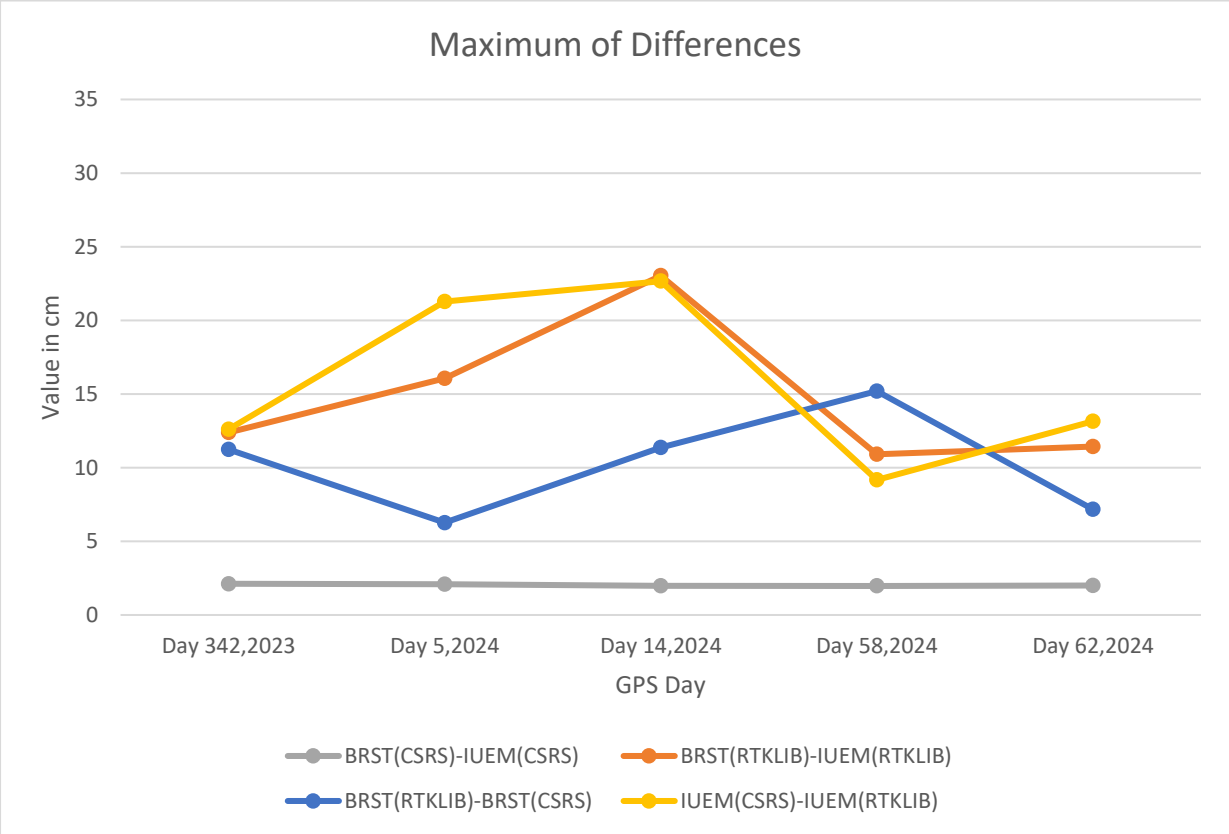

Figure 31 Maximum of Differences of ZTD for BRST-IUEM Stations

- The ZTD estimates from the two stations (BRST and IUEM) processed by CSRS-PPP show closest agreement to each other with mean differences of ZTD less than 2cm and maximum of differences of ZTD less than 3cm. It shows that the ZTD values provided by the VFCH and RDHB7 stations exhibit similar trends in terms of temporal variability.
- Mean and Maximum of ZTD differences of the two stations processed by RTKLIB show reasonable agreement with each other. The Mean of differences observed in this case is 10cm or less and maximum of differences being 15cm or lesser.
- Variability of ZTD estimates is also checked when BRST station data is processed by RTKLIB and the IUEM station data is processed by CSRS and vice versa. This comparison yields Low values of mean and maximum of ZTD differences. It suggests consistent ZTD values for Day342,2023, Day58 and Day62,2024. For January (Day 5 and 14), there are relatively high values for mean and maximum in this case.

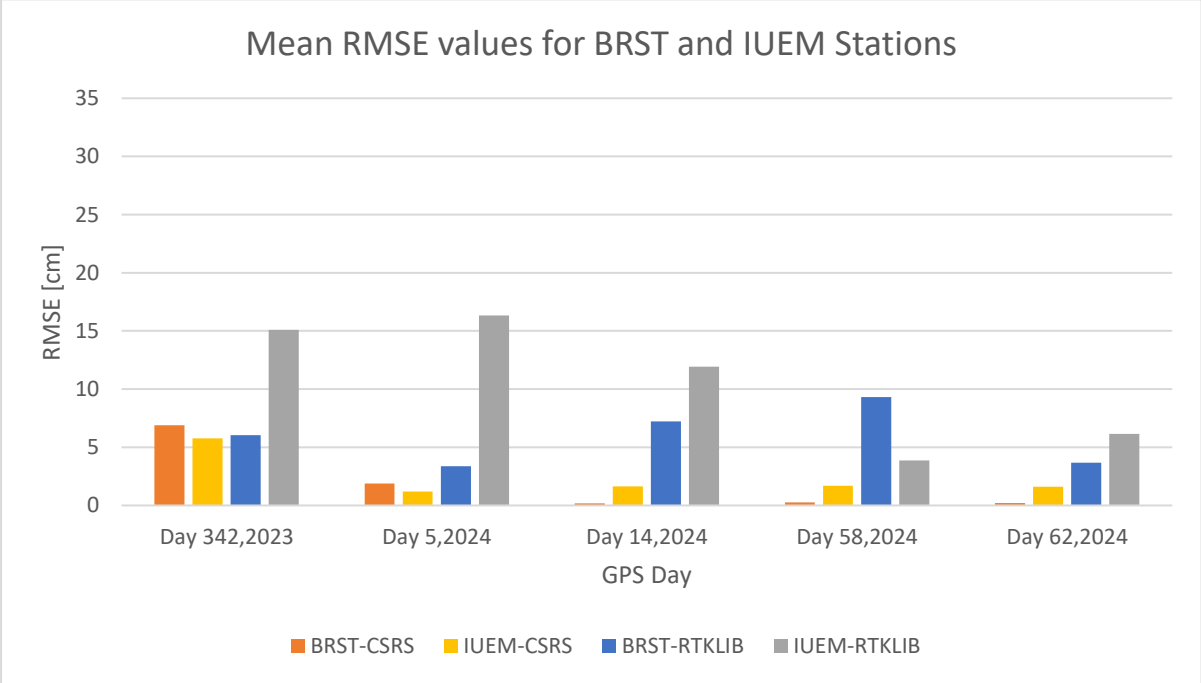

Figure 32 Mean RMSE values for BRST-IUEM Stations

- The ZTD estimates from the BRST and IUEM stations processed by CSRS-PPP indicate comparable accuracy for all the days observed. The ZTD estimates provided by the two stations have very low RMSE values (less than 2cm). For Day342, 2023, RMSE value for IUEM station data is lower than that of BRST station data.
- If we compare the RMSE values for the ZTD obtained by the BRST and IUEM stations, processed through RTKLIB, there are comparable RMSE values for Day14, Day58, and Day62, 2024. The RMSE values for BEFF station processed by RTKLIB is relatively higher for the Day 342,2023 and Day 5,2024.

Discussion

The CSRS-PPP models the tropospheric delay values closer to the EUREF tropospheric product. This is primarily because the online service uses the Global Mapping function based on numerical weather model data. RTKLIB uses Neil mapping function to estimate the zenith tropospheric delay, which depends on the site coordinates and the time of the year. Another difference is the cut-off angle set up in the software. The cut-off angle used by the EUREF tropospheric product and the CSRS online service is 7.5 degrees. RTKLIB only allows the setting up of cut-off angle as multiple of 5. Hence, a value of 10 was chosen as the closest option. Due to this difference, some satellites are discarded for the solution. The processing from RTKLIB results in more rejection of epochs due to this reason.

First, we discuss the variability of ZTD estimates obtained through CSRS. The observed limits for the Mean and Maximum of ZTD Differences are provided in table 5.

GNSS Stations	ZTD range (m)	**CSRS-PPP**	
		Mean of Differences (cm)	Maximum of Differences (cm)
1. GRAS-SOPH	2-2.1	<35	<40
2. BRON-BEFF	2.3-2.4	<2	<2
3. BRMG-BIO	2.3-2.4	<2	<2
4. VFCH-RDHB7	2.3-2.5	<3	<3
5. BRST-IUEM	2.3-2.5	<3	<3

Table 5 Limits of Mean and Maximum of Differences for CSRS-PPP

All the stations except GRAS-SOPH, show very low values of statistical indicators listed in table 5. The temporal variation of ZTD values provided by Centipede stations align closely with the EUREF provided values, when processed by CSRS-PPP. The stations located in Eastern France show lower variability of ZTD during the observed 24-hours interval while it is higher for the stations in Central and Western part of France. It is important that even in the regions of relatively high temporal variability of tropospheric delays, Centipede stations provide ZTD values very close to that of EUREF stations. The mean and maximum of ZTD differences are less than 3cm for all the stations except GRAS-SOPH which is discussed next.

For the SOPH station situated at relatively lower latitude in Eastern France, the ZTD Timeseries analysis reveal similar ZTD variability trend over time as of GRAS (EUREF) station. The only difference is that the estimated delay values are consistently greater by 30cm approximately than the GRAS station. This relatively higher estimation of ZTD values from the SOPH station is due to its low altitude of 178.85m as compared to the that of GRAS station (1319.35m). Lower altitude results in greater thickness of troposphere and consequently, higher values of Zenith tropospheric delay.

GNSS Stations	ZTD range (m)	**RTKLIB**	
		Mean of Differences (cm)	Maximum of Differences (cm)
GRAS-SOPH	2-2.1	<30	<35
BRON-BEFF	2.3-2.4	<10	<15
BRMG-BIO	2.3-2.4	<10	<15
VFCH-RDHB7	2.3-2.5	<10	<15
BRST-IUEM	2.3-2.5	<10	<15

Table 6 Limits of Mean and Maximum of Differences for RTKLIB

The Analysis of ZTD estimates processed through RTKLIB reveals a trend towards higher values in both mean and maximum differences, indicating a certain variability in estimates. Despite this variability, the analysis indicates that both Centipede and EUREF network stations exhibit comparable temporal capture of ZTD when the data is processed through RTKLIB. With mean of differences less than 10cm and Maximum of differences less than 15cm, ZTD estimates from the centipede network are consistent with the estimates obtained from the EUREF network. Again, the GRAS-SOPH stations show high values for the mean and maximum, attributable to the low elevation of SOPH station.

RMSE values for all the stations are listed in table 7 to check the quality performance of the Centipede network stations.

GNSS Station	RMSE (cm)	
	CSRS	RTKLIB
GRAS	<3	<45
SOPH	<35	<30
BRON	<1	<11
BEFF	<1	<27
BRMG	<3	<10
BIO	<3	<10
VFCH	<8	<12
RDHB7	<8	<10
BRST	<7	<10
IUEM	<7	<17

Table 7 RMSE values for all Stations

The accuracy of the ZTD estimates, processed through CSRS, for the Centipede stations is same as that of the EUREF network stations at each observed location except SOPH. As previously discussed, this high RMSE value is due to the low elevation of SOPH station while the GRAS station is located in a hilly area with much higher elevation and ZTD values very close to the EUREF tropospheric product. If the processing is done through RTKLIB, SOPH station provides lower RMSE value than the GRAS station. BIO and RDHB7 stations have similar performance as their nearest EUREF network stations in terms of tropospheric delay values. The BEFF and IUEM stations have relatively high RMSE values for RTKLIB processing. Although, RTKLIB processed estimates do not accurately model the tropospheric effects as compared to CSRS-PPP, it confirms the comparable temporal and spatial variability of ZTD estimates provided by the low-cost Centipede Network.

Conclusion

This study evaluates the performance of the low-cost Centipede Network station in providing Zenith tropospheric delay estimates. The ZTD estimates are compared to the EUREF GNSS Network processed ZTD estimates. The analysis is made independent of the processing method by using RTKLIB and CSRS-PPP. In assessing the Zenith Tropospheric Delay (ZTD) estimates, this study reveals a similar level of accuracy between the low-cost Centipede network and the EUREF network, if processed through appropriate software package such as CSRS-PPP. The ZTD values from the two networks exhibit similar temporal trends and fluctuations. The low-cost Centipede Network provided ZTD values are consistent with the EUREF provided ZTD values, irrespective of the changing geographical and atmospheric conditions. The CSRS processed ZTD values for the Centipede network have low RMSE values (<3cm for Eastern France and <8cm for Central and Western France). The results from the RTKLIB also confirm the similar temporal variability of ZTD values. The RMSE values for the RTKLIB processed data are relatively higher due to inaccurate modelling of troposphere and atmospheric conditions. This deviation from the EUREF tropospheric product is regarded due to different mapping function and cut-off angle than CSRS-PPP. Although, RTKLIB processed estimates do not accurately model the tropospheric effects as compared to CSRS-PPP, it confirms the comparable temporal and spatial variability of ZTD estimates provided by the low-cost Centipede Network.

These findings demonstrate that despite the differences in equipment costs and configurations, the spatial and temporal variability of ZTD readings across both networks aligns closely. Hence, the low cost GNSS networks can be employed for GNSS network densification. They offer a cost-effective solution to enhance the spatial resolution of tropospheric monitoring. The resulting high-resolution temporal and spatial monitoring of water vapor distribution would enable more accurate forecasts of rainfall and extreme weather events. This can have a huge positive impact to the climate change studies.

Bibliography

[1] S. Jin, Q. Wang, and G. Dardanelli, 'A Review on Multi-GNSS for Earth Observation and Emerging Applications', *Remote Sensing*, vol. 14, no. 16. 2022. doi: 10.3390/rs14163930.

[2] B. Hofmann-Wellenhof, H. Lichtenegger, and J. Collins, *Global Positioning System. Theory and Practice*, Fourth Edition. Springer Wien New-York.

[3] M. Hern´andez-Pajares, J.M. Juan Zornoza, and J. Sanz Subirana, *GPS data processing: code and phase Algorithms, Techniques and Recipes*, Second Edition. Barcelona: gAGE-NAV S.L., 2005.

[4] J. F. Zumberge, M. B. Heflin, D. C. Jefferson, M. M. Watkins, and F. H. Webb, 'Precise point positioning for the efficient and robust analysis of GPS data from large networks', *J Geophys Res Solid Earth*, vol. 102, no. B3, 1997, doi: 10.1029/96jb03860.

[5] X. Li, X. Zhang, X. Ren, M. Fritsche, J. Wickert, and H. Schuh, 'Precise positioning with current multi-constellation Global Navigation Satellite Systems: GPS, GLONASS, Galileo and BeiDou', *Sci Rep*, vol. 5, 2015, doi: 10.1038/srep08328.

[6] 'CentipedeRTK'.

[7] C. Schär *et al.*, 'Kilometer-scale climate models: Prospects and challenges', *Bull Am Meteorol Soc*, vol. 101, no. 5, 2020, doi: 10.1175/BAMS-D-18-0167.1.

[8] J. A. Milbrandt, S. Bélair, M. Faucher, M. Vallée, M. L. Carrera, and A. Glazer, 'The pan-canadian high resolution (2.5 km) deterministic prediction system', *Weather Forecast*, vol. 31, no. 6, 2016, doi: 10.1175/WAF-D-16-0035.1.

[9] B. Bramanto, I. Gumilar, T. P. Sidiq, W. Kuntjoro, and D. A. Tampubolon, 'Sensing of the atmospheric variation using Low Cost GNSS Receiver', in *IOP Conference Series: Earth and Environmental Science*, 2018. doi: 10.1088/1755-1315/149/1/012073.

[10] M. S. Garrido-Carretero, M. C. de Lacy-Pérez de los Cobos, M. J. Borque-Arancón, A. M. Ruiz-Armenteros, R. Moreno-Guerrero, and A. J. Gil-Cruz, 'Low-cost GNSS receiver in RTK positioning under the standard ISO-17123-8: A feasible option in geomatics', *Measurement (Lond)*, vol. 137, 2019, doi: 10.1016/j.measurement.2019.01.045.

[11] A. Krietemeyer, M. C. ten Veldhuis, H. van der Marel, E. Realini, and N. van de Giesen, 'Potential of cost-efficient single frequency GNSS receivers for water vapor monitoring', *Remote Sens (Basel)*, vol. 10, no. 9, 2018, doi: 10.3390/rs10091493.

[12] 'GNSS-Global Navigation Satellite Systems: GPS, GLONASS, Galileo, and more', *Choice Reviews Online*, vol. 45, no. 11, 2008, doi: 10.5860/choice.45-6185.

[13] L. Essen and K. D. Froome, 'Dielectric constant and refractive index of air and its principal constituents at 24,000 Mc./s.', *Nature*, vol. 167, no. 4248, 1951, doi: 10.1038/167512a0.

[14] K. Wilgan, F. Hurter, A. Geiger, W. Rohm, and J. Bosy, 'Tropospheric refractivity and zenith path delays from least-squares collocation of meteorological and GNSS data', *J Geod*, vol. 91, no. 2, 2017, doi: 10.1007/s00190-016-0942-5.

[15] G. D. Thayer, 'An improved equation for the radio refractive index of air', *Radio Sci*, vol. 9, no. 10, 1974, doi: 10.1029/RS009i010p00803.

[16] J. C. Owens, 'Optical Refractive Index of Air: Dependence on Pressure, Temperature and Composition', *Appl Opt*, vol. 6, no. 1, 1967, doi: 10.1364/ao.6.000051.

[17] G. Guerova *et al.*, 'Review of the state of the art and future prospects of the ground-based GNSS meteorology in Europe', *Atmospheric Measurement Techniques*, vol. 9, no. 11. 2016. doi: 10.5194/amt-9-5385-2016.

[18] J. Won, K. D. Park, J. Ha, and J. Cho, 'Effects of tropospheric mapping functions on GPS data processing', *Journal of Astronomy and Space Sciences*, vol. 27, no. 1, 2010, doi: 10.5140/JASS.2010.27.1.021.

[19] S. Nistor and A. S. Buda, 'Determination of Zenith Tropospheric Delay and Precipitable Water Vapor using GPS Technology', *Mathematical Modelling in Civil Engineering*, vol. 12, no. 2, 2016, doi: 10.1515/mmce-2016-0007.

[20] J. M. Astudillo, L. Lau, Y. T. Tang, and T. Moore, 'Analysing the Zenith tropospheric delay estimates in on-line precise point positioning (PPP) services and PPP software packages', *Sensors (Switzerland)*, vol. 18, no. 2, 2018, doi: 10.3390/s18020580.

[21] T. A. Herring, 'Modeling of atmospheric delay in the analysis space geodetic data', *Symposium on Refraction of Transatmospheric Signals in Geodesy*, no. 36, 1992.

[22] H. Schuh and J. Böhm, 'Very long baseline interferometry for geodesy and astrometry', in *Sciences of Geodesy - II: Innovations and Future Developments*, 2014. doi: 10.1007/978-3-642-28000-9_7.

[23] A. E. Niell, 'Global mapping functions for the atmosphere delay at radio wavelengths', *J Geophys Res Solid Earth*, vol. 101, no. 2, 1996, doi: 10.1029/95jb03048.

[24] J. Boehm, B. Werl, and H. Schuh, 'Troposphere mapping functions for GPS and very long baseline interferometry from European Centre for Medium-Range Weather Forecasts operational analysis data', *J Geophys Res Solid Earth*, vol. 111, no. 2, Feb. 2006, doi: 10.1029/2005JB003629.

[25] J. Boehm, A. Niell, P. Tregoning, and H. Schuh, 'Global Mapping Function (GMF): A new empirical mapping function based on numerical weather model data', *Geophys Res Lett*, vol. 33, no. 7, 2006, doi: 10.1029/2005GL025546.

[26] J. Douša, 'The impact of errors in predicted GPS orbits on zenith troposphere delay estimation', *GPS Solutions*, vol. 14, no. 3, 2010, doi: 10.1007/s10291-009-0138-z.

[27] C. Shi *et al.*, 'Seismic deformation of the M w 8.0 Wenchuan earthquake from high-rate GPS observations', *Advances in Space Research*, vol. 46, no. 2, 2010, doi: 10.1016/j.asr.2010.03.006.

[28] H. Bock, U. Hugentobler, and G. Beutler, 'Kinematic and Dynamic Determination of Trajectories for Low Earth Satellites Using GPS', in *First CHAMP Mission Results for Gravity, Magnetic and Atmospheric Studies*, 2003. doi: 10.1007/978-3-540-38366-6_10.

[29] K. Dixon, 'StarFire™: A global SBAS for sub-decimeter precise point positioning', in *Proceedings of the Institute of Navigation - 19th International Technical Meeting of the Satellite Division, ION GNSS 2006*, 2006.

[30] J. Tomaštík and T. Everett, 'Static Positioning under Tree Canopy Using Low-Cost GNSS Receivers and Adapted RTKLIB Software', *Sensors*, vol. 23, no. 6, 2023, doi: 10.3390/s23063136.

[31] T. Takasu, 'RTKLIB: An open source program package for GNSS positioning'.

[32] T. Everett, 'RTKLIB-demo-5'.

ANNEX A

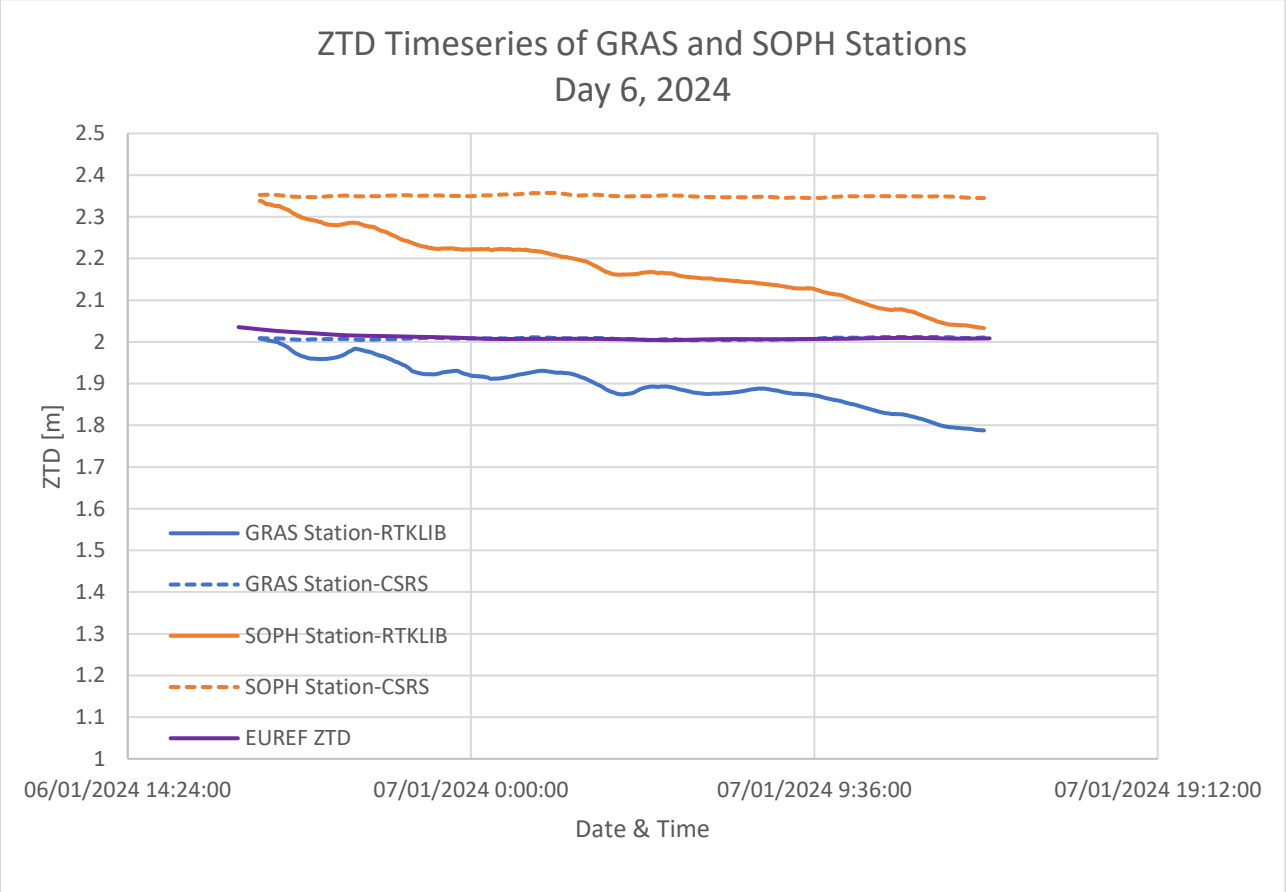
ZTD Timeseries of GRAS and SOPH Stations
Day 6, 2024
ZTD [m]
2.5
2.4
2.3
2.2
2.1
2
1.9
1.8
1.7
1.6
1.5
1.4
1.3
1.2
1.1
1
GRAS Station-RTKLIB
GRAS Station-CSRS
SOPH Station-RTKLIB
SOPH Station-CSRS
EUREF ZTD
06/01/2024 14:24:00
07/01/2024 0:00:00
07/01/2024 9:36:00
07/01/2024 19:12:00
Date & Time

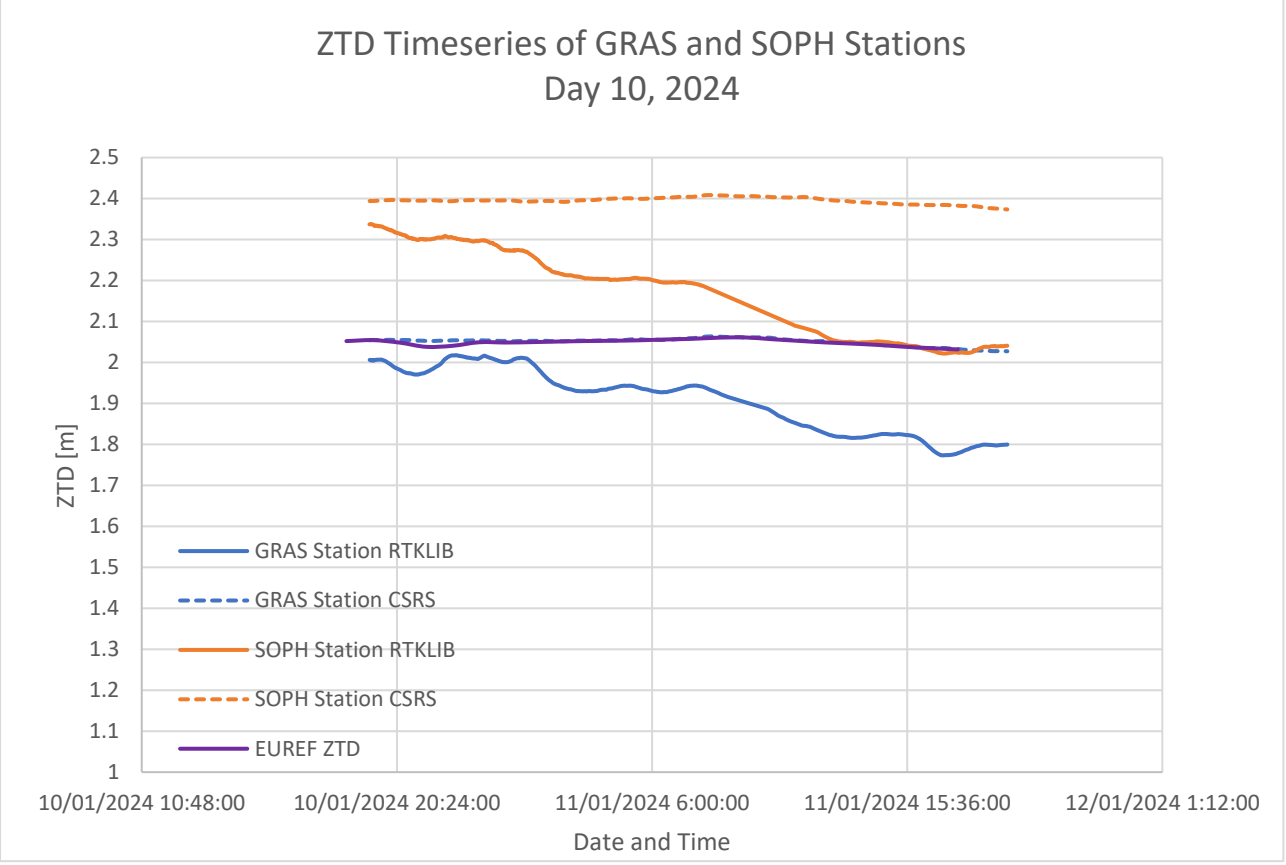
ZTD Timeseries of GRAS and SOPH Stations
Day 10, 2024
ZTD [m]
2.5
2.4
2.3
2.2
2.1
2
1.9
1.8
1.7
1.6
1.5
1.4
1.3
1.2
1.1
1
GRAS Station RTKLIB
GRAS Station CSRS
SOPH Station RTKLIB
SOPH Station CSRS
EUREF ZTD
10/01/2024 10:48:00
10/01/2024 20:24:00
11/01/2024 6:00:00
11/01/2024 15:36:00
12/01/2024 1:12:00
Date and Time

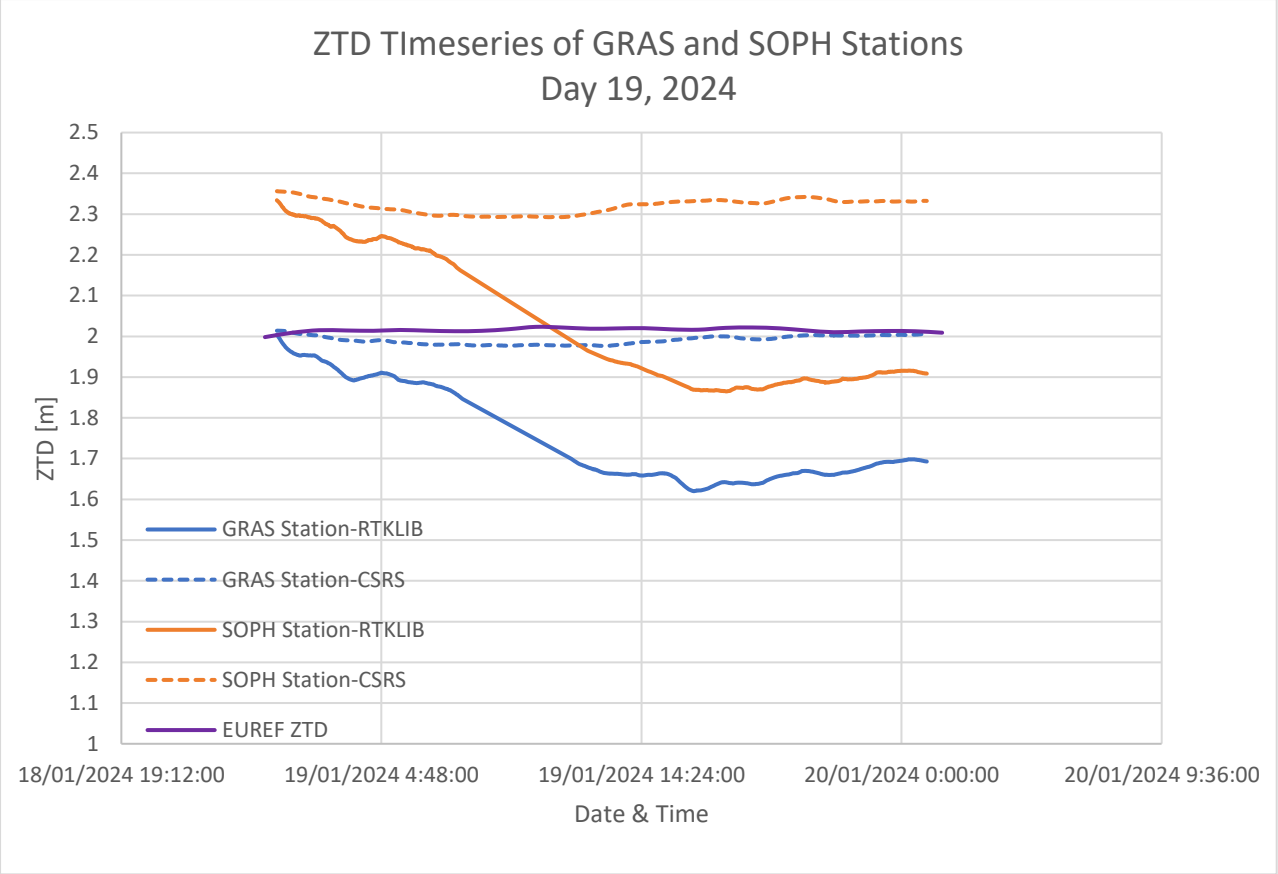
ZTD TImeseries of GRAS and SOPH Stations
Day 19, 2024
ZTD [m]
2.5
2.4
2.3
2.2
2.1
2
1.9
1.8
1.7
1.6
1.5
1.4
1.3
1.2
1.1
1
GRAS Station-RTKLIB
GRAS Station-CSRS
SOPH Station-RTKLIB
SOPH Station-CSRS
EUREF ZTD
18/01/2024 19:12:00
19/01/2024 4:48:00
19/01/2024 14:24:00
20/01/2024 0:00:00
20/01/2024 9:36:00
Date & Time

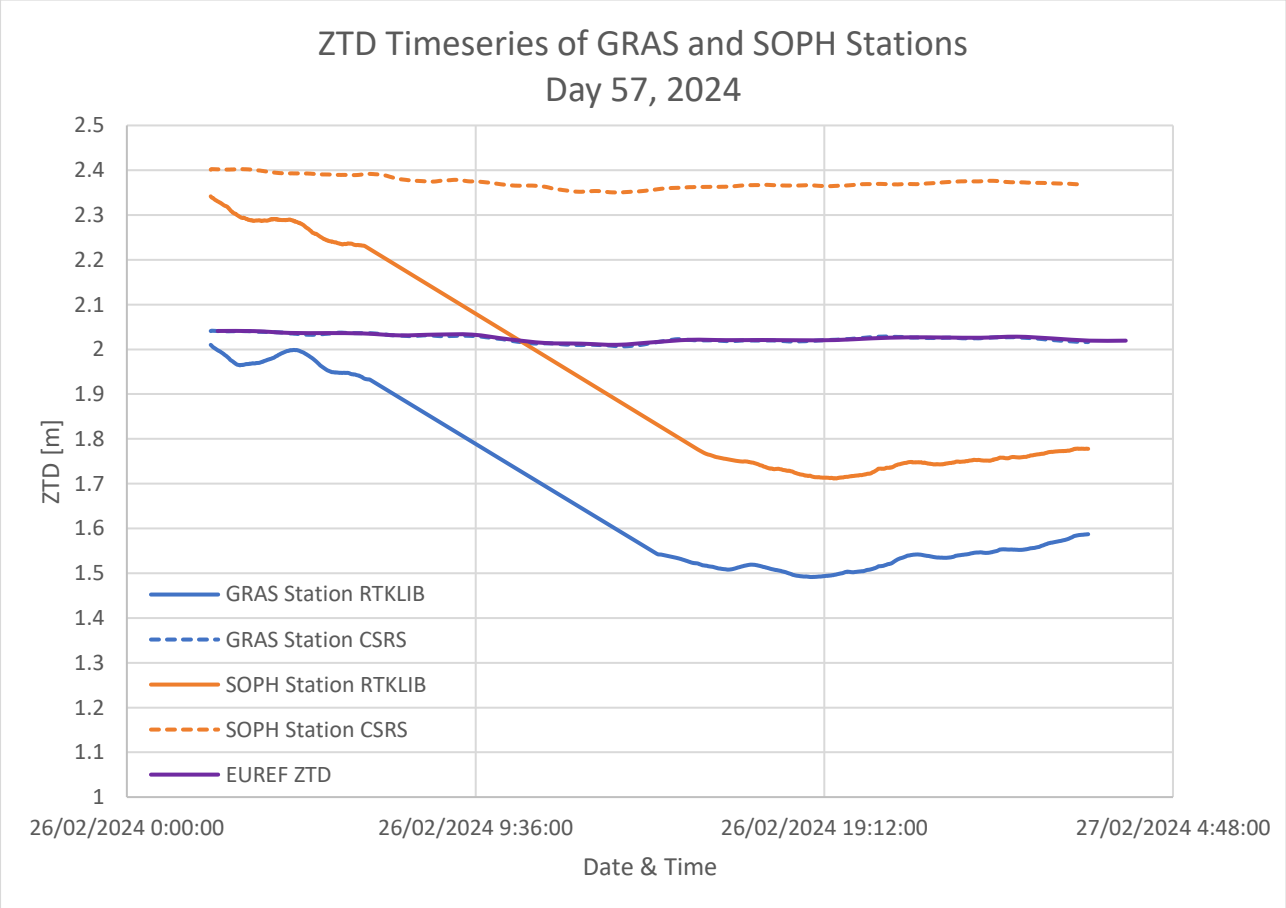
ZTD Timeseries of GRAS and SOPH Stations
Day 57, 2024
ZTD [m]
2.5
2.4
2.3
2.2
2.1
2
1.9
1.8
1.7
1.6
1.5
1.4
1.3
1.2
1.1
1
GRAS Station RTKLIB
GRAS Station CSRS
SOPH Station RTKLIB
SOPH Station CSRS
EUREF ZTD
26/02/2024 0:00:00
26/02/2024 9:36:00
26/02/2024 19:12:00
27/02/2024 4:48:00
Date & Time

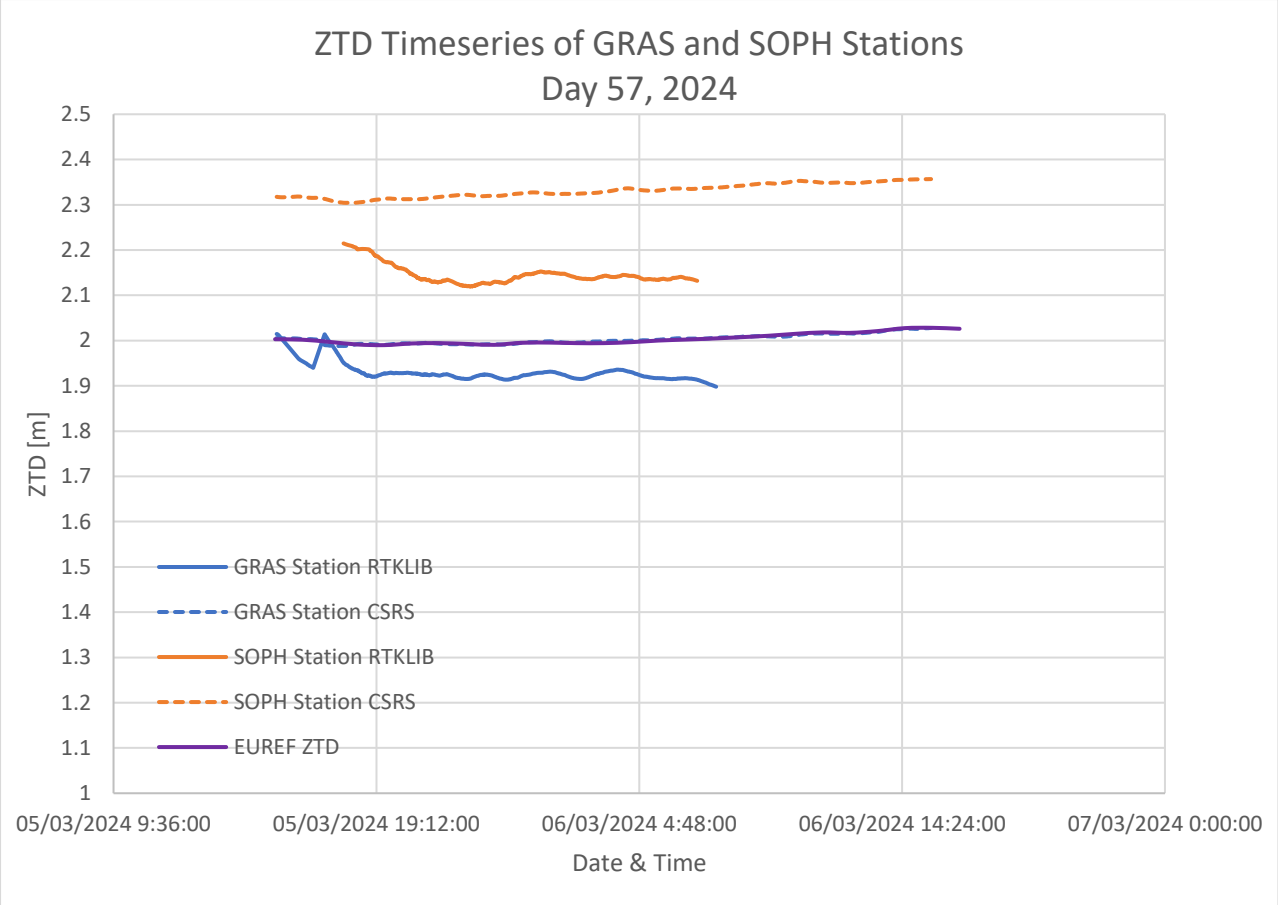
ZTD Timeseries of GRAS and SOPH Stations
Day 57, 2024
ZTD [m]
2.5
2.4
2.3
2.2
2.1
2
1.9
1.8
1.7
1.6
1.5
1.4
1.3
1.2
1.1
1
GRAS Station RTKLIB
GRAS Station CSRS
SOPH Station RTKLIB
SOPH Station CSRS
EUREF ZTD
05/03/2024 9:36:00
05/03/2024 19:12:00
06/03/2024 4:48:00
06/03/2024 14:24:00
07/03/2024 0:00:00
Date & Time

ANNEX B

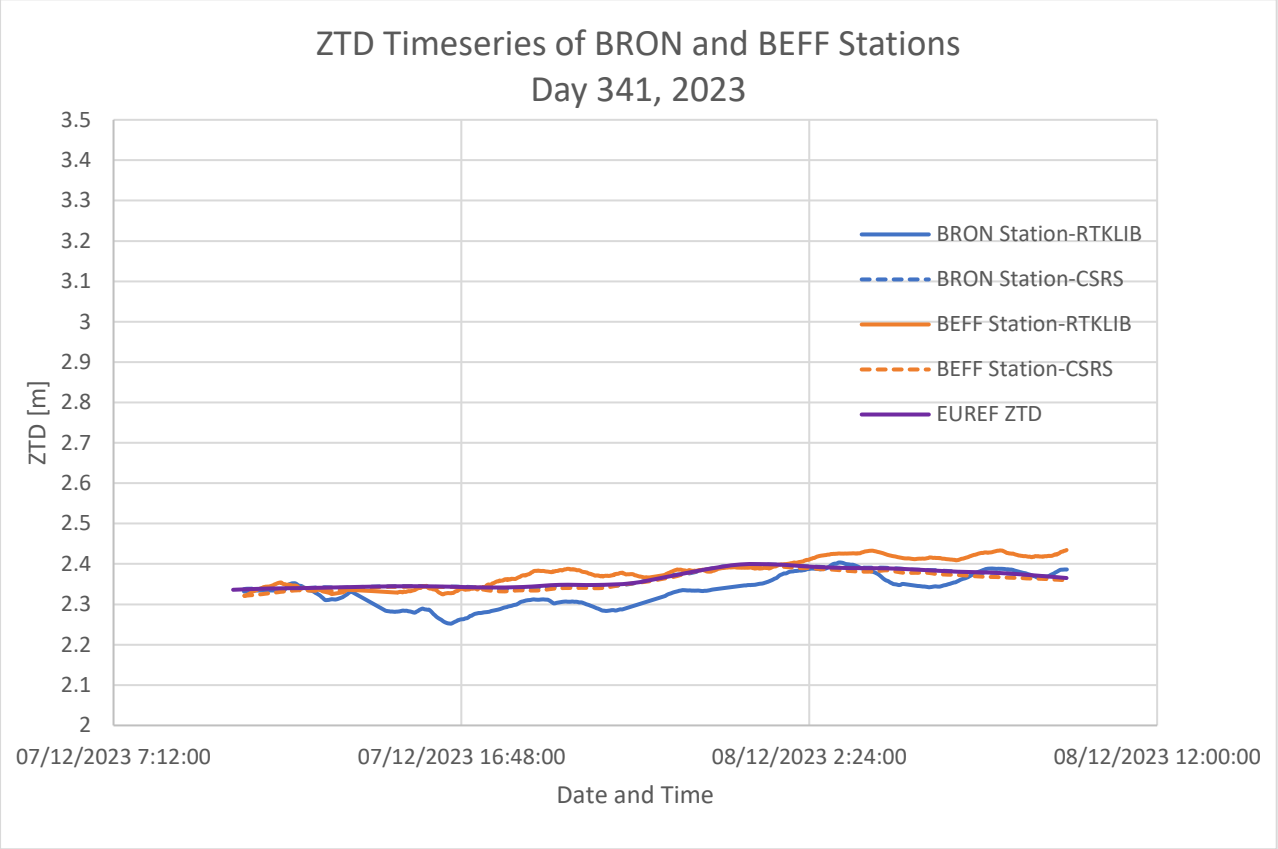
ZTD Timeseries of BRON and BEFF Stations
Day 341, 2023
ZTD [m]
3.5
3.4
3.3
3.2
3.1
3
2.9
2.8
2.7
2.6
2.5
2.4
2.3
2.2
2.1
2
BRON Station-RTKLIB
BRON Station-CSRS
BEFF Station-RTKLIB
BEFF Station-CSRS
EUREF ZTD
07/12/2023 7:12:00
07/12/2023 16:48:00
08/12/2023 2:24:00
08/12/2023 12:00:00
Date and Time

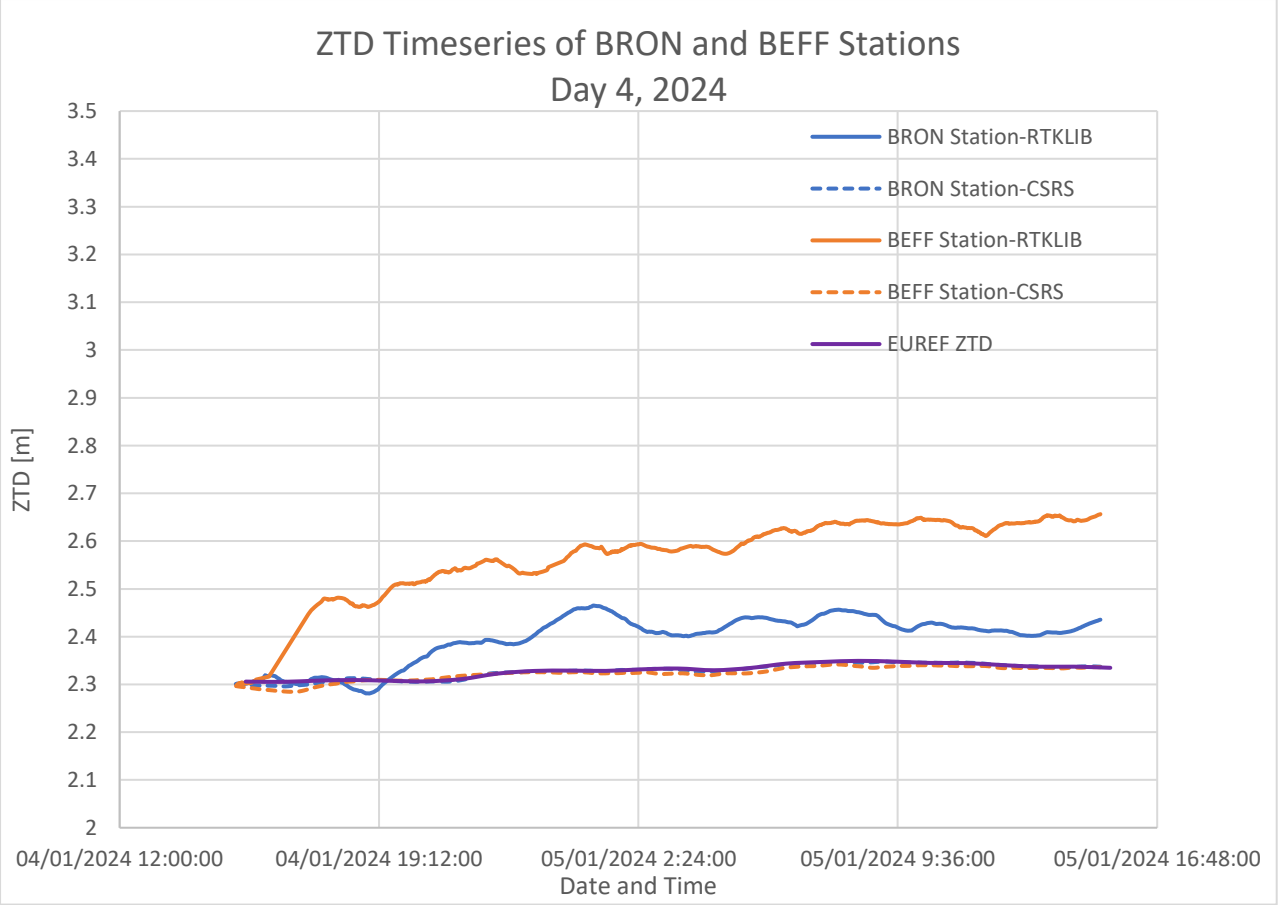
ZTD Timeseries of BRON and BEFF Stations
Day 4, 2024
ZTD [m]
3.5
3.4
3.3
3.2
3.1
3
2.9
2.8
2.7
2.6
2.5
2.4
2.3
2.2
2.1
2
BRON Station-RTKLIB
BRON Station-CSRS
BEFF Station-RTKLIB
BEFF Station-CSRS
EUREF ZTD
04/01/2024 12:00:00
04/01/2024 19:12:00
05/01/2024 2:24:00
05/01/2024 9:36:00
05/01/2024 16:48:00
Date and Time

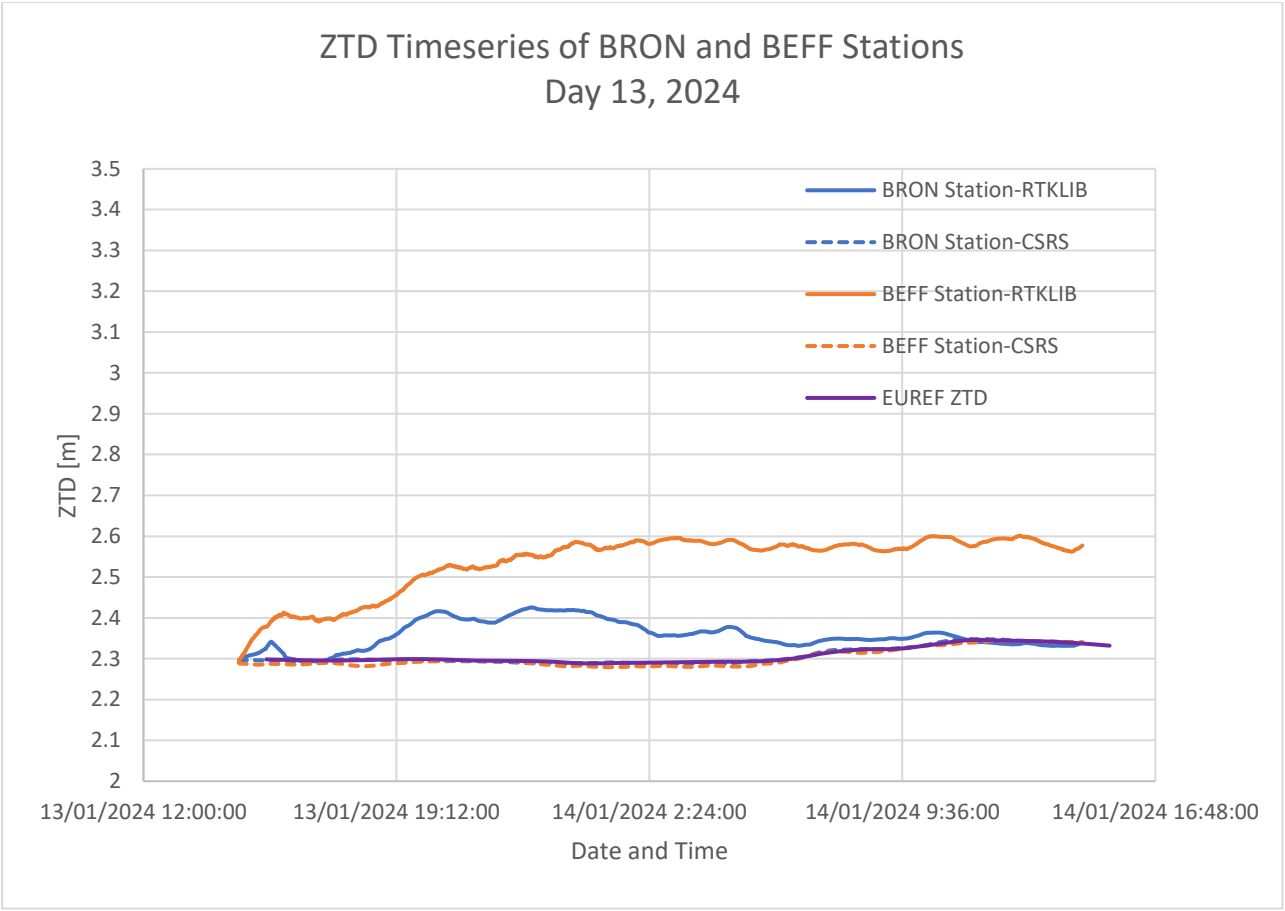
ZTD Timeseries of BRON and BEFF Stations
Day 13, 2024
BRON Station-RTKLIB
BRON Station-CSRS
BEFF Station-RTKLIB
BEFF Station-CSRS
EUREF ZTD
ZTD [m]
3.5
3.4
3.3
3.2
3.1
3
2.9
2.8
2.7
2.6
2.5
2.4
2.3
2.2
2.1
2
13/01/2024 12:00:00
13/01/2024 19:12:00
14/01/2024 2:24:00
14/01/2024 9:36:00
14/01/2024 16:48:00
Date and Time

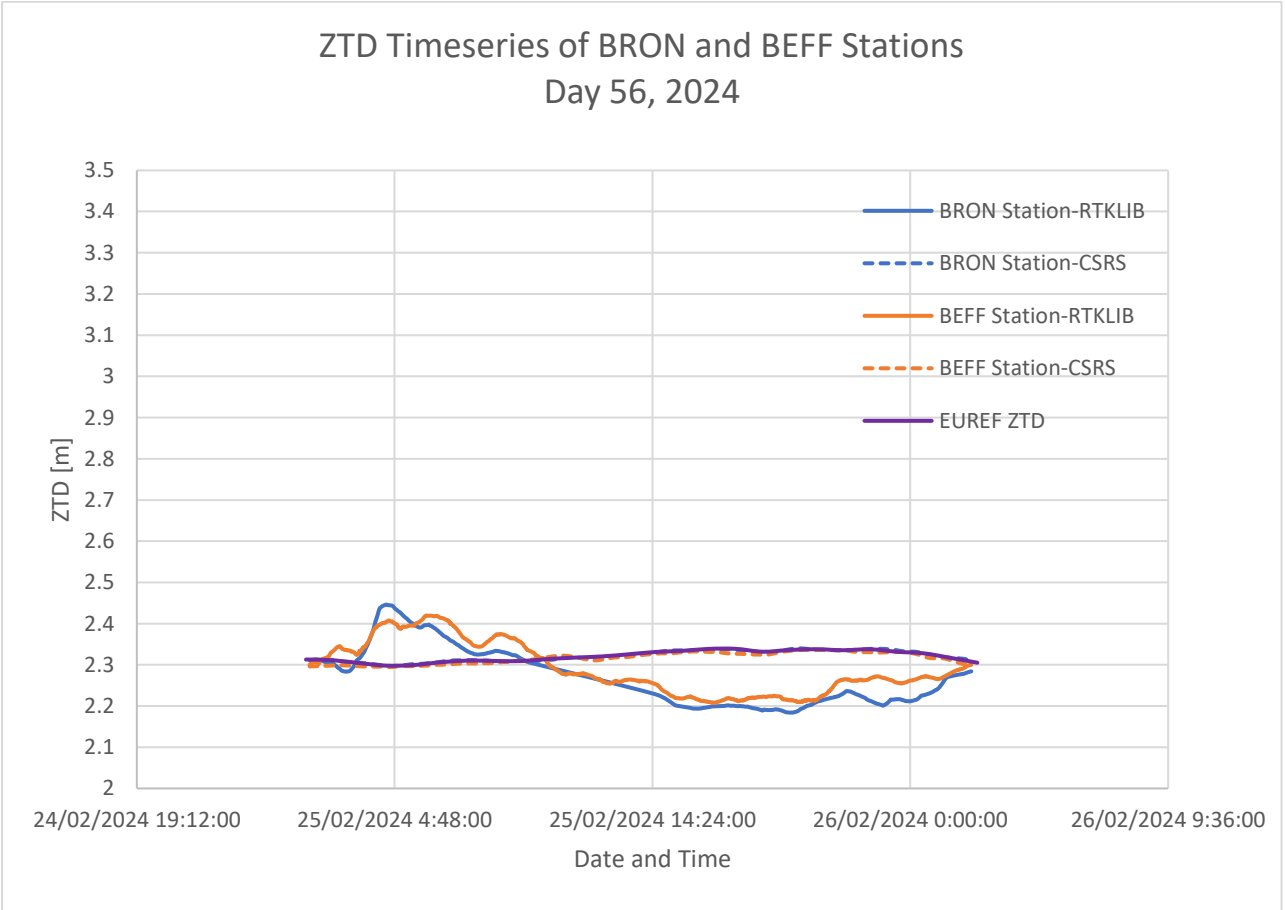
ZTD Timeseries of BRON and BEFF Stations
Day 56, 2024
BRON Station-RTKLIB
BRON Station-CSRS
BEFF Station-RTKLIB
BEFF Station-CSRS
EUREF ZTD
ZTD [m]
3.5
3.4
3.3
3.2
3.1
3
2.9
2.8
2.7
2.6
2.5
2.4
2.3
2.2
2.1
2
24/02/2024 19:12:00
25/02/2024 4:48:00
25/02/2024 14:24:00
26/02/2024 0:00:00
26/02/2024 9:36:00
Date and Time

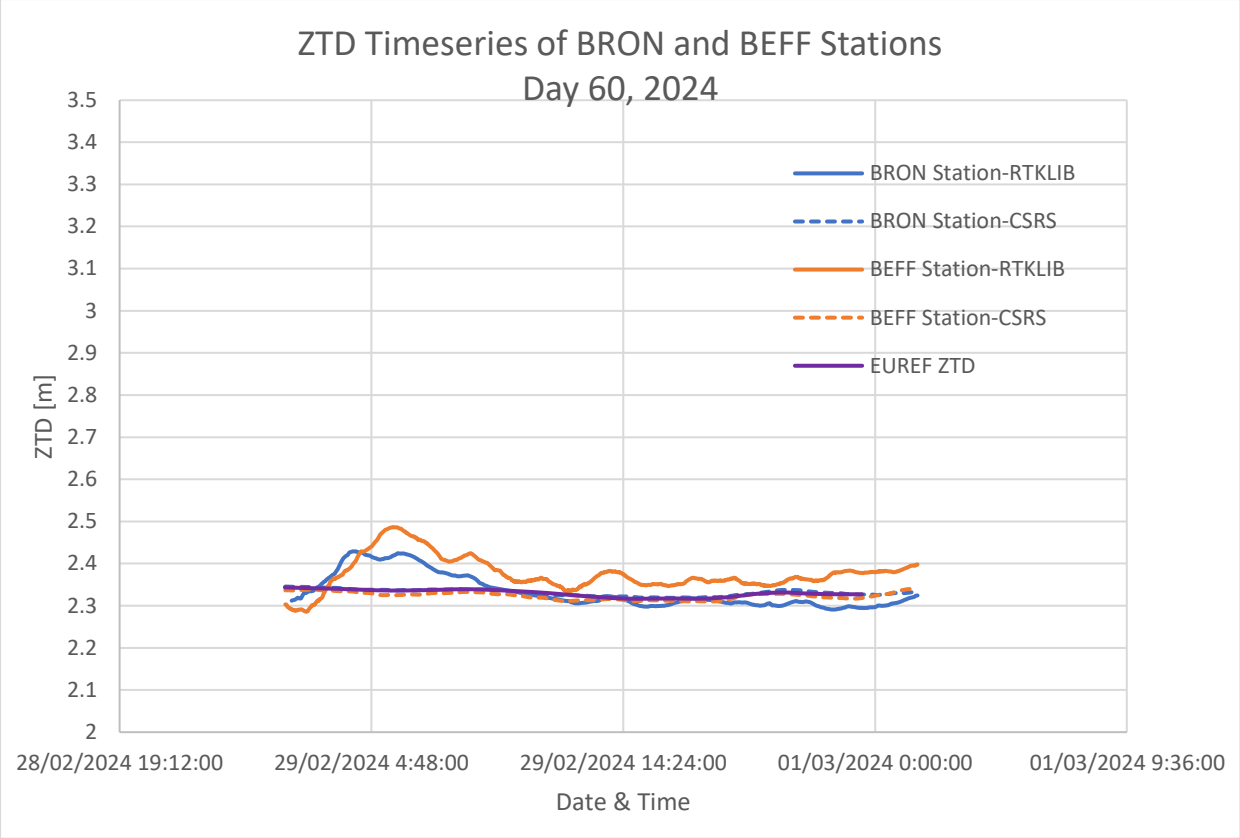
ZTD Timeseries of BRON and BEFF Stations
Day 60, 2024
ZTD [m]
3.5
3.4
3.3
3.2
3.1
3
2.9
2.8
2.7
2.6
2.5
2.4
2.3
2.2
2.1
2
BRON Station-RTKLIB
BRON Station-CSRS
BEFF Station-RTKLIB
BEFF Station-CSRS
EUREF ZTD
28/02/2024 19:12:00
29/02/2024 4:48:00
29/02/2024 14:24:00
01/03/2024 0:00:00
01/03/2024 9:36:00
Date & Time

ANNEX C

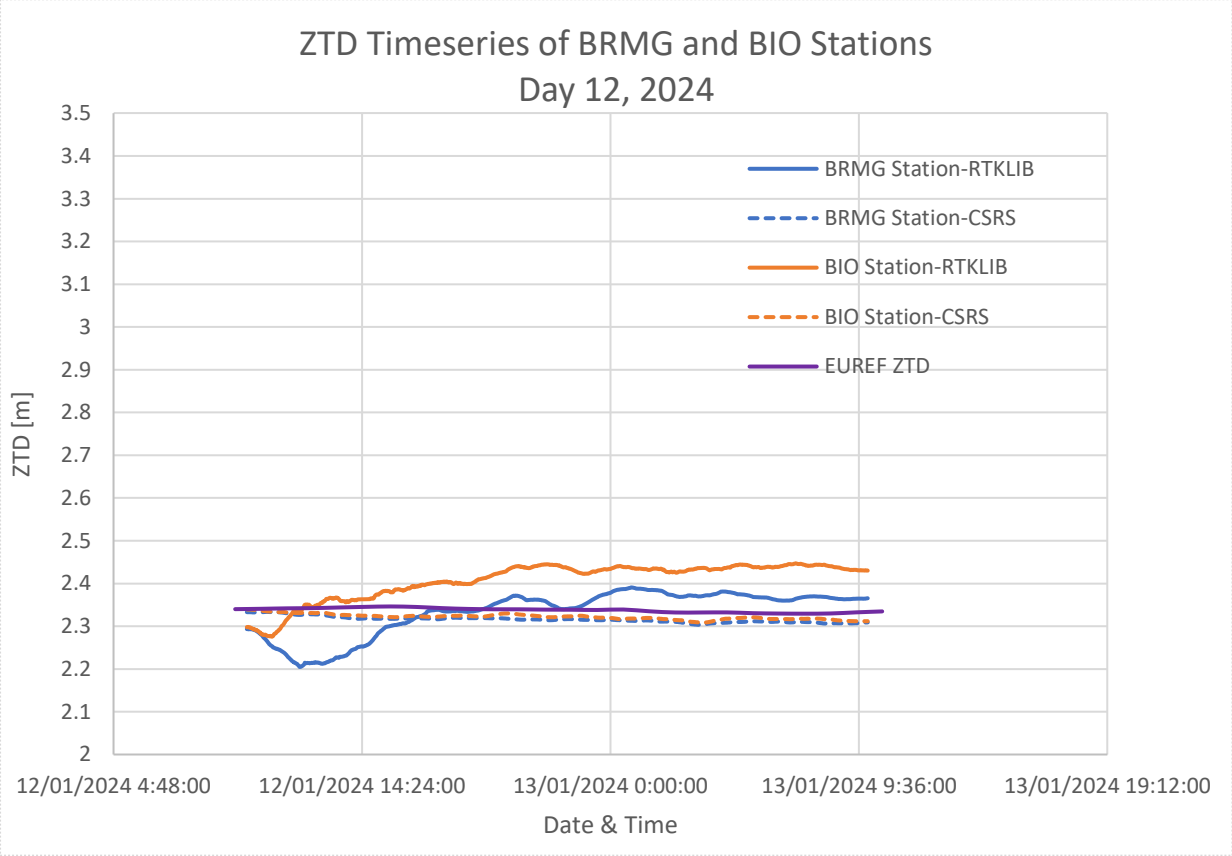
ZTD Timeseries of BRMG and BIO Stations
Day 12, 2024
ZTD [m]
3.5
3.4
3.3
3.2
3.1
3
2.9
2.8
2.7
2.6
2.5
2.4
2.3
2.2
2.1
2
BRMG Station-RTKLIB
BRMG Station-CSRS
BIO Station-RTKLIB
BIO Station-CSRS
EUREF ZTD
12/01/2024 4:48:00
12/01/2024 14:24:00
13/01/2024 0:00:00
13/01/2024 9:36:00
13/01/2024 19:12:00
Date & Time

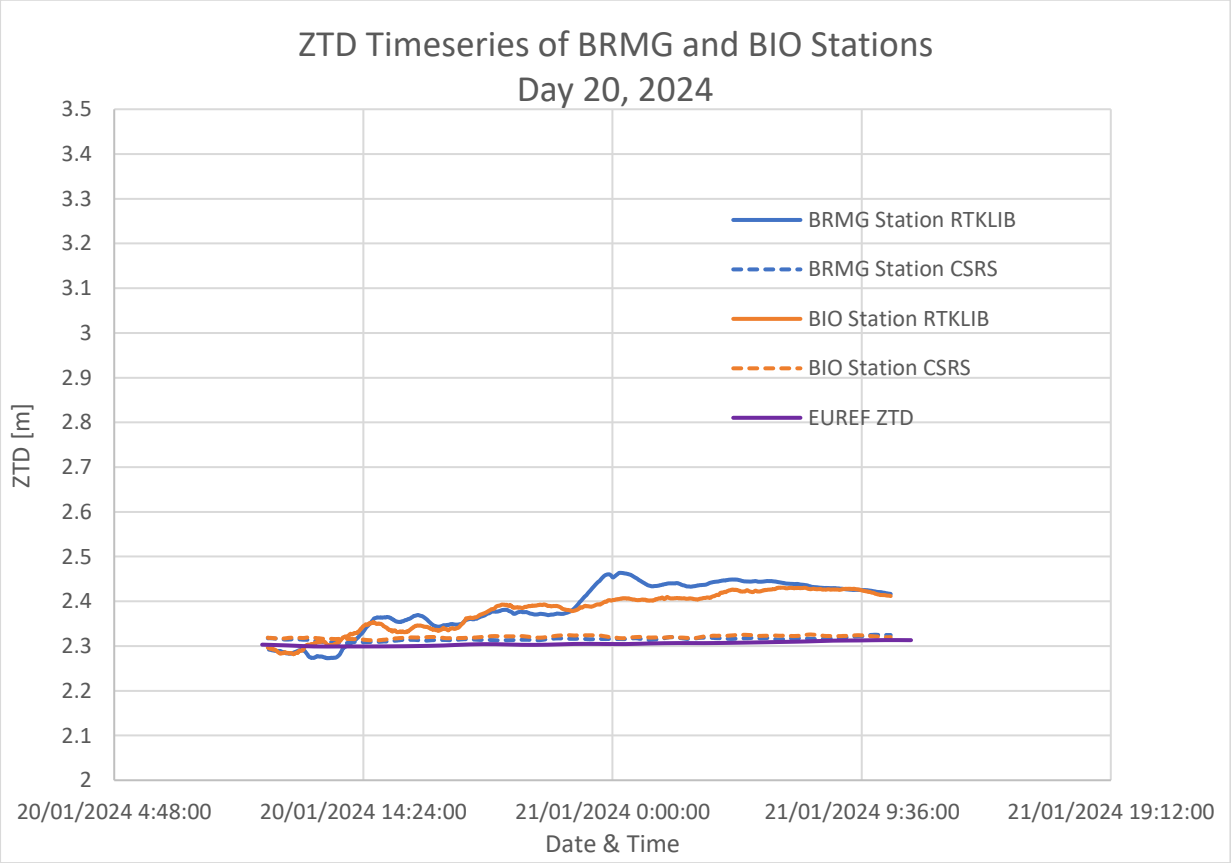
ZTD Timeseries of BRMG and BIO Stations
Day 20, 2024
ZTD [m]
3.5
3.4
3.3
3.2
3.1
3
2.9
2.8
2.7
2.6
2.5
2.4
2.3
2.2
2.1
2
BRMG Station RTKLIB
BRMG Station CSRS
BIO Station RTKLIB
BIO Station CSRS
EUREF ZTD
20/01/2024 4:48:00
20/01/2024 14:24:00
21/01/2024 0:00:00
21/01/2024 9:36:00
21/01/2024 19:12:00
Date & Time

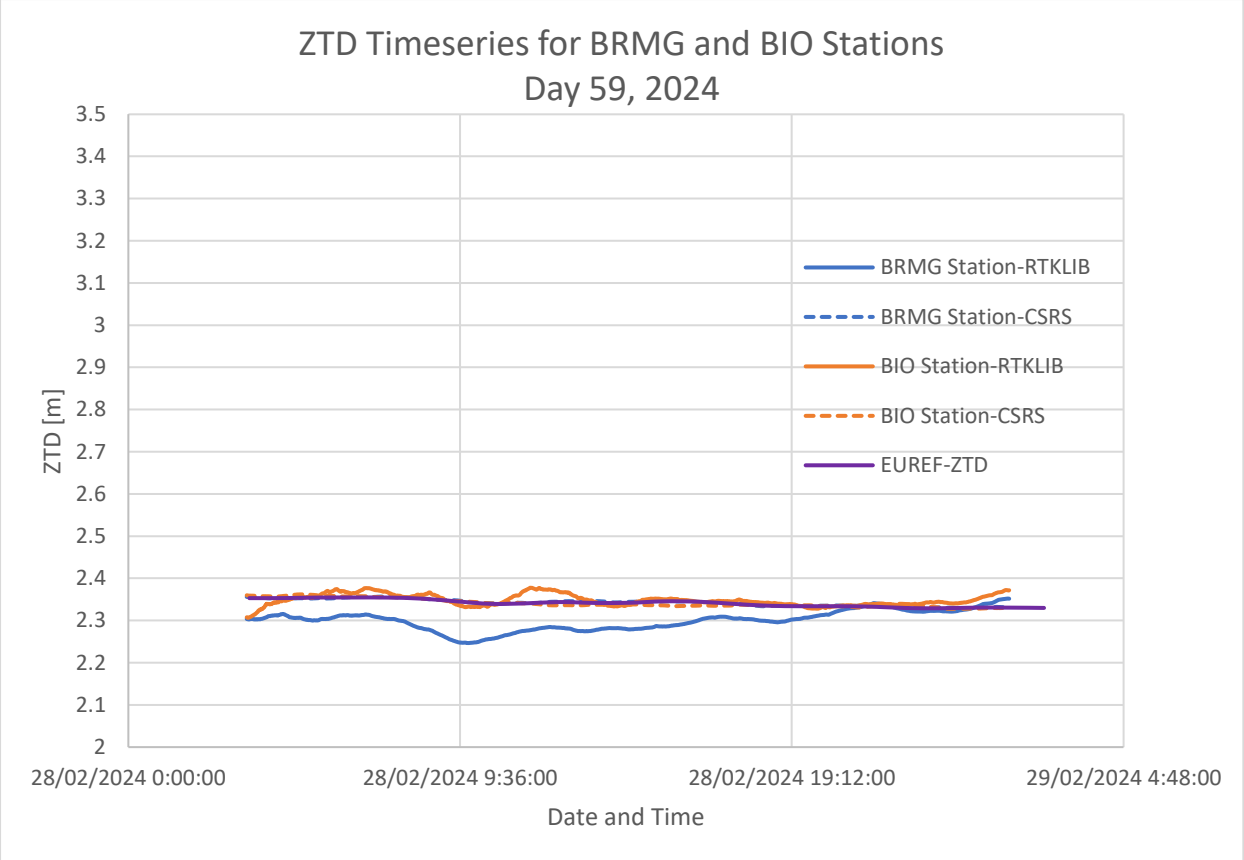
ZTD Timeseries for BRMG and BIO Stations
Day 59, 2024
ZTD [m]
3.5
3.4
3.3
3.2
3.1
3
2.9
2.8
2.7
2.6
2.5
2.4
2.3
2.2
2.1
2
BRMG Station-RTKLIB
BRMG Station-CSRS
BIO Station-RTKLIB
BIO Station-CSRS
EUREF-ZTD
28/02/2024 0:00:00
28/02/2024 9:36:00
28/02/2024 19:12:00
29/02/2024 4:48:00
Date and Time

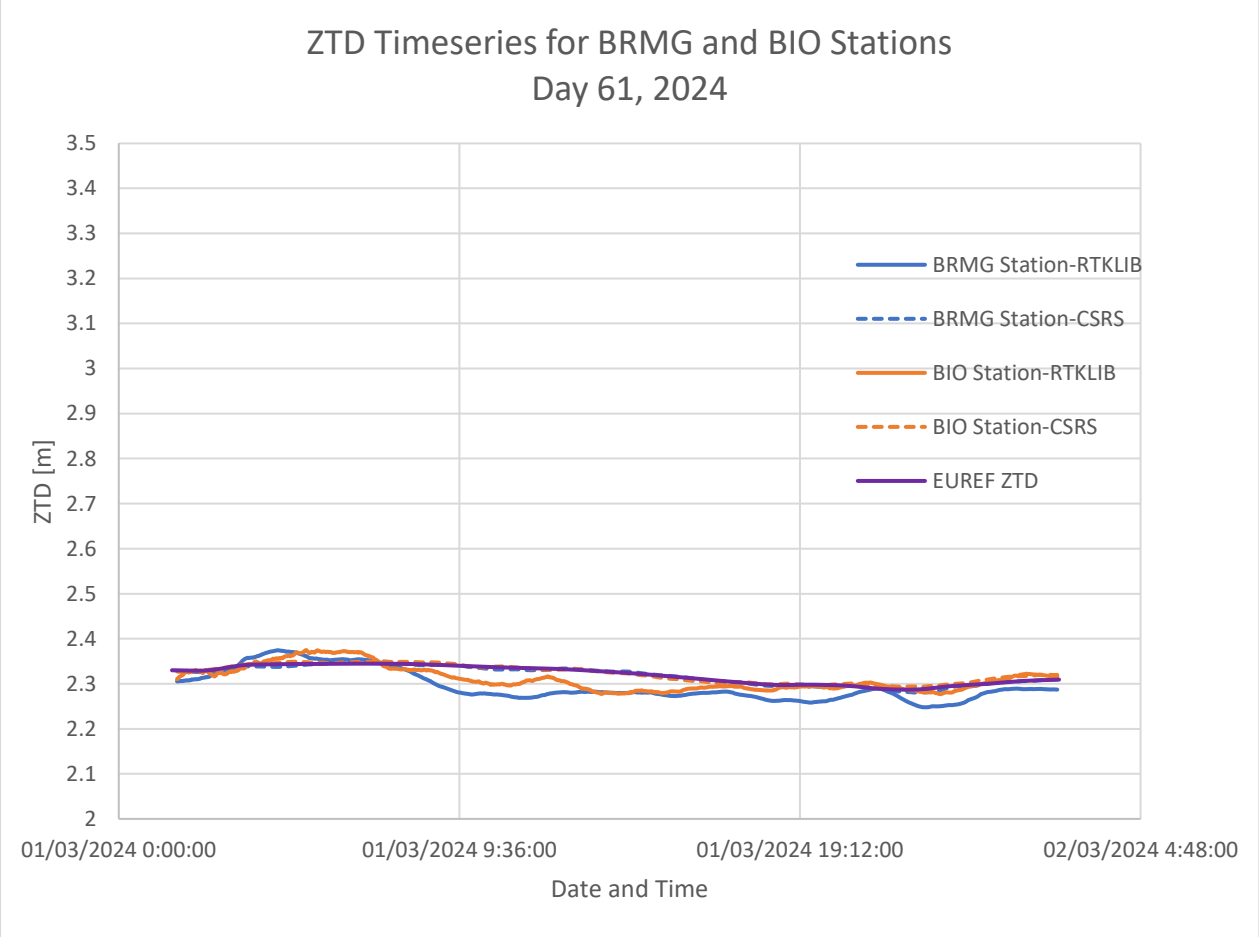
ZTD Timeseries for BRMG and BIO Stations
Day 61, 2024
ZTD [m]
3.5
3.4
3.3
3.2
3.1
3
2.9
2.8
2.7
2.6
2.5
2.4
2.3
2.2
2.1
2
BRMG Station-RTKLIB
BRMG Station-CSRS
BIO Station-RTKLIB
BIO Station-CSRS
EUREF ZTD
01/03/2024 0:00:00
01/03/2024 9:36:00
01/03/2024 19:12:00
02/03/2024 4:48:00
Date and Time

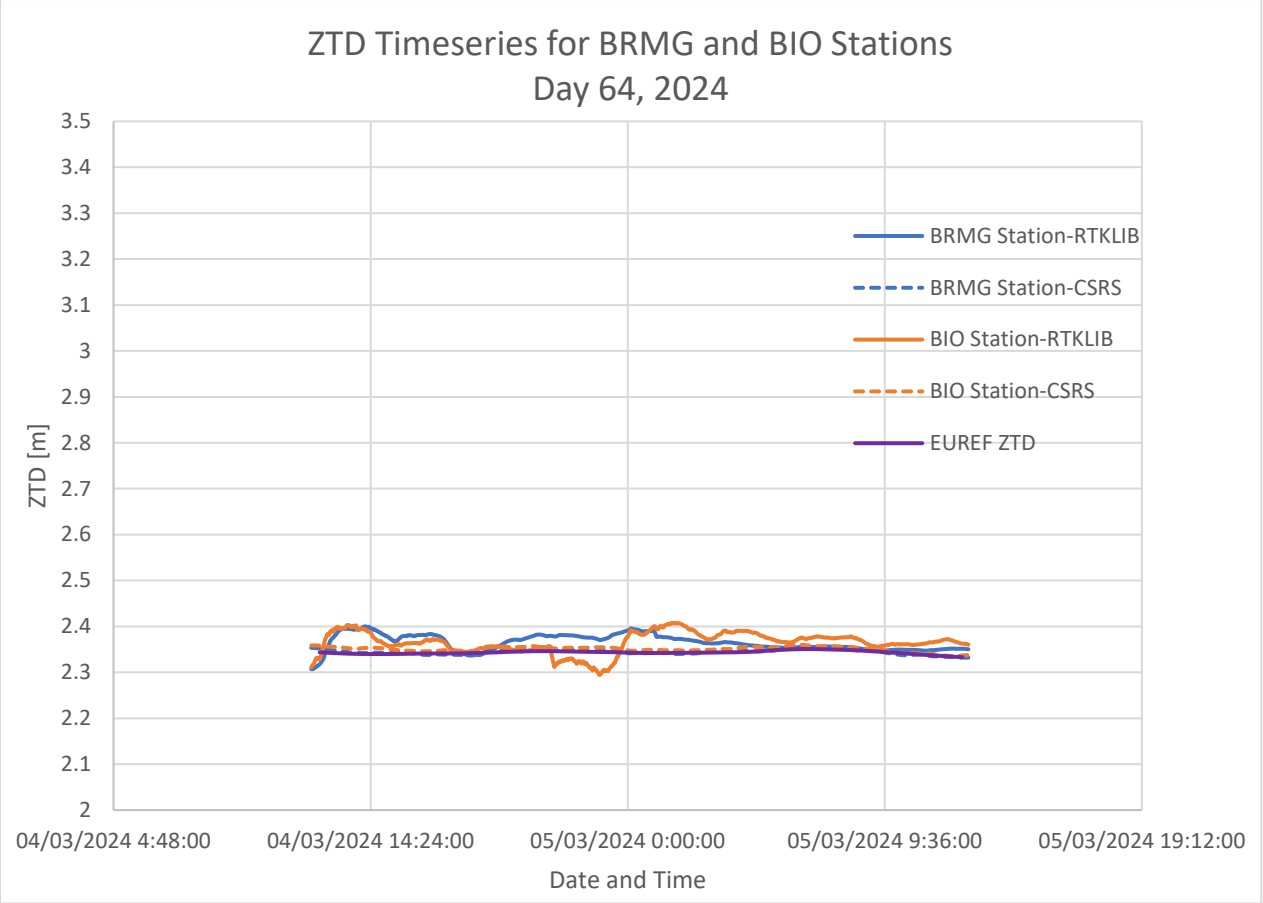
ZTD Timeseries for BRMG and BIO Stations
Day 64, 2024
ZTD [m]
3.5
3.4
3.3
3.2
3.1
3
2.9
2.8
2.7
2.6
2.5
2.4
2.3
2.2
2.1
2
BRMG Station-RTKLIB
BRMG Station-CSRS
BIO Station-RTKLIB
BIO Station-CSRS
EUREF ZTD
04/03/2024 4:48:00
04/03/2024 14:24:00
05/03/2024 0:00:00
05/03/2024 9:36:00
05/03/2024 19:12:00
Date and Time

ANNEX D

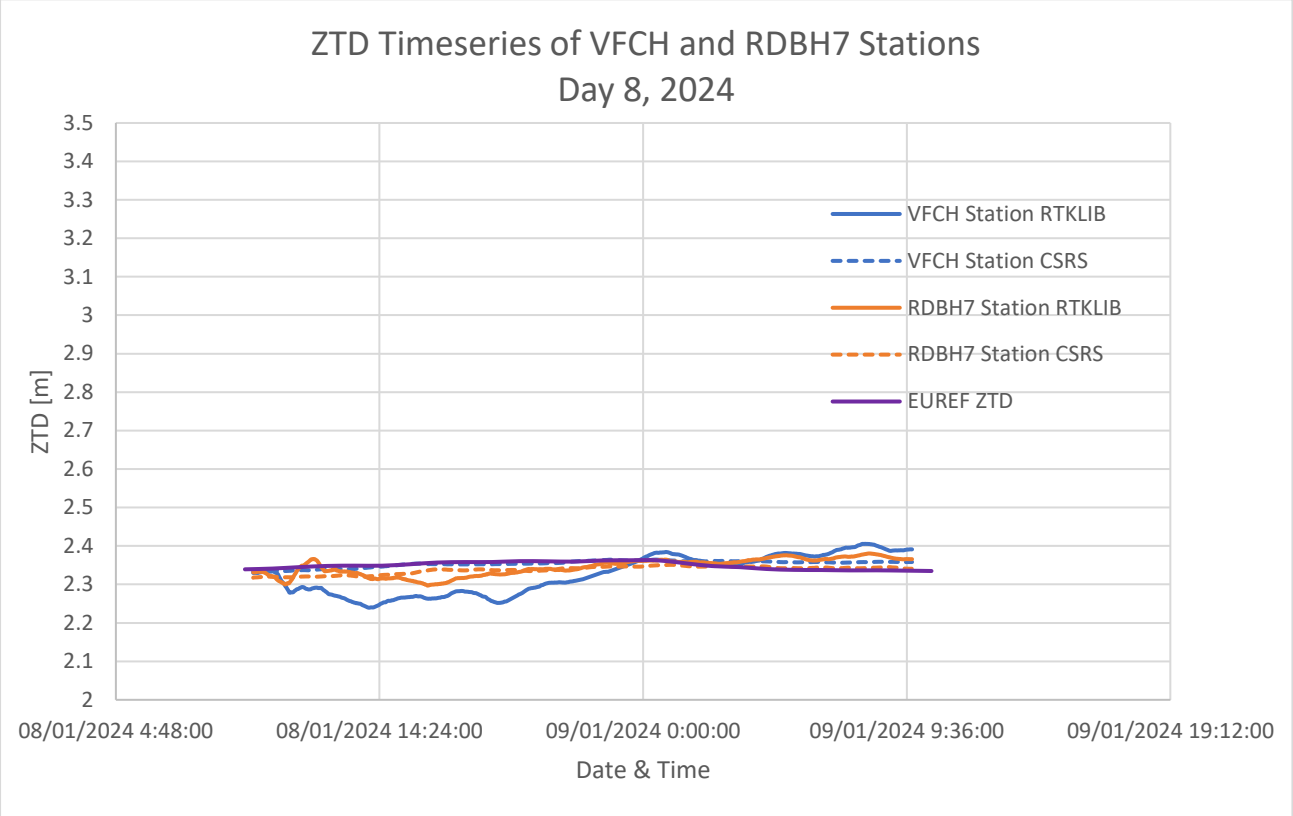
ZTD Timeseries of VFCH and RDBH7 Stations
Day 8, 2024
ZTD [m]
3.5
3.4
3.3
3.2
3.1
3
2.9
2.8
2.7
2.6
2.5
2.4
2.3
2.2
2.1
2
VFCH Station RTKLIB
VFCH Station CSRS
RDBH7 Station RTKLIB
RDBH7 Station CSRS
EUREF ZTD
08/01/2024 4:48:00
08/01/2024 14:24:00
09/01/2024 0:00:00
09/01/2024 9:36:00
09/01/2024 19:12:00
Date & Time

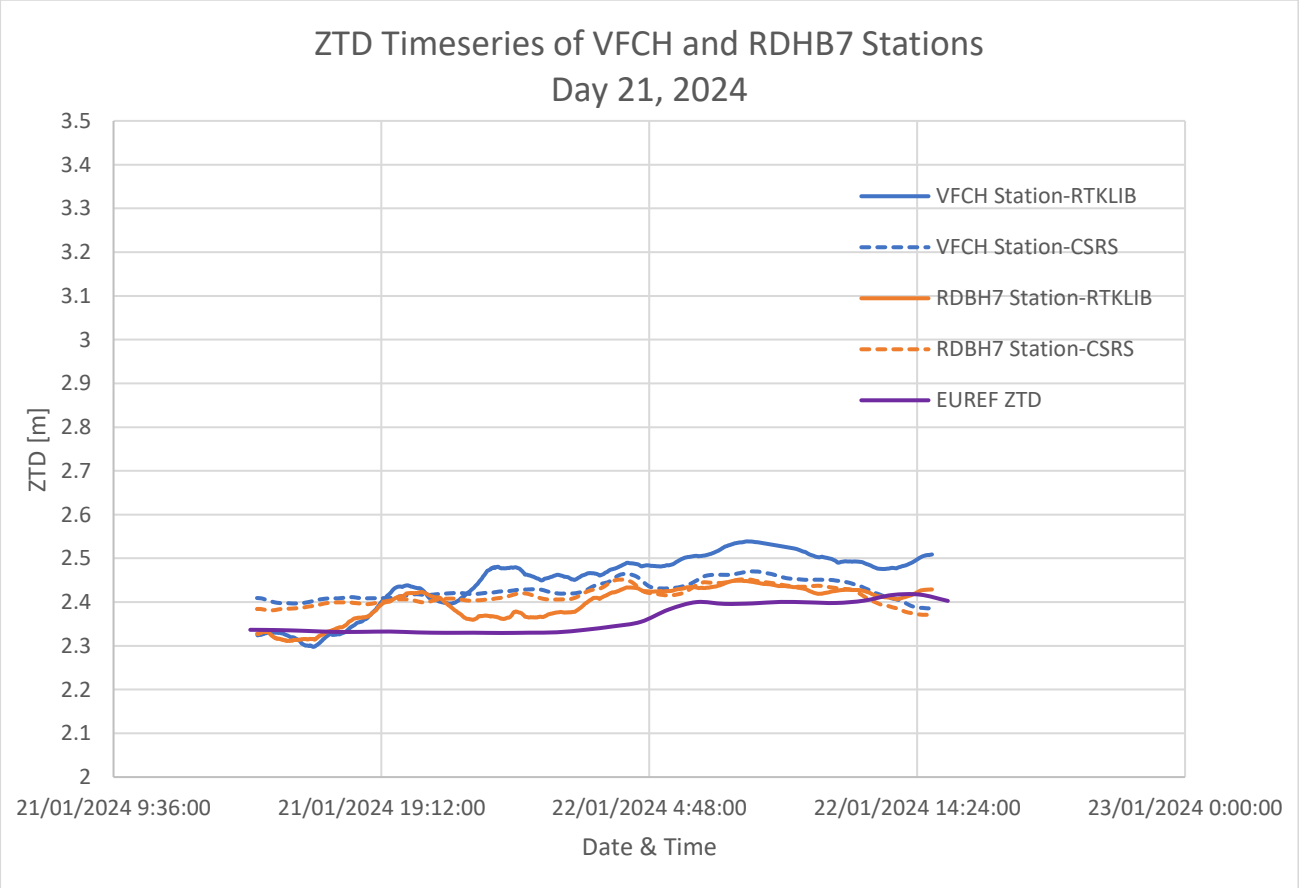
ZTD Timeseries of VFCH and RDHB7 Stations
Day 21, 2024
ZTD [m]
3.5
3.4
3.3
3.2
3.1
3
2.9
2.8
2.7
2.6
2.5
2.4
2.3
2.2
2.1
2
VFCH Station-RTKLIB
VFCH Station-CSRS
RDBH7 Station-RTKLIB
RDBH7 Station-CSRS
EUREF ZTD
21/01/2024 9:36:00
21/01/2024 19:12:00
22/01/2024 4:48:00
22/01/2024 14:24:00
23/01/2024 0:00:00
Date & Time

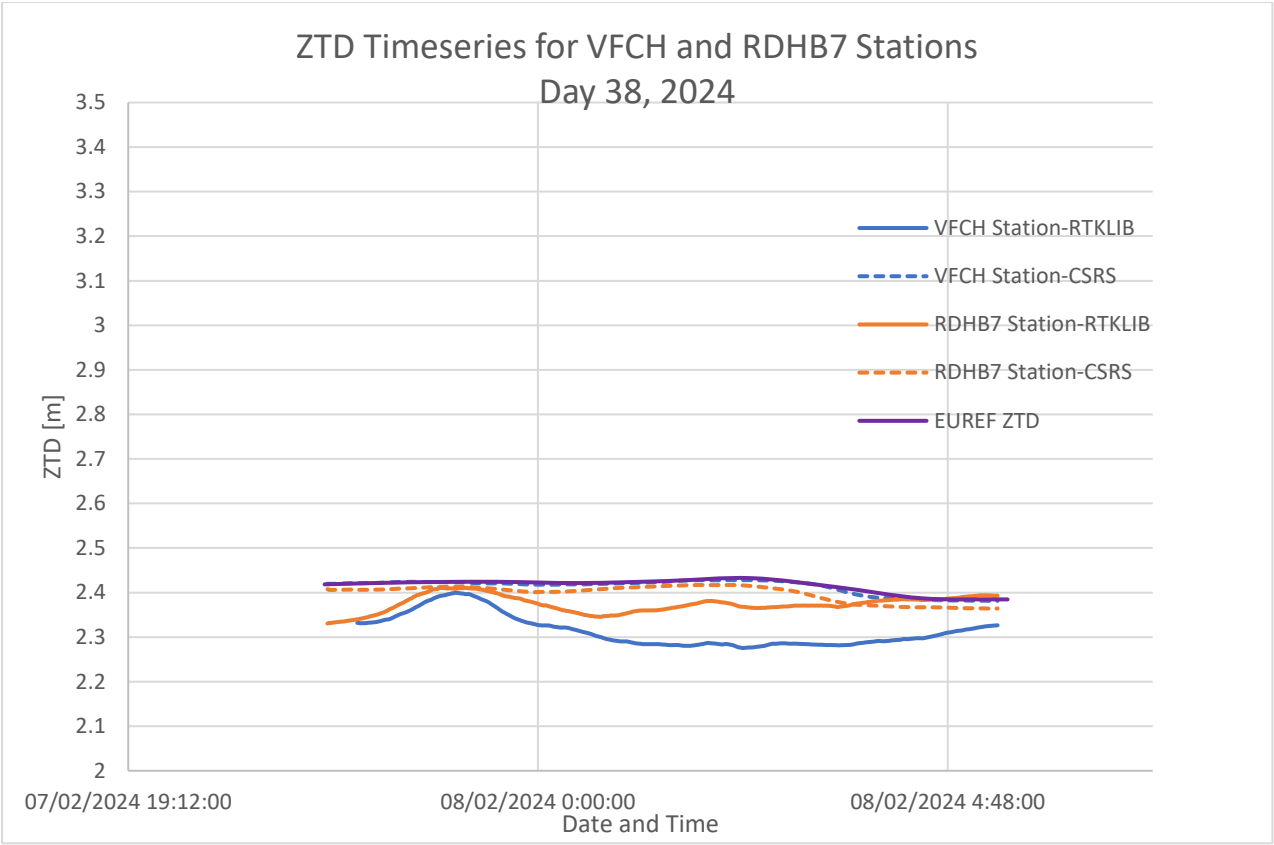
ZTD Timeseries for VFCH and RDHB7 Stations
Day 38, 2024
3.5
3.4
3.3
3.2
3.1
3
2.9
2.8
2.7
2.6
2.5
2.4
2.3
2.2
2.1
2
ZTD [m]
VFCH Station-RTKLIB
VFCH Station-CSRS
RDHB7 Station-RTKLIB
RDHB7 Station-CSRS
EUREF ZTD
07/02/2024 19:12:00
08/02/2024 0:00:00
08/02/2024 4:48:00
Date and Time

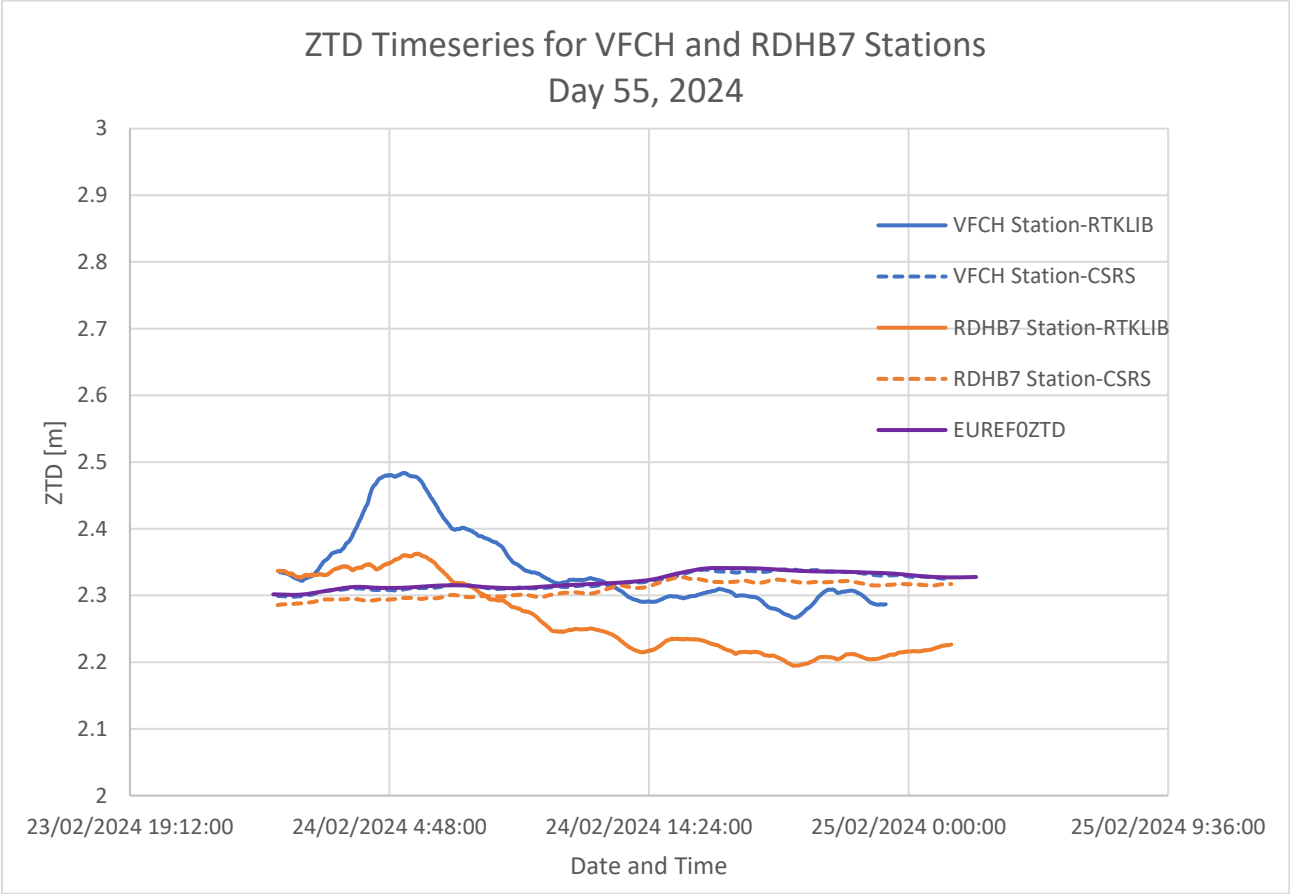
ZTD Timeseries for VFCH and RDHB7 Stations
Day 55, 2024
3
2.9
2.8
2.7
2.6
2.5
2.4
2.3
2.2
2.1
2
ZTD [m]
VFCH Station-RTKLIB
VFCH Station-CSRS
RDHB7 Station-RTKLIB
RDHB7 Station-CSRS
EUREF0ZTD
23/02/2024 19:12:00
24/02/2024 4:48:00
24/02/2024 14:24:00
25/02/2024 0:00:00
25/02/2024 9:36:00
Date and Time

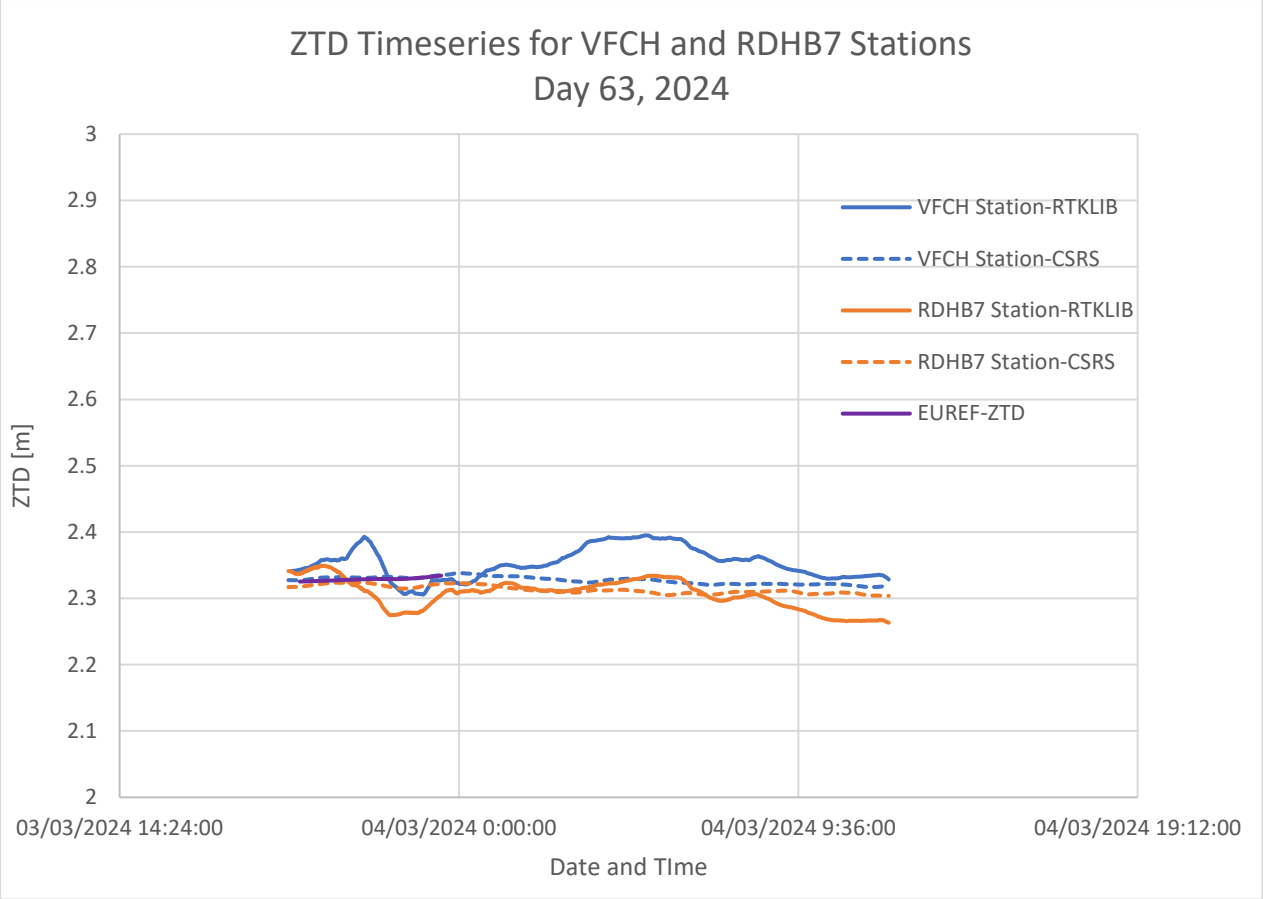
ZTD Timeseries for VFCH and RDHB7 Stations
Day 63, 2024
ZTD [m]
3
2.9
2.8
2.7
2.6
2.5
2.4
2.3
2.2
2.1
2
VFCH Station-RTKLIB
VFCH Station-CSRS
RDHB7 Station-RTKLIB
RDHB7 Station-CSRS
EUREF-ZTD
03/03/2024 14:24:00
04/03/2024 0:00:00
04/03/2024 9:36:00
04/03/2024 19:12:00
Date and TIme

ANNEX E

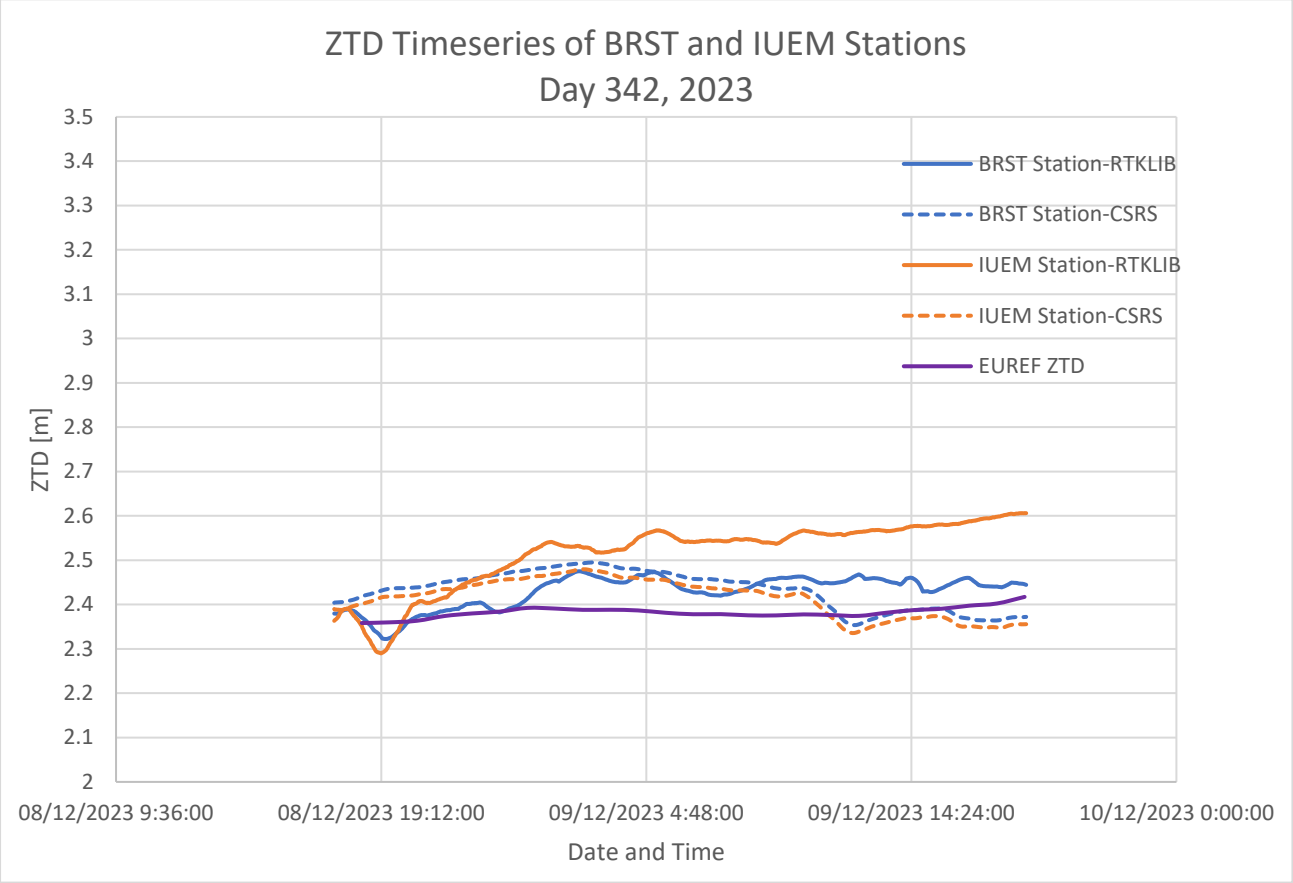
ZTD Timeseries of BRST and IUEM Stations
Day 342, 2023
ZTD [m]
3.5
3.4
3.3
3.2
3.1
3
2.9
2.8
2.7
2.6
2.5
2.4
2.3
2.2
2.1
2
BRST Station-RTKLIB
BRST Station-CSRS
IUEM Station-RTKLIB
IUEM Station-CSRS
EUREF ZTD
08/12/2023 9:36:00
08/12/2023 19:12:00
09/12/2023 4:48:00
09/12/2023 14:24:00
10/12/2023 0:00:00
Date and Time

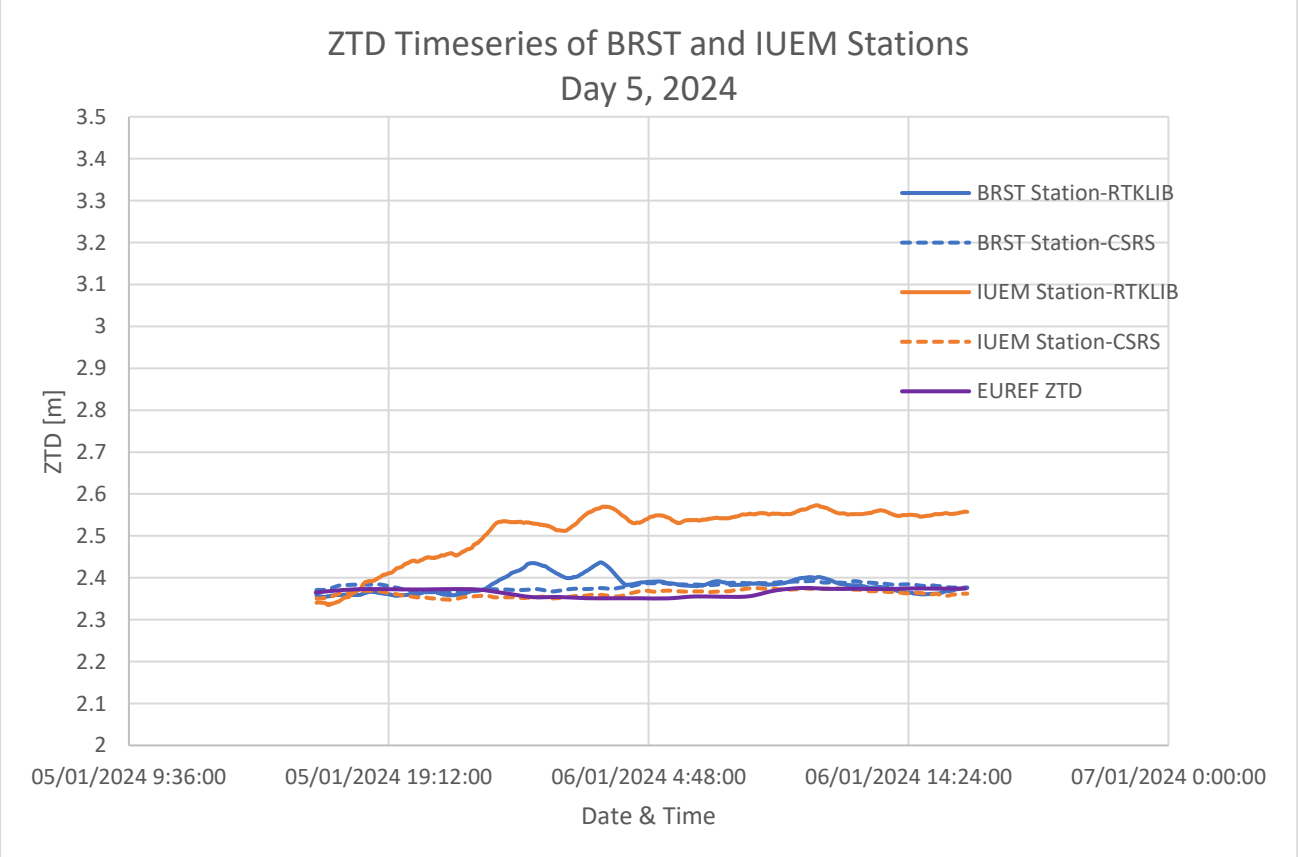
ZTD Timeseries of BRST and IUEM Stations
Day 5, 2024
ZTD [m]
3.5
3.4
3.3
3.2
3.1
3
2.9
2.8
2.7
2.6
2.5
2.4
2.3
2.2
2.1
2
BRST Station-RTKLIB
BRST Station-CSRS
IUEM Station-RTKLIB
IUEM Station-CSRS
EUREF ZTD
05/01/2024 9:36:00
05/01/2024 19:12:00
06/01/2024 4:48:00
06/01/2024 14:24:00
07/01/2024 0:00:00
Date & Time

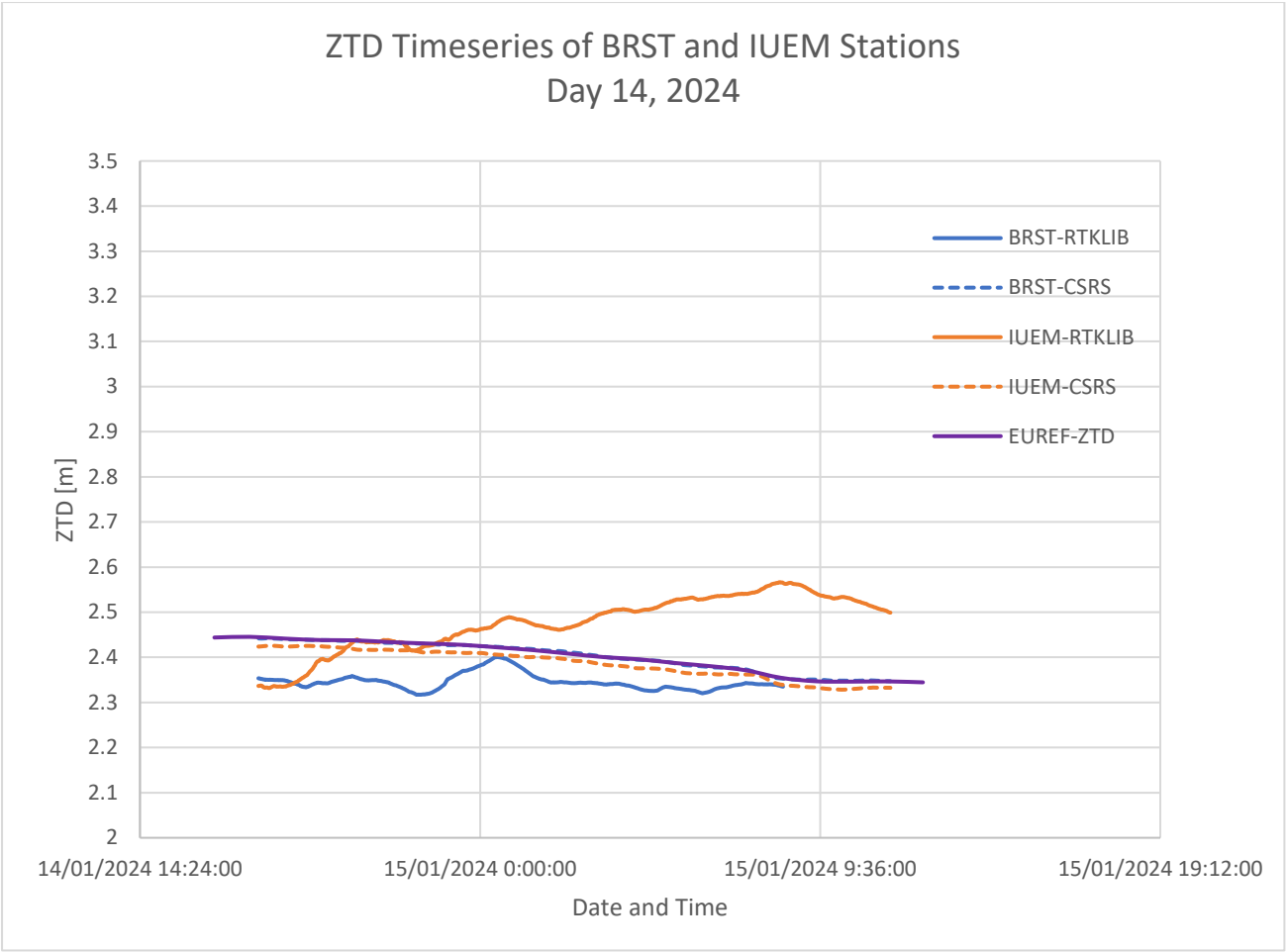
ZTD Timeseries of BRST and IUEM Stations
Day 14, 2024
ZTD [m]
3.5
3.4
3.3
3.2
3.1
3
2.9
2.8
2.7
2.6
2.5
2.4
2.3
2.2
2.1
2
BRST-RTKLIB
BRST-CSRS
IUEM-RTKLIB
IUEM-CSRS
EUREF-ZTD
14/01/2024 14:24:00
15/01/2024 0:00:00
15/01/2024 9:36:00
15/01/2024 19:12:00
Date and Time

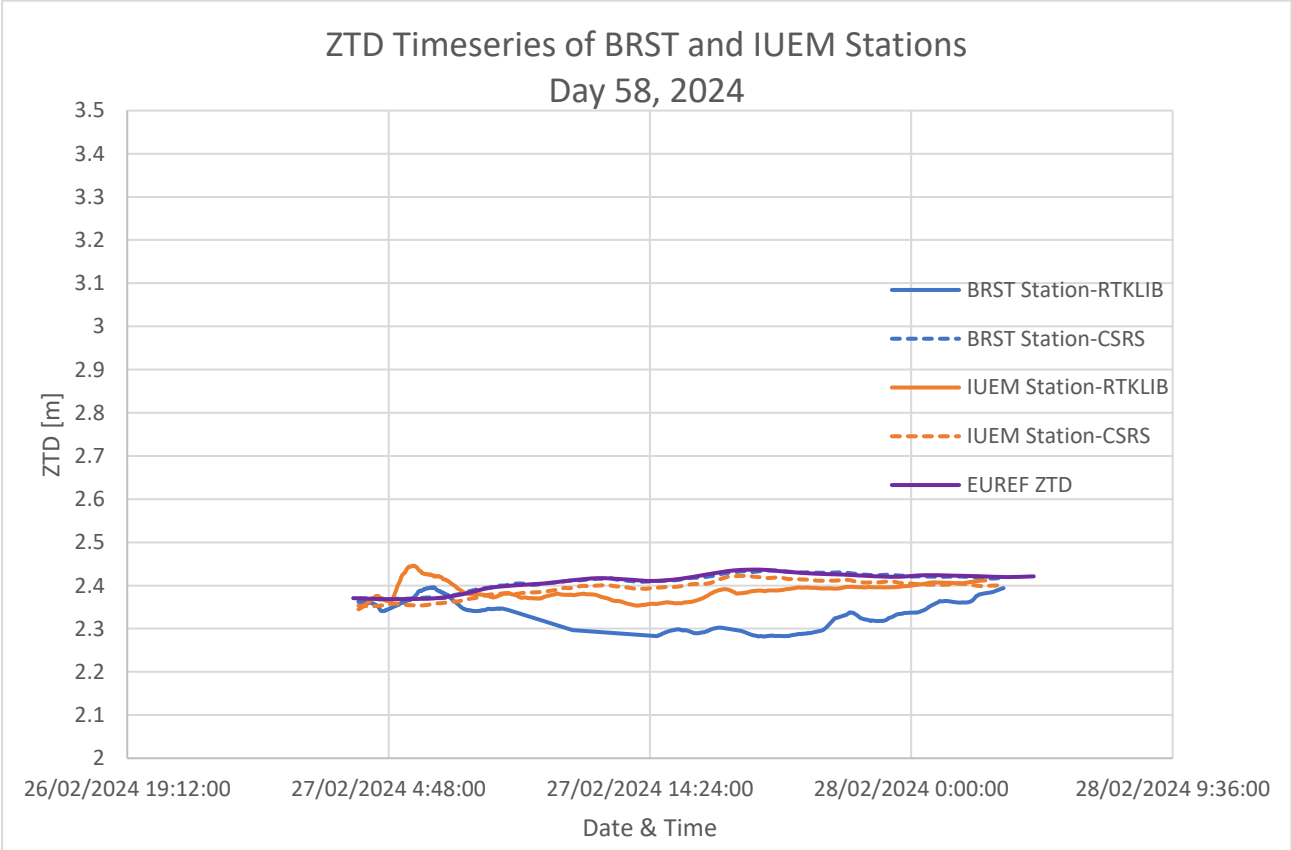
ZTD Timeseries of BRST and IUEM Stations
Day 58, 2024
ZTD [m]
3.5
3.4
3.3
3.2
3.1
3
2.9
2.8
2.7
2.6
2.5
2.4
2.3
2.2
2.1
2
BRST Station-RTKLIB
BRST Station-CSRS
IUEM Station-RTKLIB
IUEM Station-CSRS
EUREF ZTD
26/02/2024 19:12:00
27/02/2024 4:48:00
27/02/2024 14:24:00
28/02/2024 0:00:00
28/02/2024 9:36:00
Date & Time

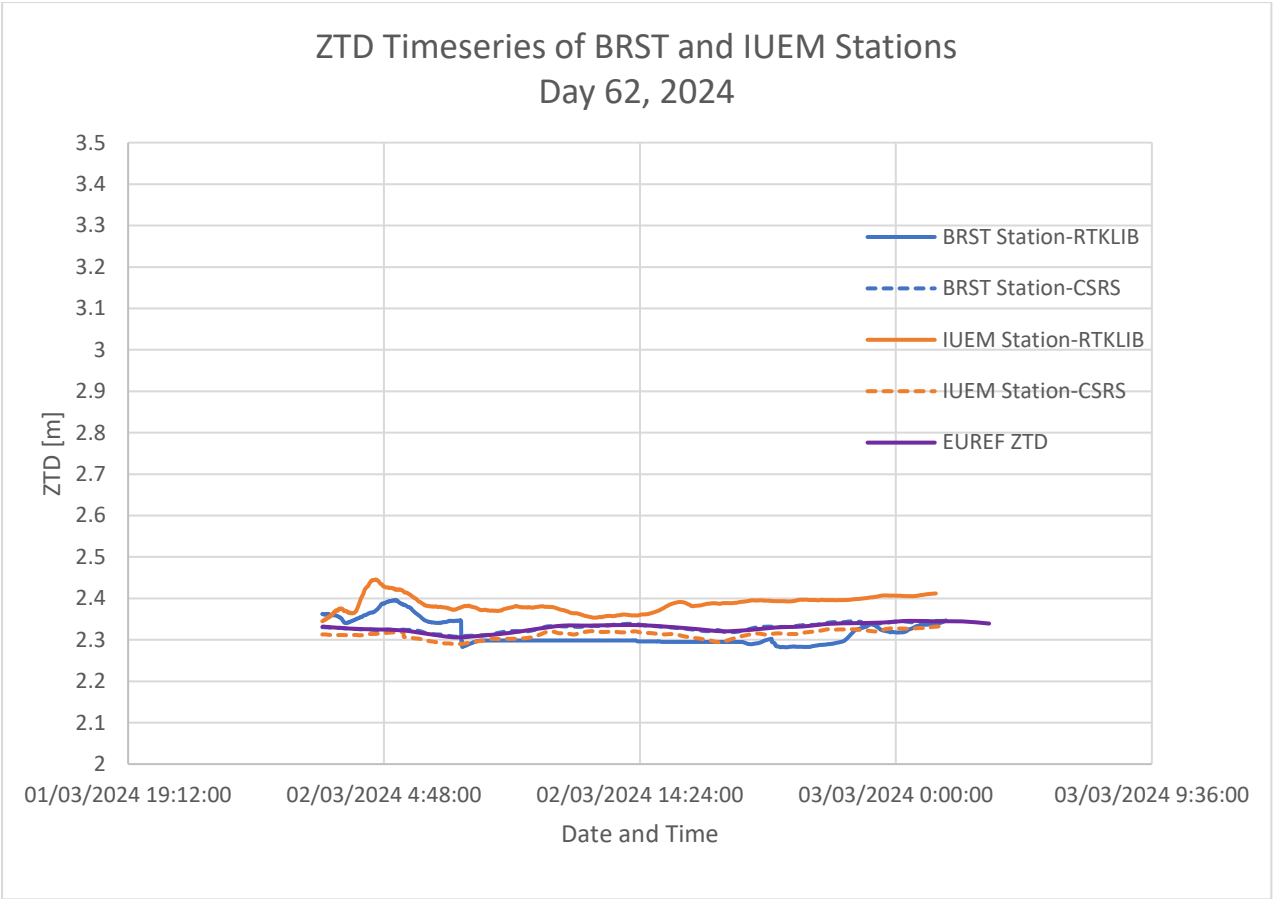
ZTD Timeseries of BRST and IUEM Stations
Day 62, 2024
ZTD [m]
3.5
3.4
3.3
3.2
3.1
3
2.9
2.8
2.7
2.6
2.5
2.4
2.3
2.2
2.1
2
BRST Station-RTKLIB
BRST Station-CSRS
IUEM Station-RTKLIB
IUEM Station-CSRS
EUREF ZTD
01/03/2024 19:12:00
02/03/2024 4:48:00
02/03/2024 14:24:00
03/03/2024 0:00:00
03/03/2024 9:36:00
Date and Time